Mass transfer in bubbly flows with or without chemical absorption

Devy Setiorini Sa’adiyah

(Degree)
博士（工学）

(Date of Degree)
2023-03-25

(Date of Publication)
2024-03-01

(Resource Type)
doctoral thesis

(Report Number)
甲第8643号

(URL)
https://hdl.handle.net/20.500.14094/0100482391

Doctoral Dissertation

Mass transfer in bubbly flows with or without chemical absorption
化学吸収を伴う気泡流の物質移動に関する研究

January 2023

Graduate School of Engineering, Kobe University

Devy Setiorini Sa'adiyah

博 士 論 文

Mass transfer in bubbly flows with or without chemical absorption
化学吸収を伴う気泡流の物質移動に関する研究

令和 5年 1月

神戸大学大学院 工学研究科

Devy Setiorini Sa’adiyah

Abstract

Post-combustion CO_2 captures such as Gas-Lift Advanced Dissolution (GLAD) systems, bubble column reactors and gas absorbers rely on mass transfer phenomena in which gas in bubbles is dissolved in the surrounding liquid phase. Learning about the flow characteristics of the system is important for designing the bubble column reactor with chemical absorption. Changes in bubble diameter, shape, and rising bubble speed due to mass transfer significantly change the flow characteristics. When determining the rate of chemical absorption, it is important to take into account the enhancement factor E. However, the existing E correlations are based on an analytical theory that has not been verified against experimental data for multi-bubble systems. Hence in this study, experiments of single CO_2 bubbles with various shapes were carried out with several NaOH concentrations and its applicability to bubbly flow was examined.

The mass transfer from a single CO_2 bubble with chemical absorption in a stagnant liquid was investigated in a vertical pipe with a diameter of D = 12.5 mm. The experiments were conducted with various sodium hydroxide concentrations ($12 \leq pH \leq 13.15$) and various bubble shapes ($0.4 \leq \lambda \leq 1.4$), where λ is the ratio of the bubble diameter to the pipe diameter. The image processing was performed for the bubble images, and the mass transfer coefficient was measured from the time change of the bubble diameter. The value of E is determined for each bubble by comparing the mass transfer coefficients of chemical and physical absorption. The experimental results confirmed that the presence of NaOH does not affect the mass transfer due to low concentration as E for $7 < pH < 12$ is almost unity. For $pH > 12.25$, E increases with increasing both pH and d. The enhancement factor E varies not only with pH but also with the shapes of bubbles d^*, where d^* ($= d/d_T$) is the ratio of the bubble diameter to the bubble diameter at the transition from ellipsoidal to semi-Taylor bubbles, putting E correlation from Fleischer et al., which is based on the two-film theory and a flat interface, inapplicable to single bubbles. The proposed empirical correlation of E for single bubbles shows good agreement with 93% of the data within 10% error margins. The correlation was also applied to bubbles in the larger pipe with a D = 18.2 mm.

Before applying the enhancement factor proposed in this study to multi-bubble systems, the applicability of obtaining good predictions for mass transfer in multi-bubble systems with different types of physical absorption was investigated. The experiments on bubbly-slug flows in a vertical pipe were carried out for three conditions: a pure water system, a system with electrolyte, NaCl, and a system including surfactant and electrolyte, NaCl-1-octanol mixture, and the obtained data were used to validate the predicted results. The spatial evolution of the flow patterns, radial void fraction distributions, and radial bubble diameter distributions of bubbles were measured for D = 25.0 mm, the liquid phase Reynolds number of 7000, and the gas volume flux of 0.120 m/s. The one-way bubble tracking method was used as the numerical simulation method. The available mass transfer correlations are implemented into the simulation. The predicted and measured spatial evolution agree well, implying that mass transfer correlations developed for single bubbles are applicable to bubbly flows with high Schmidt numbers. Due to the extremely thin concentration boundary layer present in a system with a high Schmidt number, the influence of adjacent bubbles and fluctuations in velocity surrounding the bubbles as a result of the liquid flow are negligible in terms of their effects on mass transfer. Therefore, the spatial evolutions were well predicted.

The E correlation of chemical absorption was then implemented into the bubble tracking system to test its applicability in bubbly flows with chemical absorption. In order to confirm the predicted results with or without chemical absorption, experiments were carried out for two gas volume flux conditions in a pure system and a NaOH system to validate the predicted results. Since the dissolution of bubbles in chemical absorption is very fast, the image processing method is used to calculate both mean void fractions and bubble diameter distributions at several axial locations in a vertical pipe. Good predictions of the flow patterns, mean void fractions, and bubble diameter distributions were obtained using the proposed E correlations in coupled with the available mass transfer correlations for a clean system applied to the one-way bubble tracking method

This study investigated the mass transfer with chemical absorption from single bubbles of varied shapes and NaOH concentrations flowing through a vertical pipe. A correlation of enhancement factor was also developed to predict bubble dissolution rate in aqueous NaOH solution. The bubble tracking method was used to verify the validity of available mass transfer correlations with different kinds of physical absorption before applying the proposed E correlation to the multi-bubble system. It was also clear that the proposed E correlation can predict bubbly flows in a vertical pipe with or without chemical absorption.

抄録

GLAD（Gas-Lift Advanced Dissolution）システム、バブルカラムリアクター、ガスアブソーバーなどの燃焼後 CO_2 回収は、気泡中のガスが周囲の液相に溶解する物質移動現象に依存しています。化学吸収を伴うバブルカラムリアクターの設計には、システムの流動特性を知ることが重要です。物質移動による気泡径、形状、気泡の上昇速度の変化は、流動特性を大きく変化させます。化学吸収速度を決定する際には、増進係数 E を考慮することが重要である。しかし、既存の E 相関は解析理論に基づいており、複数気泡系の実験データに対する検証はなされていない。そこで本研究では、様々な形状の単一 CO_2 気泡を複数の NaOH 濃度で実験し、気泡流への適用性を検討しました。

直径 D=12.5mm の垂直配管において、滞留液中の化学吸収を伴う単一 CO_2 気泡からの物質移動について調べた。実験は，様々な水酸化ナトリウム濃度（$12 \leq pH \leq 13.15$）と様々な気泡形状（$0.4 < \lambda < 1.4$）で行い，λ は気泡径とパイプ径の比であった．気泡画像に対して画像処理を行い、気泡径の時間変化から物質移動係数を測定した。化学吸収と物理吸収の物質移動係数を比較することで、各気泡の E 値を決定した。実験の結果、$7 \leq pH \leq 12$ では E がほぼ 1 であるため、NaOH の存在は低濃度による物質移動に影響を与えないことが確認された。ここで、d^* ($= d/d_T$) は楕円形から半テイラー形への移行点における気泡径と気泡径の比であり、2膜理論と平面界面に基づく Fleischer らの E 相関は単一気泡には当てはまらない。提案した単一気泡に対する経験的な E 相関は、10%の誤差の範囲内で 93%のデータと良い一致を示した。また、この相関関係を直径 18.2 mm の大型パイプ内の気泡に適用した。

本研究で提案した増強係数を複数気泡系に適用する前に、異なるタイプの物理吸収を持つ複数気泡系における物質移動について良好な予測値を得るための適用性を検討した。垂直配管内のバブリースラグ流について、純水系、電解質 NaCl を含む系、界面活性剤と電解質 NaCl-1-オクタノール混合系の 3 条件での実験を行い、得られたデータを用いて予測結果の検証を行った。D = 25.0mm、液相レイノルズ数

7000、ガス体積流束 0.120m/s において、流動パターンの空間展開、径方向ボイド率分布、径方向気泡径分布が計測された。数値シミュレーション手法として、ワンウェイバブルトラッキング法を用いた。利用可能な物質移動相関はシミュレーションに実装されている。予測された空間的変遷と測定された空間的変遷はよく一致し、単一気泡のために開発された物質移動相関が高いシュミット数を持つ気泡流に適用可能であることを示唆するものである。高いシュミット数の系に存在する極めて薄い濃度境界層により、隣接する気泡の影響や液体の流れによる気泡の周囲の速度変動は、物質移動への影響という点では無視できる程度である。したがって、空間的な進化をよく予測することができた。

次に、化学物質吸収の E 相関を気泡追跡システムに実装し、化学物質吸収を伴う気泡流への適用性を検証した。化学吸収の有無にかかわらず予測結果を検証するため、純水系とNaOH系の2つのガス体積フラックス条件について実験を行った。化学吸収による気泡の溶解は非常に速いため、画像処理法を用いて、垂直配管の軸方向複数箇所における平均ボイド率および気泡径分布の両方を算出した。一方向気泡追跡法を適用した清浄系において、提案した E 相関式と既存の物質移動相関式を併用することにより、流動様式、平均ボイド率、気泡径分布の良好な予測結果を得ることができた。

本研究では、垂直配管を流れる様々な形状および NaOH 濃度の単一気泡からの化学吸収を伴う物質移動について検討した。また、NaOH 水溶液中の気泡溶解速度を予測するための増強係数の相関式を開発した。提案した E 相関を多気泡系に適用する前に、気泡追跡法を用いて、異なる種類の物理吸収を伴う利用可能な物質移動相関の妥当性を検証した。また、提案した E 相関は、化学的吸収の有無にかかわらず、垂直配管内の気泡流を予測できることを明らかにした。

Table of contents

List of figures

List of tables

List of symbols

Roman symbols

A	[–]	constant value
A_B	[m^2]	bubble surface area
b_i	[m^3/kmol]	constant
$B(t)$	[–]	binarized signal
c_i	[kmol/m^3]	concentration of ion
c_s	[kmol/m^3]	concentration of solution
C_0	[kmol/m^3]	CO_2 concentration in the liquid phase
C_{int}	[kmol/m^3]	concentration of CO_2 at the bubble interface
C_D	[–]	coefficient of drag
C_L	[mol/m^3]	gas concentration in the liquid phase
C_{Li}	[–]	lift coefficient
C_N	[wt.%]	concentration of NaCl
C_P	[–]	experimental coefficient for coalescence probability
C_{sat}	[mol/m^3]	saturated concentration of CO_2
C_{sat}^0	[mol/m^3]	saturated concentration of CO_2 in clean water
C_{sol}	[mol/m^3]	concentration of solution
C_V	[kmol/m^3]	molar concentration of water in the solution (55.4 kmol/m^3)
C_{VM}	[–]	virtual mass coefficient
d	[m]	sphere-volume equivalent bubble diameter
d_E	[m]	transition bubble diameter of ellipsoidal bubble
d_{in}	[m]	initial diameter
d_T	[m]	transition bubble diameter of Taylor bubble
d^*	[–]	dimensionless bubble diameter for shape transition
D	[m]	pipe diameter
D_{CO_2}	[m^2/s]	diffusion coefficient of CO_2
$D_{CO_2}^0$	[m^2/s]	diffusion coefficient of CO_2 in water
D_L	[m^2/s]	diffusion coefficient
$\boldsymbol{e}$	[–]	unit vectors orthogonal
E	[–]	enhancement factor
Eo	[–]	Eötvös number
Eo_D	[–]	Eötvös number for large bubbles
Eo_H	[–]	Eötvös number for the major diameter d_H of the bubble

$f(r)$	[–]	radial factor
$\boldsymbol{F_B}$	[N]	buoyancy force
$\boldsymbol{F_D}$	[N]	drag force
$\boldsymbol{F_F}$	[N]	centrifugal force
$\boldsymbol{F_L}$	[N]	lift force
$\boldsymbol{F_W}$	[N]	wall force
Fr_D	[–]	Froud number
g	[m/s^2]	gravitational constant
h_G	[m^3/kmol]	gas-specific parameters
h_G^0	[m^3/kmol]	gas-specific parameter for pure gas
h_i	[m^3/kmol]	ion-specific
h_T	[m^3/(kmol·K)]	gas-specific parameter for the temperature effect
H	[Pa]	Henry constant
H_{CO_2}	[Pa]	Henry constant of CO_2
$H_{CO_2}^0$	[Pa]	Henry constant of CO_2 in water
J_G	[m/s]	gas volume flux
J_L	[m/s]	liquid volume flux
k_a	m^3/ms	adsorption rate constant
k_d	1/s	desorption rate constant
k_L	[m/s]	mass transfer coefficient
k_L^0	[m/s]	mass transfer coefficient without chemical absorption
l_m	[m]	mixture length representing the turbulence length scale
l_{Gi}	[m]	major axis length of the ellipsoid of bubble
l_{Ri}	[m]	minor axis length of the ellipsoid of bubble
L	[m]	length of Taylor bubble
L_m	[m]	distance from the bubble trailing edge
m	[–]	total number of ions
m_p	mol	the amount of material of the gas p (= CO_2, N_2, O_2)
M_{H2O}	[g/mol]	molar mass of water (=18 g/mol)
M	[–]	Morton number
n	mol	species mole
n_i	[kmol/m^3]	number of ions
$\boldsymbol{n}_r$	[–]	unit vector in the radial direction of the pipe
$\boldsymbol{n}_z$	[–]	unit vector pointing vertically upward
N	[–]	total number of elliptical plates
P_C	[–]	coalescence probability
P_{atm}	[Pa]	atmospheric pressure

Pe	[–]	Peclet number
Pe_D	[–]	Peclet number for large bubble
$P(z)$	[Pa]	pressure inside a bubble at z position
Q	[mol/m^3·s]	CO_2 transfer rate
r	[–]	radial direction
r_T	[m]	radial position of the bubble interface
R	[J/mol.K]	universal gas constant
R_P	[m]	pipe radius
Re	[–]	Reynold number
Re_D	[–]	Reynold number for large bubble
Re_L	[–]	liquid Reynold number
R_W	[m]	radius of the updraft region in the wake
Sc	[–]	Schmidt number
Sh	[–]	Sherwood number
Sh^0	[–]	Sherwood number without chemical absorption
Sh_D	[–]	Sherwood number for large bubble
Sh_D^0	[–]	Sherwood number for large bubble without chemical absorption
St	[–]	Strouhal number
t	[s]	time
t_1	[s]	measurement start time
t_M	[s]	measurement time
T	[K]	temperature
V_B	[m/s]	bubble rising velocity
V_{B0}	[m/s]	terminal velocity
V_{max}	[m/s]	maximum rise velocity in the wake region of the large bubble
$\boldsymbol{V_L}$	[m/s]	liquid velocity
V_T	[m/s]	terminal velocity of semi-Taylor and Taylor bubbles
V_W	[m/s]	wake velocity of a preceding large bubble
$\boldsymbol{V'}$	[m/s]	velocity fluctuation due to turbulence
V^*	[–]	the dimensionless value (V_{max}/ V_T)
x	[m]	the bubble position
X	[–]	mole fraction of CO_2 in the gas phase
z_B	[m]	vertical coordinate
z_i	[m]	vertical coordinate of i-th plates
z_T	[m]	vertical downward distance from the bubble tip

Greek symbols

α	[–]	bubble-shape dependent constant
α_G	[–]	void fraction
β	[–]	coefficient indicating the degree of turbulence vorticity influence on bubble motion
γ	[–]	parameter to calculate Fr_D
Γ_m	mol/m^2	saturation concentration
δ	[m]	thickness of elliptic plate
ε	[–]	parameter to calculate Fr_D
ζ	[–]	Standard deviation
η	[–]	parameter to calculate Fr_D
θ	[–]	circumferential direction
Θ_B	[m^3]	total bubble volume
Θ_{Bn}	[m^3]	total gas volume of each bubble class
λ	[–]	diameter ratio (= d/D)
μ_L	[Pa·s]	liquid viscosity
ρ_{H2O}	[kg/m^3]	water density (= 997 kg/m^3)
ρ_G	[kg/m^3]	gas density
ρ_L	[kg/m^3]	liquid density
σ	[N/m]	surface tension
τ	[s]	time
Φ	[–]	wall effect multiplier
ξ	[–]	parameter to account for the fact that there is no pressure gradient in the axial direction in the descending free-falling liquid film around Taylor bubbles
χ	[–]	coefficient to calculate Vw

Chapter 1
Introduction

1.1 Background

Reduction of carbon dioxide (CO_2) emission remains the critical issue in controlling global warming. In the petroleum, natural gas, coal-fired power plants, and chemical industries, physical and chemical absorption methods are frequently used to remove CO_2, i.e., Gas-Lift Advanced Dissolution (GLAD) system [1], bubble column reactor and gas absorber (Fig. 1.1) [2,3]. CO_2 gas dissolved in the liquid, and the mass transfer from bubbles to liquid have become essential in designing those gas-liquid two-phase flow devices. In the GLAD system, physical absorption takes place in the CO_2 dissolution into seawater as they rise in J-shaped pipes installed in the ocean. For chemical absorption, flue gas from industries containing CO_2 is purged into a reactive liquid so that CO_2 not only dissolves but also changes to other products very quickly due to chemical reactions. Many reactive liquids have been examined to obtain the maximum efficiency of CO_2 removal, and sodium hydroxide (NaOH) has the highest removal percentage, 92–99% [4].

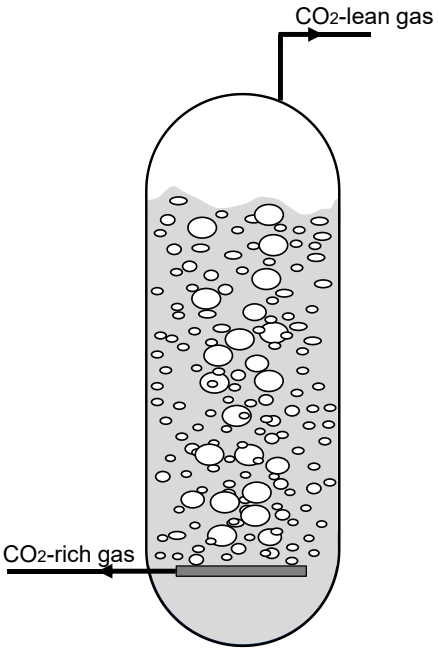

Fig. 1.1 Bubble column reactor

In designing the bubble column reactor with chemical absorption, it is necessary to understand the flow characteristics of the equipment. The flow characteristics change significantly due to changes in the bubble diameter, shape, and rising speed of the bubbles due to mass transfer. Also, the enhancement factor E needs to be considered to define how fast the absorption rate in the system. E is a dimensionless number that compares the mass transfer coefficient from chemical absorption to physical absorption [5]:

$$E = \frac{k_L}{k_L^0} \simeq \frac{Sh}{Sh^0} \tag{1.1}$$

where k_L and k_L^0 are the mass transfer coefficients with and without chemical absorption, respectively, and Sh and Sh^0 are the Sherwood numbers with and without chemical absorption.

Most studies on CO_2 absorption in NaOH solutions have been carried out for flows in bubble column reactors, both experimental and numerical [6–12]. Some numerical simulations have implemented the enhancement factor based on an analytical approximation derived from several enhancement factor theories, such as the penetration [13,14], the surface renewal [14], and the two-film theories [15,16]. Fleischer et al. [6] used the two-film theory to estimate E for a wide range of NaOH concentration ($7 \leq \text{pH} \leq 14$). Then for simplicity, E estimated from the theory was extracted as a function of pH and implemented into the numerical simulation for bubbly flows (see Fig. 1.2) as follows

$$E = 1 + 7x10^{-7}\exp\left(1.98pH - 10.6\right) \tag{1.2}$$

Basically, the theoretical derivations of E considered only the rate of diffusion through a flat interface. The bubble column reactor is, however, a multi-bubble system including a wide range of bubble diameters. The flat interface assumption cannot be adopted unless the radius of the interface curvature is infinitely large. Hence, it is required to obtain knowledge of mass transfer with chemical reactions from single bubbles of various diameters and shapes.

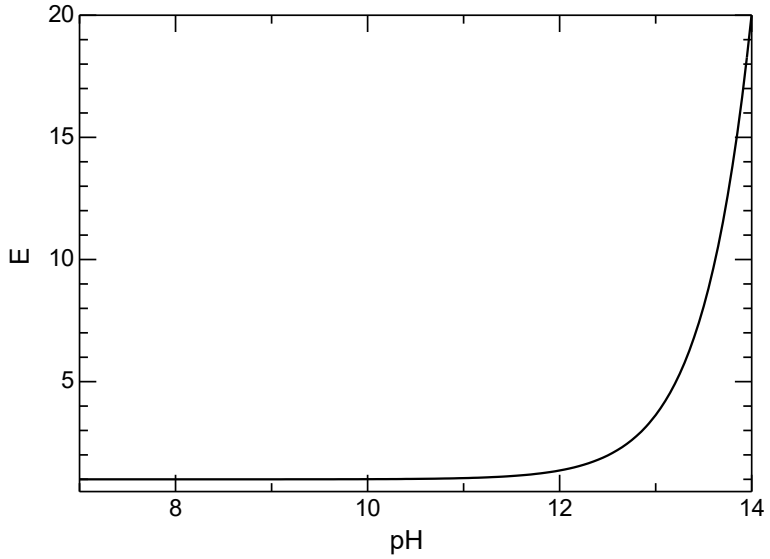

Fig. 1.2 Enhancement factor proposed by Fleischer et al. [6]

Madhavi et al. [17] experimentally observed a single spherical CO_2 bubble rising through infinite stagnant NaOH aqueous solutions at pH = 14, 14.18, and 14.4 in the range of bubble diameter from 0.45 to 0.65 mm. The experiments showed that the bubble diameter decreased significantly as the NaOH concentration increased, i.e., the increase in the NaOH concentration enhanced the mass transfer. This tendency was well reproduced by a prediction model taking E into account [18]. Jia and Zhang [19] used the experimental results by Madhavi et al. for comparison with their numerical predictions. Their simulation showed that the chemical reaction dominated the local mass transfer rate. The chemical absorption from Taylor bubbles was studied by Kundu et al. [20], who focused only on the percentage of removed CO_2 during experiments with several pipe diameters and NaOH concentrations. The observation of various kinds of bubble shapes is very limited. To this point, our knowledge of the chemical absorption of deformed bubbles is insufficient. In particular, the relationship between E and pH for single bubbles proposed by Fleischer et al., which is used by many researchers to perform numerical prediction of multi-bubble systems, lacks experimental evidence. Therefore, experiments of single CO_2 bubbles with various shapes were carried out with several NaOH concentrations to obtain an empirical E correlation by comparing k_L of the chemical absorption with those of the physical absorption k_L^0. Then the empirical E correlation will be implemented in the numerical simulation of the multi-bubble systems.

1.2 Mass transfer from a single CO_2 bubbles

The mass transfer from a single bubble is affected by various factors such as bubble diameter, shape, rising speed, liquid phase physical properties, and pipe wall [21]. In addition, for chemical absorption, the enhancement factor also becomes one of the factors controlling rapid mass transfer. For this reason, many studies have investigated the effects of these factors on mass transfer. The Sherwood number *Sh* defined by the following equation is often used for mass transfer evaluation.

$$Sh = \frac{k_L d}{D_L} \tag{1.3}$$

where k_L [m/s] is the mass transfer coefficient, d [m] is the sphere-volume equivalent bubble diameter, and D_L [m^2/s] is the diffusion coefficient.

Following Eq. (1.1), the Sh for chemical absorption for small bubbles can be evaluated by using

$$Sh = E\ Sh^0 \tag{1.4}$$

and for large bubbles, using

$$Sh_D = E\ Sh_D^0 \tag{1.5}$$

Here, Sh and Sh_D are the Sherwood number considering chemical absorption for small bubble and large bubbles (cf. Eq. (1.8)), respectively. Sh^0 is the Sherwood number for clean system without chemical reaction. Hori et al. [22] proposed the following correlation for Sh^0, which is applicable to ellipsoidal and semi-Taylor bubbles in water of $L/D < 1$, where L is the length of Taylor bubble and D is the pipe diameter:

$$Sh^0 = \begin{cases} \frac{2}{\sqrt{\pi}}\left(0.34\ d^{*2} + 0.28 d^* + 1\right)\sqrt{Pe} & \text{for } d^* < 1 \\ (0.18\ d^* + 1.6)\ \sqrt{Pe} & \text{for } d^* \geq 1 \end{cases} \tag{1.6}$$

Here d^* (= d/d_T) is the ratio of the bubble diameter to the bubble diameter at the transition from ellipsoidal to semi-Taylor bubbles [23]. Pe is the Peclet number defined by

$$Pe = \frac{V_B d}{D_L} \tag{1.7}$$

where V_B [m/s] is the bubble rising velocity.

For Taylor bubbles of $L/D \geq 1$, Sh_D^0 in clean water proposed by Filla [24] is available:

$$Sh_D^0 = 5.1(L/D)^{0.8}\sqrt{Pe_D} \tag{1.8}$$

where Sh_D^0 is defined by

$$Sh_D^0 = \frac{k_L A_B}{D_L D} \tag{1.9}$$

where A_B (= πd^2) is the bubble surface area. Pe_D is the Peclet number defined by

$$Pe_D = \frac{V_B D}{D_\mathrm{L}} \quad , \tag{1.10}$$

The L/D in Eq. (1.7) can be evaluated by using the following correlation proposed by Nakahara and Tomiyama [25]:

$$L/D = (0.586 - 0.216\lambda + 0.844\lambda^2)\lambda \tag{1.11}$$

where λ is the diameter ratio (= bubble diameter d [m] / pipe diameter D [m]).

For all bubble shapes, E will be evaluated by comparing the mass transfer coefficient obtained from the chemical absorption experiment and mass transfer coefficient for clean system.

1.3 Multi-bubble system

In order to investigate complex multi-bubble system, many numerical methods have been proposed. The one-way bubble tracking method is well-known method that significantly reduces computational costs by utilizing models for the liquid flow instead of solving the momentum equation for the liquid phase [26]. This bubble tracking method predicts bubbly flows in a Lagrangian manner, and the local variables such as the bubble diameter, velocity, and position of each bubble in the flow field are directly obtained as dependent variables. Therefore, the volume fraction of each phase and the gas-liquid boundary area are calculated without any numerical diffusion. By implementing a mass transfer model for a clean water system to the one-way bubble tracking method, Abe et al. [27] successfully obtained a good prediction of the spatial evolution between predicted and measured dissolving bubbly pipe flows. However, the mass transfer correlation of single bubbles used in Abe et al. was obtained from the experimental results for D = 25.0 mm only, so it is not applicable to other pipe diameters [28].

Before applying the enhancement factor proposed in this study to multi-bubble systems, it would be necessary to examine whether we can obtain good prediction for mass transfer in multi-bubble systems with various kinds of physical absorption. Therefore, the experiments in multi-bubble system in a vertical pipe were carried out for three different conditions: a pure water system, a system with electrolyte, NaCl, and a system including surfactant and electrolyte, NaCl-1-octanol mixture. Mass transfer correlations proposed in previous studies for each scenario [22,29] were implemented into a three-dimensional one-way bubble tracking method [26,30], and new experimental data were used to validate the extended pure method. Experiments of multi-bubble systems with chemical absorption were carried out for a pure water system and a NaOH aqueous solution of pH = 13. The applicability of the proposed empirical correlation of E to numerical simulation of bubbly pipe flows with chemical absorption is validate by comparing measured and predicted spatial evolutions.

1.4 Objectives

Understanding the behavior of CO_2 bubbles is important in designing the bubble column reactor with chemical absorption. The presence of reactive liquid in the system increases significantly the bubble dissolution, therefore, the enhancement factor E is an essential factor that needs to be considered. Many studies have been made to develop a model of E for the bubble column reactor. However, the E correlations obtained so far have been

based on an analytical theory which has not been validated against experimental data for multi-bubble systems. In this study, we investigate the mass transfer of single CO_2 bubbles with various shapes in a vertical pipe for $7 \leq \text{pH} \leq 13.15$, and develop an empirical E correlation that can predict the bubble dissolution process. First, a dissolution experiment of a single CO_2 bubble in an aqueous NaOH solution rising in a vertical pipe is performed to obtain k_L data. Bubble dissolution in a wide range of λ is measured, and the obtained k_L were compared with k_L^0 in a pure water system.

Then, experiments of multi-bubble system with various kind of physical absorption including surfactant and electrolyte were carried out. The mass transfer correlation proposed in previous studies were implemented into the one-way bubble tracking method to examine whether they give good predictions by comparing numerical prediction of various kinds of physical absorption of multi-bubble system with measured data. Then, the experiments of multi-bubble system with chemical absorption were carried out. The spatial evolution such as flow patterns, mean void fraction, and bubble diameter distributions for chemical absorption were obtained from multi-bubble experiments for aqueous NaOH solution (pH=13). The applicability of the proposed empirical correlation of the enhancement factor E to the bubbly pipe flow with chemical absorption is validated by comparing predicted and measured data.

1.5 Dissertation structure

This dissertation consists of five chapters. The outline of each chapter is summarized below:

1. Chapter 1 describes the background of this study and the previous studies on mass transfer from bubbles with/without chemical absorption. After showing that there is insufficient knowledge about the dissolution of CO_2 bubbles in aqueous NaOH solution especially for single bubbles, the purpose and method of this study were described.
2. In Chapter 2, the effect of chemical absorption on bubble dissolution is investigated. The experiments of a single CO_2 bubbles in a stagnant liquid in a vertical pipe are carried out using aqueous NaOH solution whose pH is varied from 12 to 13.15. k_L is measured from the experiments and compared with k_L^0 for a clean system to construct empirical E correlation.
3. In Chapter 3, gas-liquid two-phase flows in a vertical pipe are measured for mass transfer with various kinds of physical absorption. The experiments are for a pure water system, a system with electrolyte, NaCl, and a system including surfactant and

electrolyte, NaCl-1-octanol mixture. The available mass transfer correlations are implemented into the bubble tracking method and the validity of the correlation is examined. The predicted and measured spatial evolutions are compared.

4. In Chapter 4, the applicability of enhancement factor proposed in Chapter 2 to bubbly flows is validated through comparison with experimental results. The E correlation is implemented into the bubble tracking method together with available mass transfer correlations for a clean system. The flow patterns, mean void fraction, and bubble diameter distributions are measured and compared with numerical predictions.
5. Chapter 5 concludes the overall achievements obtained in this research.

References

[1] T. Kajishima, T. Saito, R. Nagaosa, S. Kosugi, "A gas-lift method for CO_2 disposal into the ocean," *Energy*, vol. 22, no. 2-3, pp. 257–262, 1997, doi: 10.1016/S0360-5442(96)00125-9.

[2] M. K. Mondal, H. K. Balsora, and P. Varshney, "Progress and trends in CO_2 capture/separation technologies: A review," *Energy*, vol. 46, no. 1, pp. 431–441, 2012, doi: 10.1016/j.energy.2012.08.006.

[3] J. G. Shim, D. W. Lee, J. H. Lee, and N. S. Kwak, "Experimental study on capture of carbon dioxide and production of sodium bicarbonate from sodium hydroxide," *Environmental Engineering Research*, vol. 21, no. 3, pp. 297–303, 2016, doi: 10.4491/eer.2016.042.

[4] Y. Peng, B. Zhao, and L. Li, "Advance in Post-Combustion CO_2 Capture with Alkaline Solution: A Brief Review," *Energy Procedia*, vol. 12, no. 2012, pp. 1515–1522, 2012, doi: 10.1016/j.egypro.2011.12.1126.

[5] P. V. Danckwerts, *Gas-Liquid Reactions*. New York: McGraw-Hill, 1970.

[6] C. Fleischer, S. Becker, and G. Eigenberger, "Detailed modeling of the chemisorption of CO_2 into NaOH in a bubble column," *Chem Eng Sci*, vol. 51, no. 10, pp. 1715–1724, 1996, doi: 10.1016/0009-2509(96)00030-9.

[7] T. Schulzke, S. Schlüter, and P. M. Weinspach, "Experimental studies and simulation of the dynamic behaviour of bubble column reactors," *Comput Chem Eng*, vol. 22, no. SUPPL.1, pp. S667–S670, 1998, doi: 10.1016/s0098-1354(98)00120-3.

[8] D. Darmana, N. G. Deen, and J. A. M. Kuipers, "Detailed modeling of hydrodynamics, mass transfer and chemical reactions in a bubble column using a discrete bubble model," *Chem Eng Sci*, vol. 60, no. 12, pp. 3383–3404, 2005, doi: 10.1016/j.ces.2005.01.025.

[9] D. Darmana, R. L. B. Henket, N. G. Deen, and J. A. M. Kuipers, "Detailed modelling of hydrodynamics, mass transfer and chemical reactions in a bubble column using a discrete bubble model: Chemisorption of CO_2 into NaOH solution, numerical and experimental study," *Chemical Engineering Science*, vol. 62, no. 9. pp. 2556–2575, 2007. doi: 10.1016/j.ces.2007.01.065.

[10] K. T. Sujatha, D. Jain, S. Kamath, J. A. M. Kuipers, and N. G. Deen, "Experimental and numerical investigation of a micro-structured bubble column with chemisorption," *Chem Eng Sci*, vol. 169, pp. 225–234, 2017, doi: 10.1016/j.ces.2016.12.035.

[11] M. Krauβ and R. Rzehak, "Reactive absorption of CO_2 in NaOH: Detailed study of enhancement factor models," *Chem Eng Sci*, vol. 166, pp. 193–209, 2017, doi: 10.1016/j.ces.2017.03.029.

[12] M. Krauß and R. Rzehak, "Reactive absorption of CO_2 in NaOH: An Euler-Euler simulation study," *Chem Eng Sci*, vol. 181, pp. 199–214, 2018, doi: 10.1016/j.ces.2018.01.009.

[13] H. Hikita, S. Asai, and T. Takatsuka, “Gas absorption with a two-step instantaneous chemical reaction,” *The Chemical Engineering Journal*, vol. 4, no. 1, pp. 31–40, 1972, doi: 10.1016/0300-9467(72)80050-9.

[14] W. J. DeCoursey, “Absorption with chemical reaction: development of a new relation for the Danckwerts model,” *Chem Eng Sci*, vol. 29, no. 9, pp. 1867–1872, 1974, doi: 10.1016/0009-2509(74)85003-7.

[15] D. W. van Krevelen and P. J. Hoftijzer, “Kinetics of gas-liquid reactions part I. General theory,” *Recueil des Travaux Chimiques des Pays-Bas*, vol. 67, no. 7, pp. 563–586, 1948, doi: 10.1002/recl.19480670708.

[16] H. Hikita and S. Asai, “Gas absorption with a two-step chemical reaction,” *The Chemical Engineering Journal*, vol. 11, no. 2, pp. 123–129, 1976, doi: 10.1016/S0300-9467(76)80034-2.

[17] T. Madhavi, A. K. Golder, A. N. Samanta, and S. Ray, “Studies on bubble dynamics with mass transfer,” *Chemical Engineering Journal*, vol. 128, no. 2–3, pp. 95–104, 2007, doi: 10.1016/j.cej.2006.10.019.

[18] P. L. T. Brian, J. F. Hurley, and E. H. Hasseltine, “Penetration theory for gas absorption accompanied by a second order chemical reaction,” *AIChE Journal*, vol. 7, no. 2, pp. 226–231, 1961, doi: 10.1002/aic.690070212.

[19] H. W. Jia and P. Zhang, “Mass transfer of a rising spherical bubble in the contaminated solution with chemical reaction and volume change,” *Int J Heat Mass Transf*, vol. 110, pp. 43–57, 2017, doi: 10.1016/j.ijheatmasstransfer.2017.02.095.

[20] A. Kundu, J. K. Basu, and G. Das, “A novel gas-liquid contactor for chemisorption of CO_2,” *Sep Purif Technol*, vol. 94, pp. 115–123, 2012, doi: 10.1016/j.seppur.2011.11.016.

[21] R. Clift, J. R. Grace, and M. E. Weber, *Bubbles, Drops, and Particles*. New York: Academic Press, 1978.

[22] Y. Hori, K. Hayashi, S. Hosokawa, and A. Tomiyama, “Mass transfer from single carbon-dioxide bubbles in electrolyte aqueous solutions in vertical pipes,” *Int J Heat Mass Transf*, vol. 115, pp. 663–671, 2017, doi: 10.1016/j.ijheatmasstransfer.2017.07.087.

[23] J. Aoki, K. Hayashi, S. Hosokawa, and A. Tomiyama, “Effects of surfactants on mass transfer from single carbon dioxide bubbles in vertical pipes,” *Chem Eng Technol*, vol. 38, no. 11, pp. 1955–1964, 2015, doi: 10.1002/ceat.201500063.

[24] M. Filla, “Gas absorption from a slug held stationary in downflowing liquid,” *The Chemical Engineering Journal*, vol. 22, no. 3, pp. 213–220, 1981, doi: 10.1016/0300-9467(81)80016-0.

[25] Y. Nakahara and A. Tomiyama, “Shapes and Rising Velocities of Single Bubbles in Vertical Pipes,” *Trans. Jpn. Soc. Mech. Eng. B*, vol. 69, no. 685, pp. 2001–2009, 2003, doi: 10.1299/kikaib.69.2002.

[26] H. Tamai and A. Tomiyama, “Prediction of Undeveloped Bubbles and Slag Flows

Based on Three-Dimensional One-Way Bubble Tracking Method (1st Report, Model and Calculation Example, in Japanese)," *Transactions of the Japan Society of Mechanical Engineers (Part B)*, vol. 70, pp. 880–887, 2004.

[27] S. Abe, "Study on gas-liquid mass transfer in carbon dioxide-water bubble flow in vertical pipe (in Japanese)," Doctoral dissertation, Kobe University, 2009.

[28] Shogo Hosoda, "Study on Mass Transfer of Single Bubble in Vertical Circular Pipe (in Japanese)," Doctoral dissertation, Kobe University, 2015.

[29] Y. Hori, D. Bothe, K. Hayashi, S. Hosokawa, and A. Tomiyama, "Mass transfer from single carbon-dioxide bubbles in surfactant-electrolyte mixed aqueous solutions in vertical pipes," *International Journal of Multiphase Flow*, vol. 124, Mar. 2020, doi: 10.1016/j.ijmultiphaseflow.2020.103207.

[30] H. Tamai, "Prediction of gas-liquid two-phase bubble and slag flow in a vertical pipe based on three-dimensional one-way bubble tracking method (in Japanese)," Doctoral dissertation, Kobe University, 2002.

Chapter 2
Mass transfer with chemical absorption

2.1 Introduction

The mass transfer coefficients k_L of single carbon-dioxide bubbles with chemical absorption in a vertical pipe were examined in this section using aqueous sodium hydroxide solutions. The pH of the solution was varied from 12 to 13.15. The pipe diameter D was 12.5 mm. To accommodate a wide range of bubble shapes, the bubble diameter d was verified for $0.4 < d/D < 1.4$. Measured mass transfer coefficients were used to obtain the enhancement factor defined by

$$E = \frac{k_L}{k_L^0} \simeq \frac{Sh}{Sh^0} \qquad (2.1)$$

where k_L and k_L^0 are the mass transfer coefficients with and without chemical absorption, respectively, and Sh and Sh^0 are the Sherwood numbers with and without chemical absorption. Then, an empirical E correlation was developed to account for the effects of bubble size and NaOH concentration on mass transfer. The applicability of the correlation was verified through the experimental results of larger pipe diameter (D = 18.2 mm).

2.2 Experiment and measurement method

2.2.1 Gas and liquid properties

The concentration of aqueous sodium hydroxide solutions has a noticeable impact on the physical properties of gas and liquid phases as shown in Table 2.1. A standard hydrometer (JIS B-1525) was used to determine the liquid density, ρ_L. The liquid viscosity, μ_L, was measured using a tuning fork vibrating viscometer (A&D, SV-A10). The pendant bubble method [1] was used to measure surface tension, σ.

Table 2.1 Gas and liquid properties (T = 298 K, $P \simeq$ 1 atm)

$[OH^-]$ [mol/L]	pH	Liquid phase			Gas phase	
		ρ_L [kg/m^3]	μ_L [10^{-3} Pa·s]	σ [N/m]	D_{CO2} [10^{-9}m^2/s]	C_{sat} [mol/m^3]
10^{-7} (water)	7	997	0.89	0.072	1.92[2]	34.0[3]
0.01	12	998	0.89	0.071	1.92	33.9
0.018	12.25	998	0.90	0.071	1.92	33.8
0.032	12.5	999	0.90	0.071	1.92	33.6
0.063	12.8	1000	0.90	0.070	1.91	33.2
0.08	12.9	1001	0.91	0.070	1.91	33.0
0.1	13	1001	0.91	0.069	1.90	32.7
0.14	13.15	1003	0.92	0.068	1.90	32.2

Himmelblau [2] and van Krevelen and Hoftijzer [3] provided the diffusion coefficient, D_{CO_2}, and the saturated concentration, C_{sat}, of CO_2 in clean water. The D_{CO_2} in NaOH solution was calculated using [4]:

$$D_{CO_2} = D^0_{CO_2}(1 + 0.624\sum_{i=1}^{m} b_i c_i) \quad (2.2)$$

$$D^0_{CO_2} = 2.35 \times 10^{-6} \exp\left(\frac{-2119}{T}\right) \quad (2.3)$$

$$c_i = n_i c_s \quad (2.4)$$

where $D^0_{CO_2}$ is the diffusion coefficient of CO_2 in water [5] . The constants b_i are given in Table 2.2, c_i [kmol/m^3] is the concentration of ion and m is the total number of ions. The n_i and c_s [kmol/m^3] are the number of ions and the concentration of solution, respectively. The T is temperature in Kelvin.

The presence of reactive ions affects the saturated concentration, C_{sat}, and the Henry constant, H_{CO_2}, which can be calculated as [6] :

$$\log_{10}\left(\frac{C_{sat}}{C_{sat}^0}\right) = \log_{10}\left(\frac{H_{CO_2}^0}{H_{CO_2}}\right) = -\sum_{i=1}^{m}(h_i + h_G)c_i \quad (2.5)$$

$$H_{CO_2}^0 = \frac{1}{3.54 \times 10^{-7}\exp(2044/T)}\frac{\rho_{H2O}}{M_{H2O}} \quad (2.6)$$

$$h_G = h_G^0 + h_T(T - 298.15) \quad (2.7)$$

where C_{sat}^0 and $H_{CO_2}^0$ are the saturated concentration and the Henry constant of CO_2 in clean water, h_i and h_G are ion-specific and gas-specific parameters, respectively, h_G^0 is the gas-specific parameter for pure gas, and h_T is the gas-specific parameter for the temperature effect. The parameters in Eqs. (2.5) and (2.7) are summarized in Table 2.2. The $H_{CO_2}^0$[Pa] is calculated as a function of temperature [5], ρ_{H2O} and M_{H2O}, i.e., the water density (997 kg/m^3) and its molar mass (18 g/mol). Uncertainties in D_{CO_2} and C_{sat} estimated at 95% confidence were $\pm$0.28% and $\pm$0.42%, respectively.

Table 2.2 Parameters in Eqs. (2.2), (2.5) and (2.7)

Ion	b_i [m^3/kmol][4]	h_i [m^3/kmol][6]	Gas	$h_G{}^0$ [m^3/kmol][6]	h_T [m^3/(kmol·K)][6]
Na^+	- 0.0857	0.1143	CO_2	- 0.0172	- 0.338 x 10 $^{-3}$
OH^-	- 0.1088	0.0839			

2.2.2 Experimental setup

Fig. 2.1 illustrates the experimental setup. The apparatus used to make the aqueous sodium hydroxide solution consisted of the glove box, the water tank, and the vacuum pump, which were all integrated within the stirrer. NaOH granules (Fuji Film Wako Pure Chemical, 1310-73-2) were originally weighed to a predetermined quantity in the glove box. The stirrer was then used to thoroughly mix the purewater (Millipore, Elix Essential UV5) from the tank

and the NaOH granules. The concentration of the solution was checked using a pH-meter (TOA DKK, HDM-136A) with uncertainties ± 0.03. Argon was used as a purge gas in the tank and glove box to prevent NaOH from reacting with CO_2 in the atmosphere.

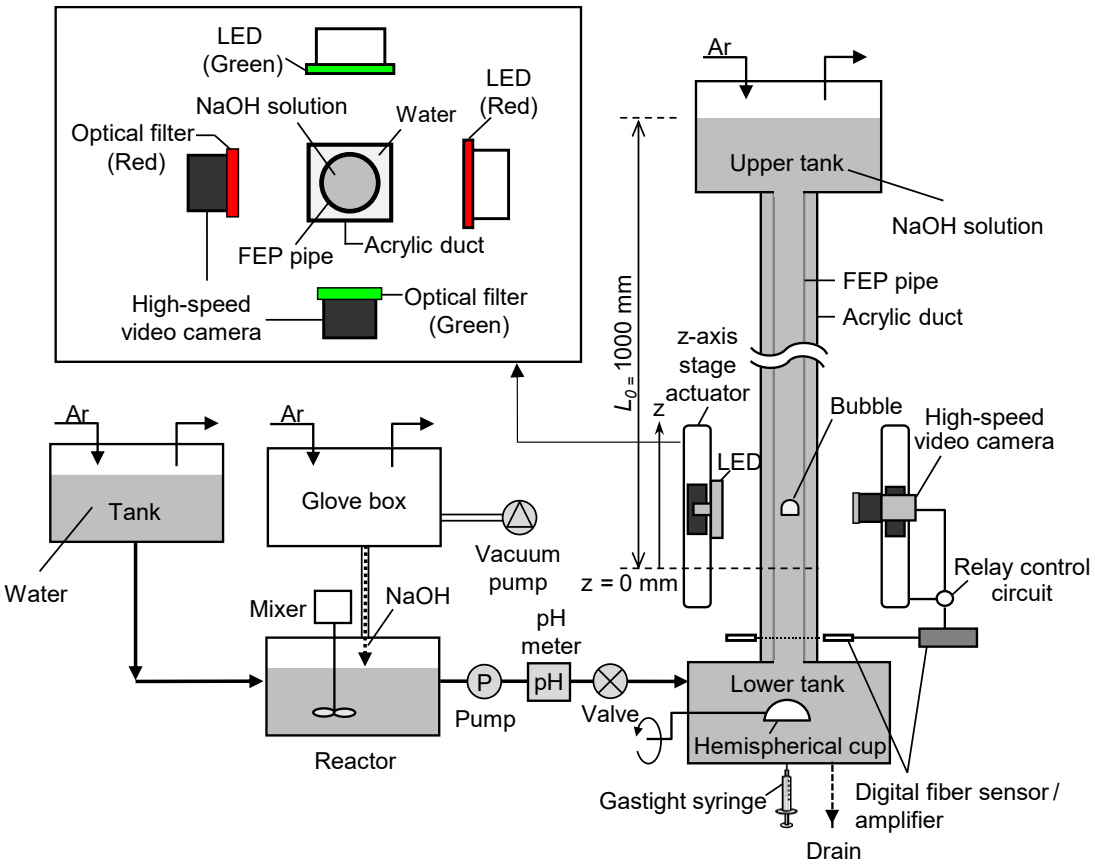

Fig. 2.1 Experimental setup

The test section consists of the lower tank, circular pipe, acrylic duct, upper tank, pump, high-speed video cameras with optical filters, z-axis stage actuators, fiber sensor, and LED lighting. Fluorinated ethylene propylene (FEP) resin was used as the material of the 12.5 mm inner diameter circular pipe. The FEP pipe was inserted in the acrylic duct, and water was used to fill the space between the pipe and the duct. Due to the fact that the refractive indices of water and FEP resin are almost identical, 1.333 and 1.338 respectively, it is feasible to capture bubble images without optical distortion. The water in the gap was circulated through a water bath that was adjusted to 298 K. All tests were performed at room temperature and atmospheric pressure (T = 298 K and P ≃ 1 atm, respectively).

CO_2 gas (Sumitomo Seika, purity 99.9 vol%) injected from the bottom of the lower tank was kept in the hemispherical cup using the gastight syringe and then released by spinning the cup. Using two synchronized video cameras, images of a bubble in the pipe were captured from the front and sides. For back illumination, the green and red LED light sources were utilized. Cameras and LED light sources were installed on the actuators, and their motions were synchronized. Bubbles were tracked from 0 to 400 mm along the z-axis by using a video camera with the following settings: 400 frames/s for frame rate and 0.04–0.05 mm/pixel for spatial resolution. After releasing no more than five small bubbles or three Taylor bubbles, the NaOH solution was refilled in order to prevent the change in NaOH concentration caused by the interaction with CO_2. In addition to neutralization, the test section and reactor were cleaned with pure water following the completion of the experiments, and k_L^0 of CO_2 in clean water was measured before the next set of experiments to confirm that all equipments were free of contamination.

2.2.3 Measurement method of bubble diameter and rising speed

Hosoda [7] applied image processing [8] to bubble images taken from two directions perpendicular to one another for bubbles of various shapes rising in a vertical pipe to obtain a sphere volume equivalent diameter (hereafter, referred to as bubble diameter) d [m] and the bubble rising velocity V_B [m/s]. The d and V_B of the target range were estimated in this investigation using their method. The image processing procedure is described below.

(1) Acquire front and side photos of bubbles simultaneously from two orthogonal directions using two high-speed video cameras (Fig 2.2(a)).
(2) Binarize the captured image and extract the contour of the bubble (Fig. 2.2(b)).
(3) Assuming that the bubble's horizontal cross-section is elliptical, the bubble is divided into an elliptic plate with a thickness of δ [m], represents the length of one bubble picture pixel. The lengths of the ellipsoid's major and minor axes are the horizontal lengths acquired from the bubble pictures (l_{Gi} [m] or l_{Ri} [m] in Fig. 2.2 (c)).
(4) Reconstruct the bubble shape by vertically stacking disassembled elliptical plates (Fig. 2.2(d)).
(5) Bubble volume Θ_B [m^3] and d are obtained by the following equations respectively.

$$\Theta_B = \sum_{i=1}^{N} \frac{\pi l_{Gi} l_{Ri} \delta}{4} \quad (2.8)$$

$$d = \left[\frac{6}{\pi}\Theta_B\right]^{1/3} \quad (2.9)$$

where N is the total number of elliptical plates stacked vertically.

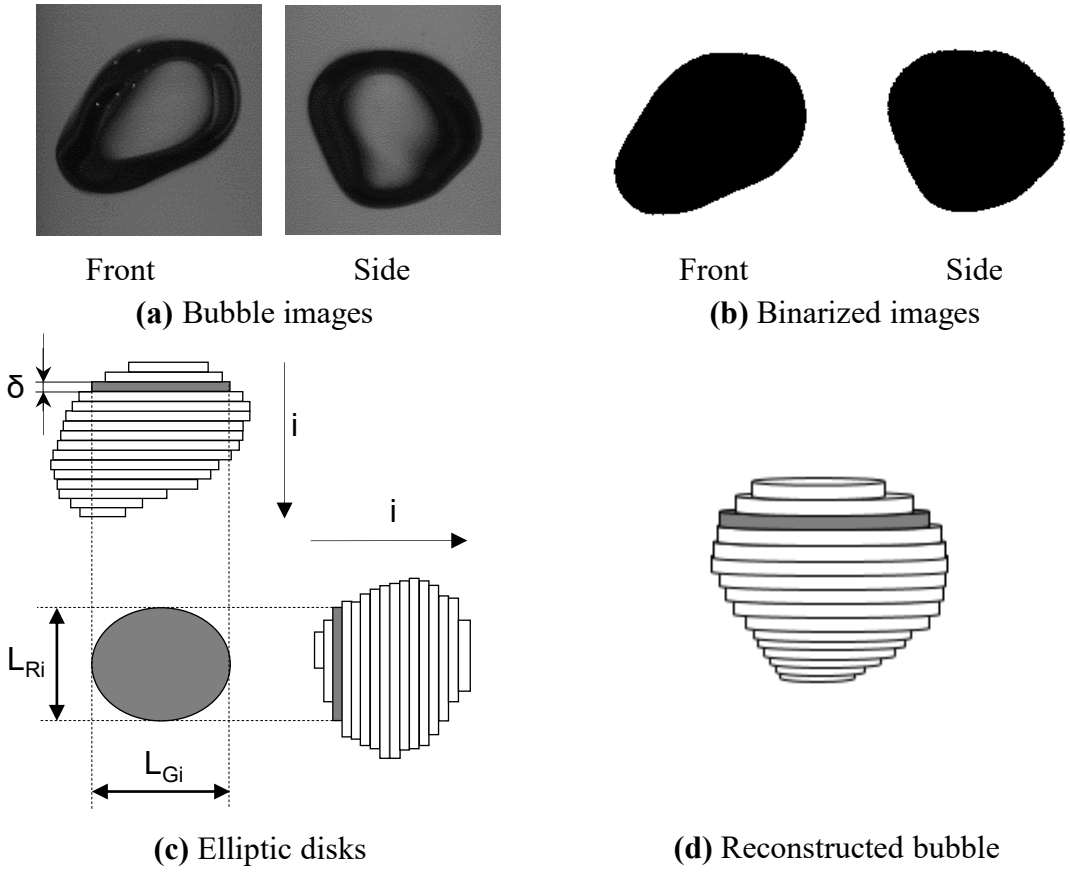

(a) Bubble images **(b)** Binarized images

(c) Elliptic disks **(d)** Reconstructed bubble

Fig. 2.2 Image processing procedure

This technique of image processing was validated by measuring the d of a single air bubble rising in a stationary liquid in a vertical pipe. In Fig. 2.3, the calculated bubble diameters using one-sided and two-sided images (method of image processing) are compared. The solid line on the graph represents an ellipsoidal air bubble in purewater system (D = 12.5 mm) with an initial bubble diameter d_{in} of 5.8 mm. The triangles and inverted triangles represented front and side single bubble images, whereas the circles symbolize the image processing method that includes two-side images. The calculation begins at 0 seconds (τ = 0 s), as shown by the

horizontal axis. Compared with the solid line, the *d* calculated from bubble images taken from two directions is more accurate than the d taken from one direction.

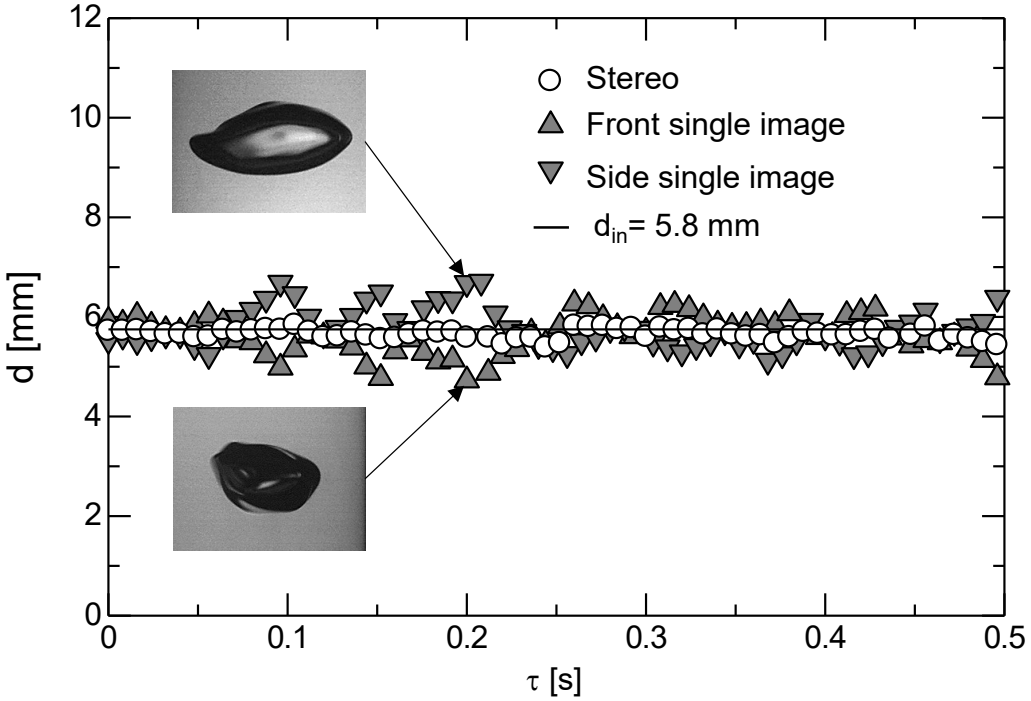

Fig. 2.3 Measured diameter of air bubble in pure water

The time variation of the vertical coordinate z_B [m] of a CO_2 bubble (d_{in} = 8.3 mm) rising in a stationary liquid in a pipe is shown in Fig. 2.4. For Taylor bubbles, the coordinates of the bubble tip are used, and for bubbles smaller than Taylor bubbles, the coordinates of the center of gravity are used as z_B because the shape of the bubble changes with time. The center-of-gravity coordinate is obtained by the following equation

$$\frac{\pi d^3}{6} z_B = \sum_{i=1}^{N} \left(\frac{\pi l_{Gi} l_{Ri} \delta}{4} \right) z_i \qquad (2.10)$$

Using the least-squares method, the linear interpolation equation for the time variation of z_B was produced, and the slope of the equation was determined to be V_B.

Since the present experiments dealt with dissolving CO_2 bubbles with volume change, it was difficult to directly estimate the uncertainties in d and V_B. Hosoda et al. [7] obtained experimental data of d and V_B for 250 air bubbles rising through clean water in the range of 5

$\leq d \leq$ 25 mm in vertical pipes of D = 12.5, 18.2 and 25.0 mm and showed that the uncertainties in d and V_B estimated at 95% confidence were $\pm$2.1% and $\pm$0.2%, respectively. The present experiment adopted the same method verified by Hosoda et al. for the camera settings such as the spatial resolution of images and the light sources; that is, the uncertainties in d and V in the present experiments are regarded as the same degree as those in their experiments.

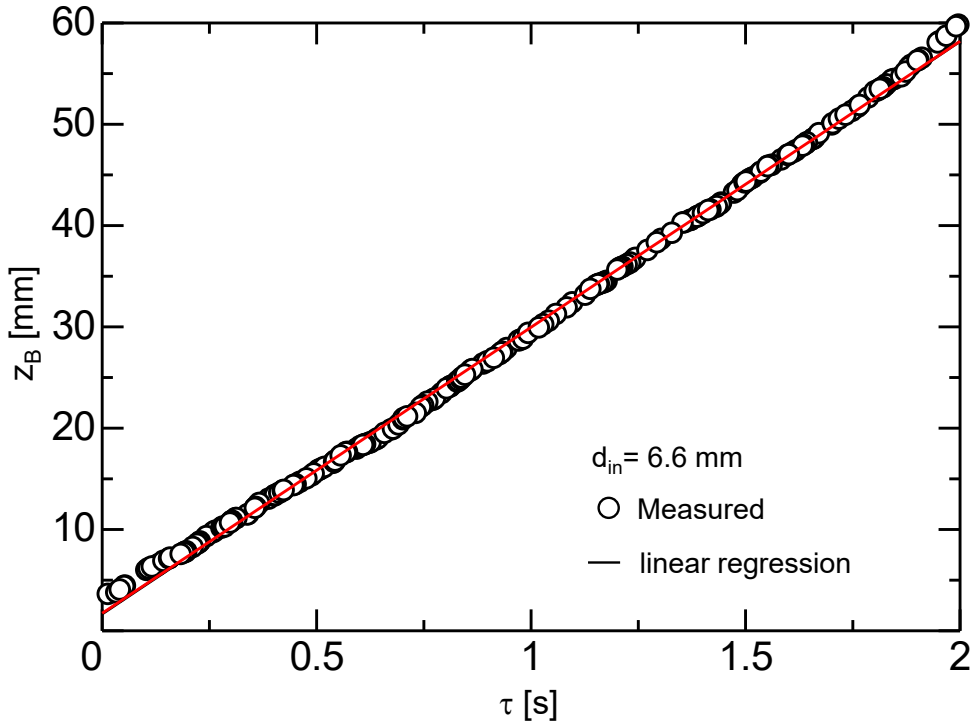

Fig. 2.4 Measured axial position of CO_2 bubble in pure water

2.2.4 Mass transfer coefficient calculation method

The rate of decrease in d was utilized to evaluate k_L and Sh. The rate of change in CO_2 moles inside a bubble is given by

$$\frac{\mathrm{d}n}{\mathrm{d}t} = -k_L A_B (C_{int} - C_0) \qquad (2.11)$$

where n is the moles, t is the time, A_B (= πd^2) is the bubble surface area, C_0 is the CO_2 concentration in the liquid phase, and C_{int} is the concentration of CO_2 at the bubble interface. The C_0 in Eq. (2.11) can be neglected since the concentration of CO_2 in the liquid phase is much smaller than C_{int} which is calculated by Henry's law:

$$P(z)X = \frac{C_{int}}{C_{int} + C_V} H_{CO_2} \quad (2.12)$$

where $P(z)$ is the pressure inside a bubble, X is the mole fraction of CO_2 in the gas phase, which is assumed to be unity, and C_V is the molar concentration of water in the solution (55.4 kmol/m^3). The $P(z)$is calculated by

$$P(z) = P_{atm} + \rho_L g(L_0 - z) + \frac{4\sigma}{d} \quad (2.13)$$

where P_{atm} is the atmospheric pressure, g is the acceleration of gravity, and the surface tension effect in P in the third term is very small and was neglected in Eq. (2.13). Substituting Eq. (2.12) into Eq. (2.11) yields

$$k_L = -\frac{1}{\pi d^2} \frac{H_{CO2} - P(z)}{C_V P(z)} \frac{\mathrm{d}n}{\mathrm{d}t} \quad (2.14)$$

The dn/dt can be expressed as the following equation by assuming that CO_2 is an ideal gas:

$$\frac{\mathrm{d}n}{\mathrm{d}t} = \frac{\pi}{6RT} \frac{\mathrm{d}(P(z)d^3)}{\mathrm{d}t} \quad (2.15)$$

where R is the universal gas constant. The $\mathrm{d}(P(z)d^3)/\mathrm{d}t$ was evaluated as

$$\frac{\mathrm{d}(P(z)d^3)}{\mathrm{d}t} = -\frac{P_2 d_2^3 - P_1 d_1^3}{t_2 - t_1} \quad (2.16)$$

where the subscripts 1 and 2 represent the start and end time of a recording period of a single bubble, respectively.

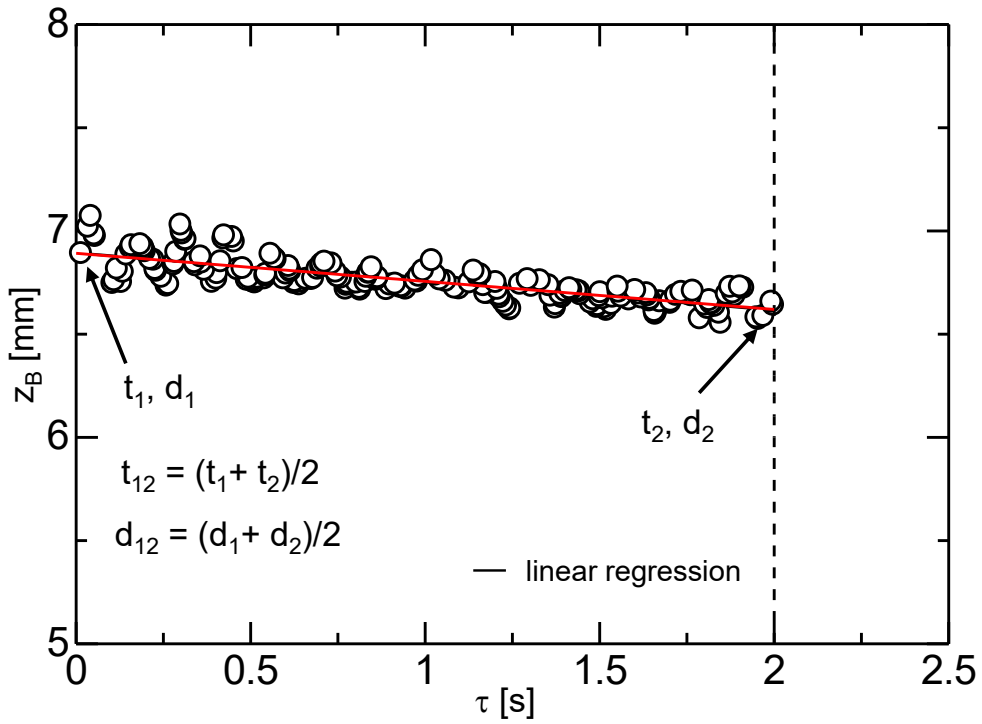

Fig. 2.5 Measured diameter of CO_2 bubble in pure water

The mass transfer coefficient can be evaluated by the following equation:

$$k_L = \frac{(H_{CO2} - P_{12})(P_2 d_2^3 - P_1 d_1^3)}{6RT(t_2 - t_1)d_{12}^2 C_V P_{12}} \quad (2.17)$$

where the subscript 12 represents the mean value between t_1 and t_2, i.e. $P_{12} = (P_1 + P_2)/2$ and $d_{12} = (d_1 + d_2)/2$ as shown in Fig. 2.5.

2.3 Mass transfer of a single bubble in an aqueous sodium hydroxide solution in a vertical pipe

2.3.1 Bubble shape and velocity

In the experiments, d ranged from 5 to 17 mm, and therefore, the range of the diameter ratio, λ (= d/D), was from 0.4 to 1.4. The shapes of CO_2 bubbles in water and in the NaOH solution at pH = 13 are compared in Fig. 2.6. Regardless of the presence of NaOH, ellipsoidal bubbles (Fig. 2.6 (a)) showed shape fluctuation and wobbling motion. At the interface of semi-Taylor bubbles of $\lambda = 0.75$, capillary waves are seen under both conditions (Fig. 2.6 (b)). In the

Taylor bubbles of a larger λ (=1.2), capillary waves are more clearly seen in the tail region. Figure 2.6 (c) confirms that the presence of NaOH in the solution had no effect on the shapes of Taylor bubbles.

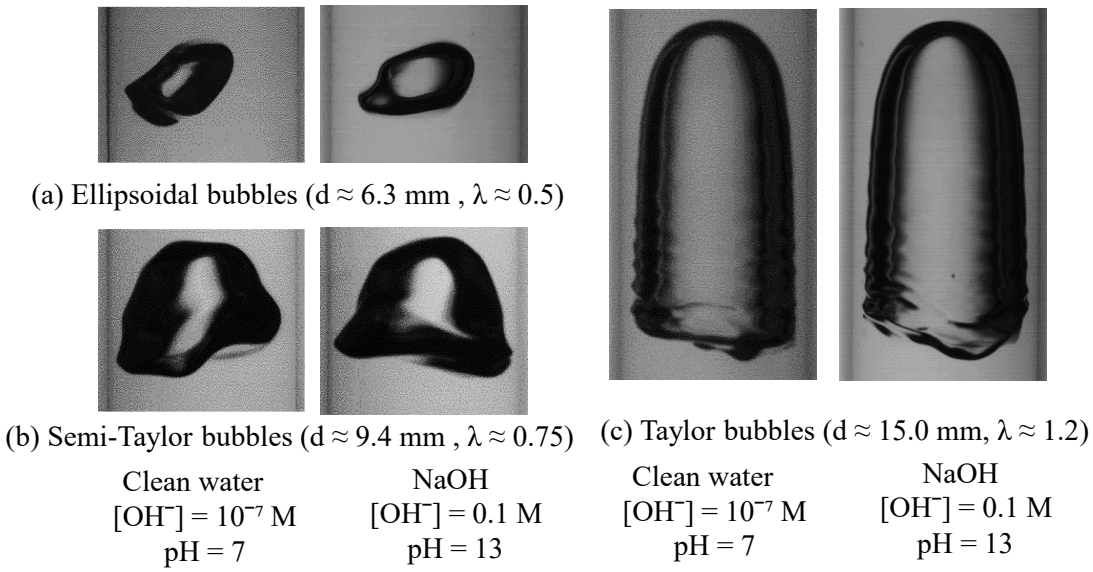

Fig. 2.6 Shapes and rise velocities of bubbles

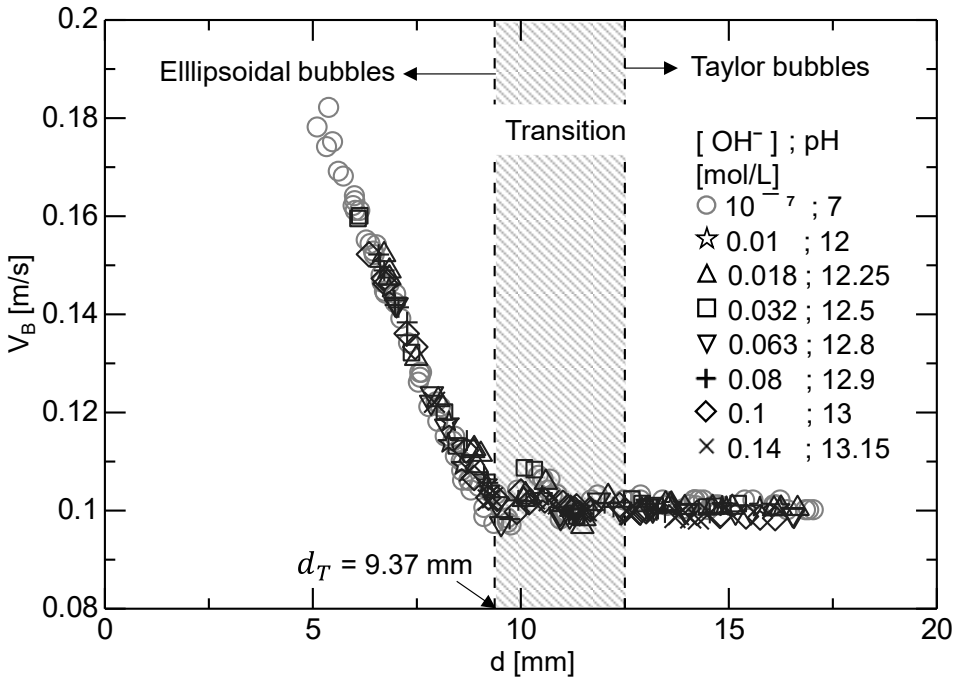

Fig. 2.7 Rise velocities of bubbles

The bubble velocities are shown in Fig. 2.7 which classified into three regimes: ellipsoidal, transition, and Taylor bubble regimes. As d increases, the bubble shape in the transition regime changes from ellipsoidal to Taylor bubble or so-called semi-Taylor bubble. The bubble diameter at the transition from ellipsoidal to semi-Taylor bubbles [9] is shown by d_T in the figure. Due to the wall effect, V_B in the ellipsoidal bubble regime decreases as d increases, but V_B in the Taylor bubble regime is independent of d. In the transition regime, there is a complicated relationship between V_B and d. The presence of NaOH had no effect on V_B under all conditions. Therefore, the behavior of bubbles at the current concentrations of aqueous NaOH solutions is comparable to that of bubbles in pure water.

2.3.2 Mass transfer coefficient and enhancement factor

Fig. 2.8 shows the mass transfer coefficients against the bubble diameter. The k_L of ellipsoidal bubbles in clean water (pH = 7) decreases with increasing d, while k_L is nearly constant in the Taylor bubble regime. The k_L at pH = 12 are identical to those at pH = 7, indicating that for pH $\leq$ 12, physical absorption continues to outweigh chemical absorption. While k_L of semi-Taylor and Taylor bubbles at pH = 12.25 is slightly larger than at pH = 12, the ellipsoidal bubbles at pH = 12.25 also have k_L similar to those at pH = 7. When pH is raised above 12.25, the data for k_L in aqueous NaOH solutions increases as pH increases.

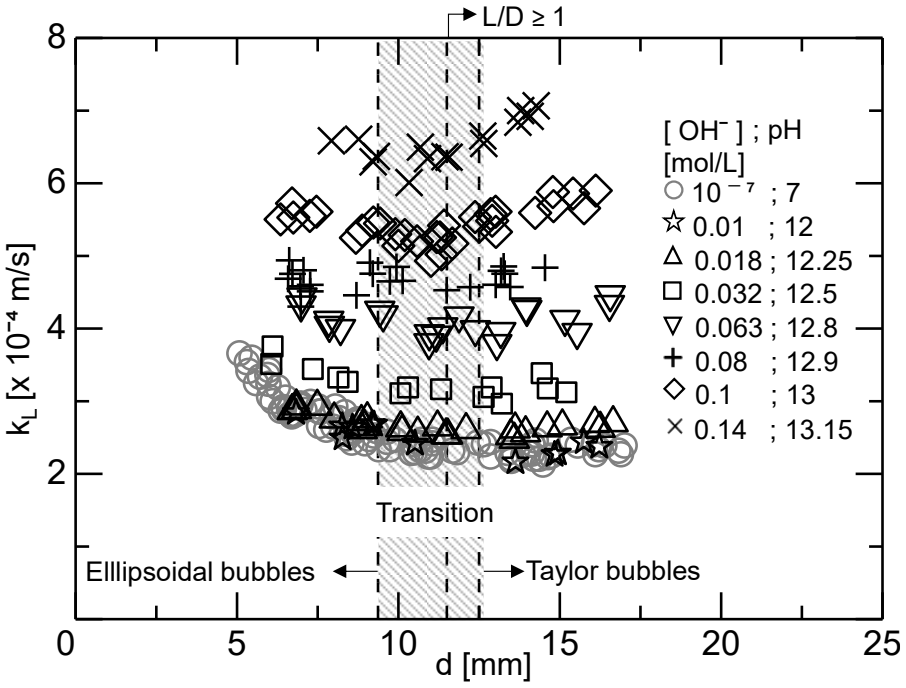

Fig. 2.8 Mass transfer coefficients of bubbles

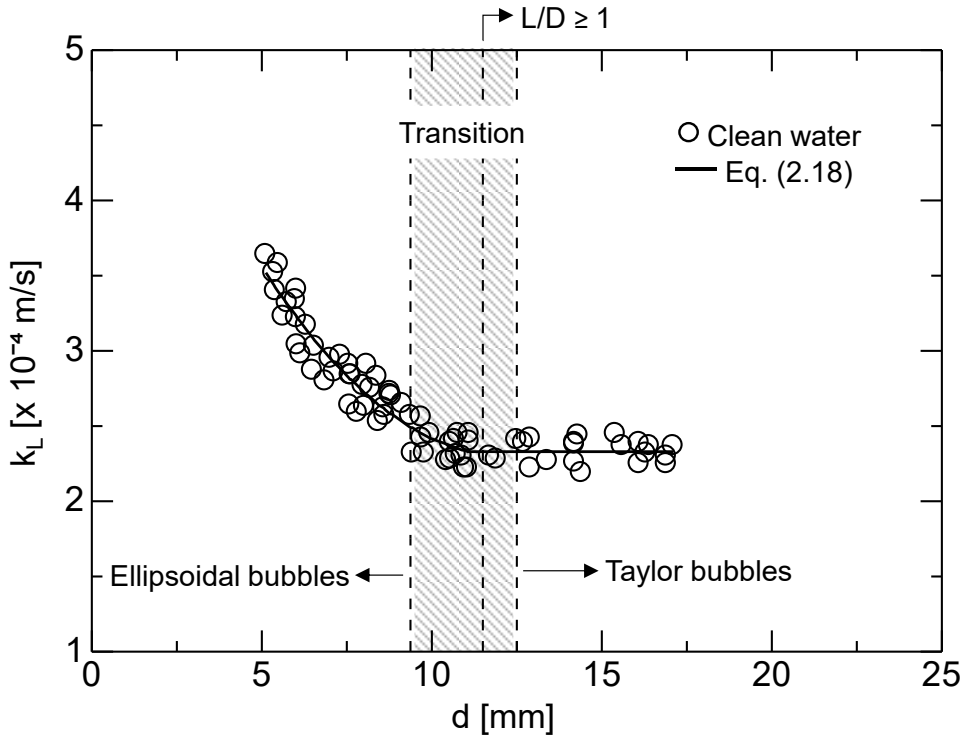

Fig. 2.9 Fitting equations of k_L^0 (D = 12.5 mm)

The enhancement factor E was calculated using k_L of bubbles in the NaOH solution and clean water. Since it was difficult to obtain data for the exactly same bubble diameter for both k_L and k_L^0, a fitting equation for k_L^0 was created using the least-square method (Fig. 2.9). For $L/D < 1$, a parabolic curve is fitted, and for $L/D \geq 1$, a constant value is preferred. The equations are then written as

$$k_L^0 = \begin{cases} 2.45d^2 - 0.06d + 6 \times 10^{-4} & \text{for } L/D < 1 \\ 2.33 \times 10^{-9} & \text{for } L/D \geq 1 \end{cases} \quad (2.18)$$

where it is assumed that the constants have the proper units in order to make [m/s] the unit of each term. A maximum deviation of 7.75% exists between the equations and the experimental data.

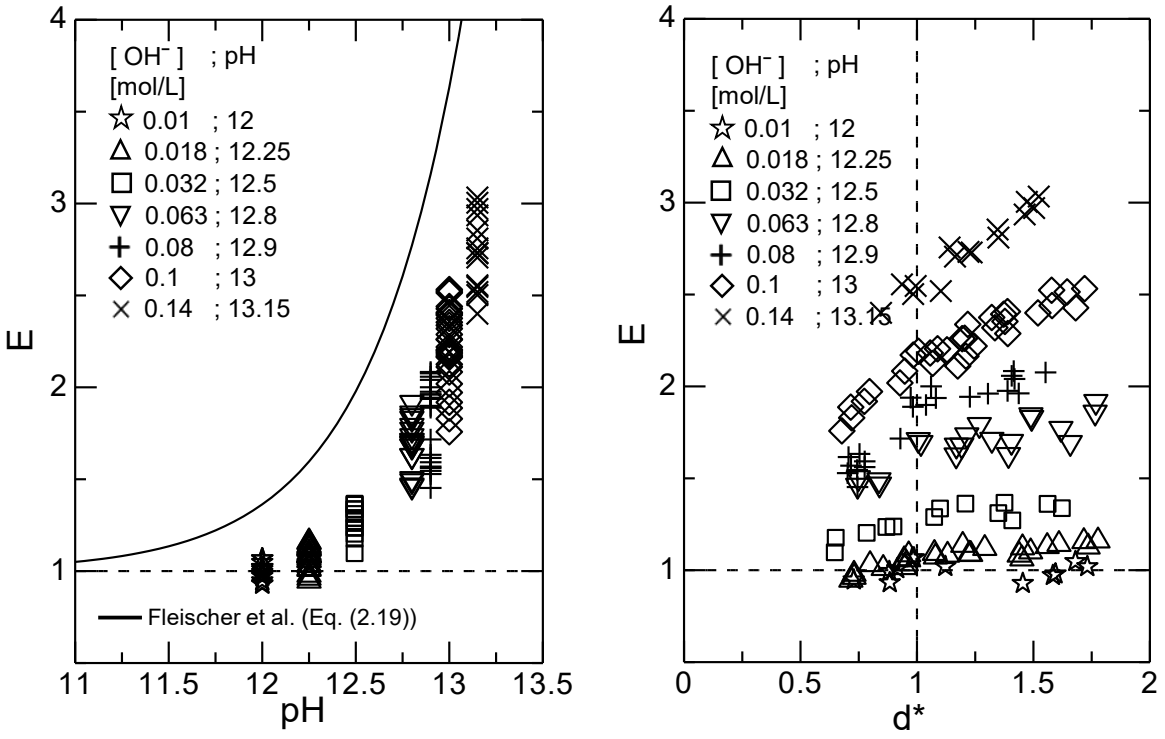

Enhancement factor for each pH (b) Enhancement factor for each d^*

Fig. 2.10 Enhancement factor

In Fig. 2.10(a), the solid line represents E as predicted by Fleischer [10] which is extracted from the two-film theory for a flat interface:

$$E = 1 + 7x10^{-7}\exp\left(1.98\,\mathrm{pH} - 10.6\right) \qquad (2.19)$$

The measured E at pH = 12 is nearly one, which is much less than the expected E (≈ 1.3). Both measured and predicted E show similar pH dependence, albeit measured E is much less than expected E. Fleischer's model is based on the two-film theory for flat surfaces. In addition, the flow at the interface and the oscillation of the interface that exists in reality are not taken into account. In the case of a bubble, oscillation and capillary wave would increase the diffusion of species at the interface during physical absorption, which contribute to the increase in k_L^0. In contrast, these phenomena do not exist at a flat surface. Therefore, k_L^0 is less for flat surfaces than for bubbles. The measured E of a bubble is thus less than Fleischer's E.

In Fig. 2.10(b), the measured E is plotted against d^*, the dimensionless bubble diameter $d^*=d/d_T$. E increases with increasing d^*. As presumed, the surface area of bubble increases with d^*. Considering physical absorption, dissolved CO_2 at the bubble front region in clean water flows down along the bubble interface and a thin concentration boundary layer of higher CO_2 concentration is formed [11] The development of the boundary layer, in other words, the attenuation of the concentration gradient at the interface, hinders CO_2 dissolution from the interface except for the front region of a bubble or the wake region where the vortex shedding facilitates the renewal of CO_2 concentration [12]. In NaOH solutions, the CO_2 concentration in the boundary layer is lower due to rapid chemical reaction of CO_2 molecules, which contributes to the increase in CO_2 dissolution [13].The mass transfer coefficient is thus enhanced with increasing the NaOH concentration and the bubble diameter. The increase rate of E with respect to d^* is not constant for all bubble shape regimes, i.e. the increase rate is larger for $d^* < 1$. As shown in Fig. 2.6(a), the transition of the shape from an ellipsoidal bubble to a semi-Taylor bubble evolves in both radial and axial directions, while that from a semi-Taylor bubble to a Taylor bubble evolves only in the axial direction. The larger increase rate of the interfacial area for $d^* < 1$, therefore, contributes to the larger increase rate of E on d^*.

Using nonlinear multiple regression, the following enhancement factor correlation was developed in terms of d^* and pH:

$$E = \begin{cases} 1 + \exp(2.98\ \mathrm{pH} + 1.04d^* - 39.7) & \text{for } d^* < 1 \\ 1 + \exp(2.69\ \mathrm{pH} + 0.40d^* - 35.3) & \text{for } 1 \le d^* < 1.8 \end{cases} \quad (2.20)$$

This correlation consists of two equations to take into account the change in the dependence on d^* at $d^* = 1$ shown in Fig. 2.10(b). Enhancement factors obtained using Eq. (2.20) are compared with the data in Fig. 2.11. The comparison showed good agreement, with 93% of the predicted E falling within 10% margins of error.

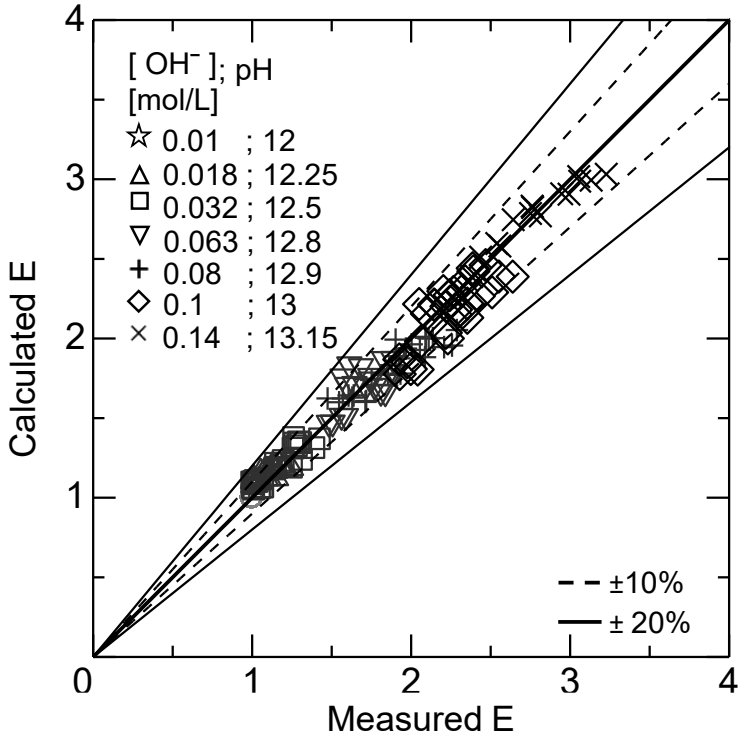

Fig. 2.11 Measured and calculated E using Eq. (2.20)

Sh was calculated from the measured k_L. For a spherical bubble, the *Sh* in clean water can be expressed as $Sh = \alpha Pe^{1/2}$ [14], where α is a bubble-shape dependent constant, *Sh* is defined by

$$Sh = \frac{k_L d}{D_{CO_2}} \qquad (2.21)$$

and *Pe* is the Peclet number defined by

$$Pe = \frac{V_B d}{D_{CO_2}} \qquad (2.22)$$

An empirical *Sh* correlation was proposed by Hosoda [7] for CO_2 bubbles in clean water. In this correlation, the constant α is expressed as a function of λ (= *d/D*). However, Hori et al. [15] found that α cannot be easily defined as α(λ), and instead, the expression d^* (= d/d_T) is more appropiate for α. This is due to the fact that d_T increases with decreasing *D*, which means that α does not always offer the same $Sh/Pe^{1/2}$ in the transition phase for pipes with

different diameters. As a result, Hori et al. presented the following correlation, which is applicable to ellipsoidal and semi-Taylor bubbles in water with $L/D < 1$:

$$Sh^0 = \begin{cases} \frac{2}{\sqrt{\pi}}\left(0.34\, d^{*2} + 0.28 d^* + 1\right)\sqrt{Pe} & \text{for } d^* < 1 \\ (0.18\, d^* + 1.6)\ \sqrt{Pe} & \text{for } d^* \geq 1 \end{cases} \qquad (2.23)$$

In Fig. 2.12, the observed $Sh/Pe^{1/2}$ of ellipsoidal and semi-Taylor bubbles for $L/D < 1$ are shown versus d^*. The data that were collected show that there is a rise in $Sh/Pe^{1/2}$ with an increase in pH. This indicates that there is an enhancement in mass transfer as a consequence of a chemical absorption. The values that were derived by applying Eqs. (2.1), (2.20) and (2.23) agree well with the data that were provided for each pH and d^*. Fig. 2.13 also shows a comparison between the calculated and measured Sh. 80% of the data are assessed with errors that are less than 10%.

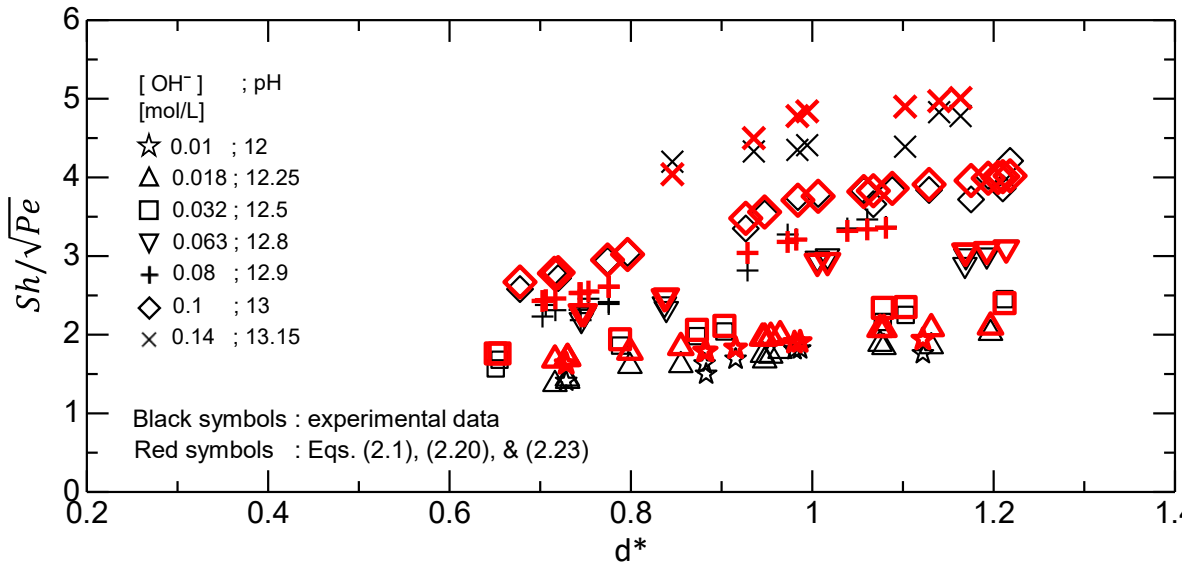

Fig. 2.12 $Sh/Pe^{1/2}$ vs. d^*

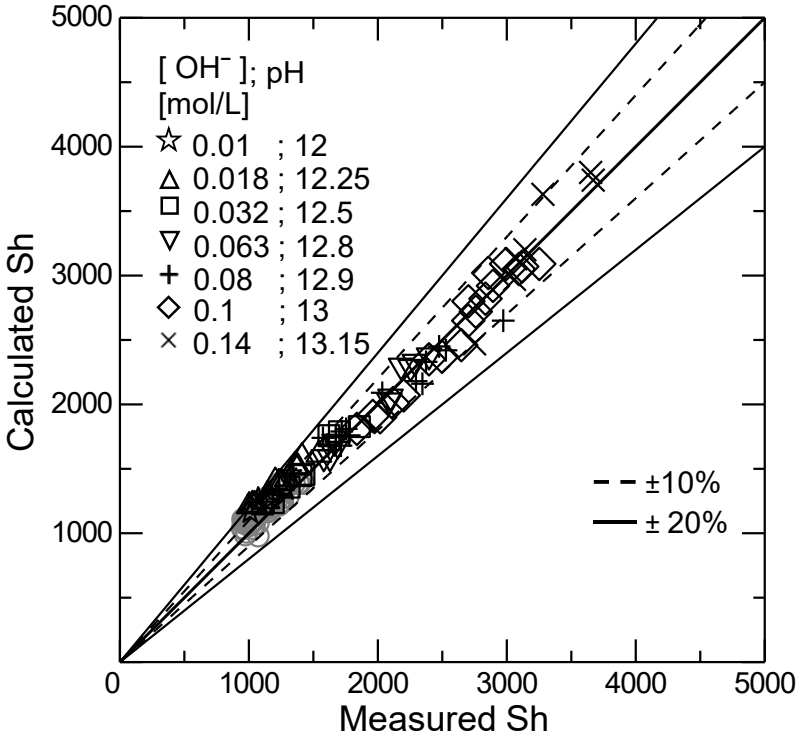

Fig. 2.13 Comparison between measured and calculated *Sh*

For Taylor bubbles with $L/D \geq 1$, the following Sherwood number correlation in clean water was proposed by Filla [16]:

$$Sh_D^0 = 5.1(L/D)^{0.8}\sqrt{Pe_D} \qquad (2.24)$$

where $Sh_D{}^0$ and Pe_D are the modified Sherwood number and the modified Peclet number defined by

$$Sh_D^0 = \frac{k_L A_B}{D_{CO_2} D} \qquad (2.25)$$

and

$$Pe_D = \frac{V_B D}{D_{CO_2}} \quad , \qquad (2.26)$$

respectively. The *L*/*D* can be evaluated by using the following correlation proposed by Nakahara and Tomiyama [17]:

$$L/D = (a_1 + 2a_2\lambda + 4a_3\lambda^2)\lambda \quad (2.27)$$

where the coefficients a_1, a_2 and a_3 are given by

$$\begin{aligned} a_1 &= \min\left(9.39 \times 10^{-5} Re_L + 0.586, 7.20 \times 10^{-6} Re_L + 0.722\right) \\ a_2 &= 5.93 \times 10^{-11} Re_L^2 + 5.95 \times 10^{-7} Re_L - 0.108 \\ a_3 &= -2.06 \times 10^{-7} Re_L + 0.211 \end{aligned} \quad (2.28)$$

Due to the fact that the liquid volumetric flux is zero in this experiment, the liquid Reynold number, denoted by the notation Re_L, is equal to zero. As a result, Eq. (2.27) is simplified to

$$L/D = (0.586 - 0.216\lambda + 0.844\lambda^2)\lambda \quad (2.29)$$

$Sh_D/Pe_D^{1/2}$ is shown against *L*/*D* for $L/D \geq 1$ in Fig. 2.14. $Sh_D/Pe_D^{1/2}$ values increase with increasing pH and *L*/*D*. Eq. (2.24) was coupled with Eq. (2.20) to evaluate the Sherwood number considering chemical absorption, Sh_D:

$$Sh_D = E\, Sh_D^0 \quad (2.30)$$

This equation well reproduces the dependence of $Sh_D/Pe_D^{1/2}$ on pH and *L*/*D* as shown in Fig. 2.15, where 74% of the data are within 10% error margins.

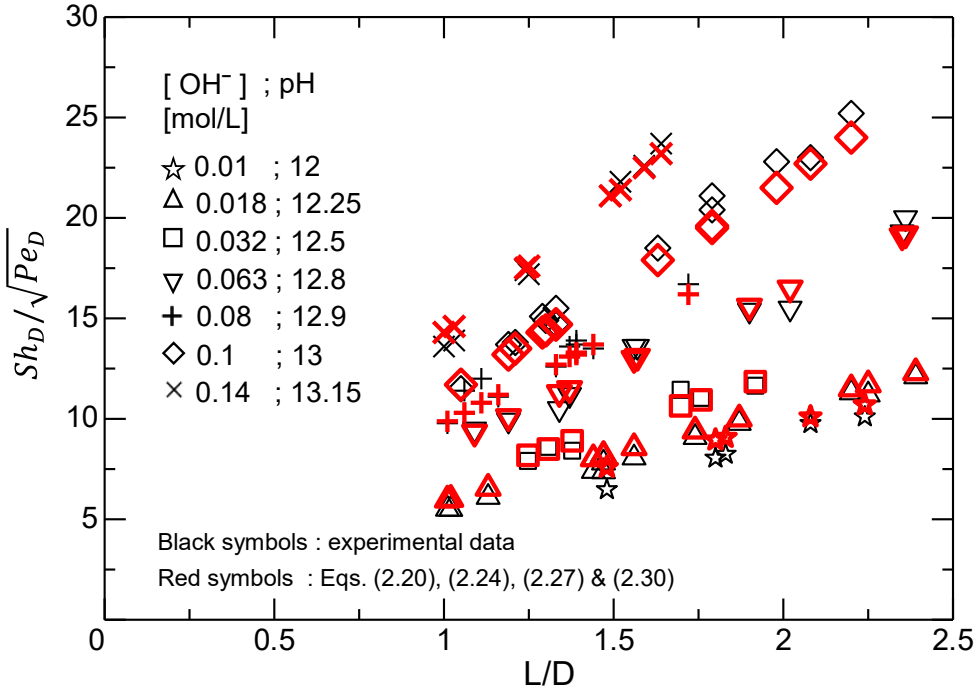

Fig. 2.14 $Sh_D/Pe_D^{1/2}$ vs. L/D

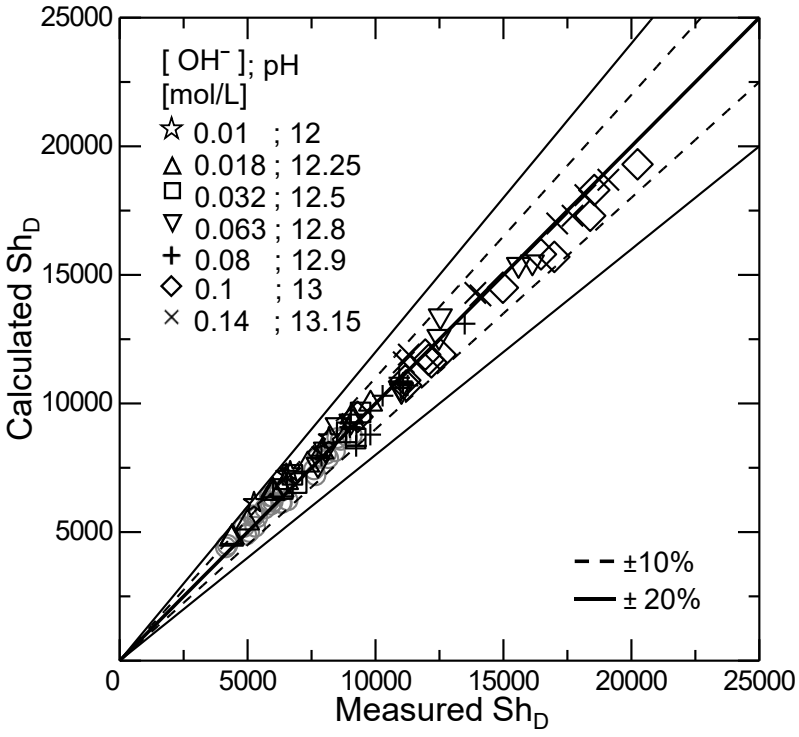

Fig. 2.15 Comparison between measured and calculated Sh_D

2.3.3 Applicability of enhancement factor correlation to bubbles in larger pipe diameter

Further observation of bubbles in three different NaOH concentrations in a pipe of D = 18.2 mm was carried out to confirm the applicability of Eq. (2.20), obtained for D = 12.5 mm, to the larger D. Fig. 2.16 shows that bubbles with pH = 12.5, 12.8 and 13 have the same V_B as pure water. The bubble velocity V_B is larger for D = 18.2 mm than D = 12.5 mm because λ are smaller. Fig. 2.17 shows the mass transfer coefficients for all bubbles in D = 18.2 mm. The amount of data for $L/D > 1$ is limited since it's difficult to generate large d bubbles in the cup during rapid dissolution, particularly at high pH. Chemical absorption boosts mass transfer at D = 12.5 mm, however k_L is nearly constant under the Taylor bubble regime D = 18.2 mm, even at high pH.

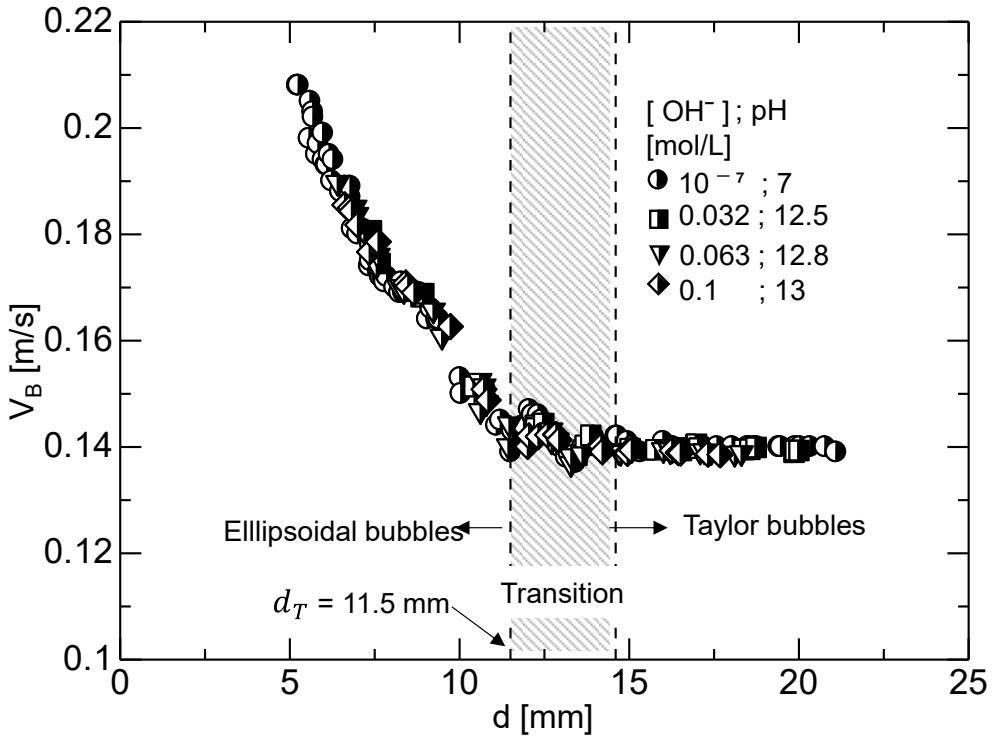

Fig. 2.16 Rise velocity of bubbles in D = 18.2 mm

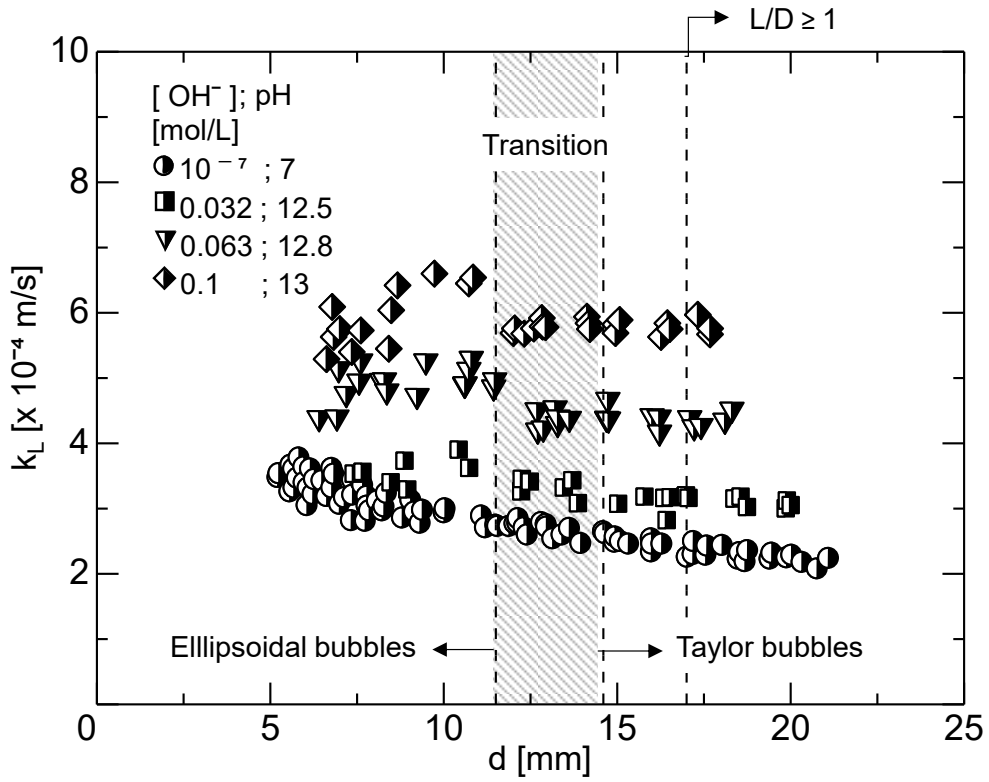

Fig. 2.17 Mass transfer coefficient of bubbles in D = 18.2mm

As in the bubbles in D = 12.5 mm, the enhancement factors of bubbles for D = 18.2 mm were calculated by comparing k_L in the NaOH solution with approximated k_L^0 which provided by using the least-squares method shown in Fig. 2.18. k_L^0 for D = 18.2 mm is fitted as

$$k_L^0 = 0.36d^2 - 0.017d + 4 \times 10^{-4} \quad (2.31)$$

The maximum deviation between the equation and the experimental data is 14%.

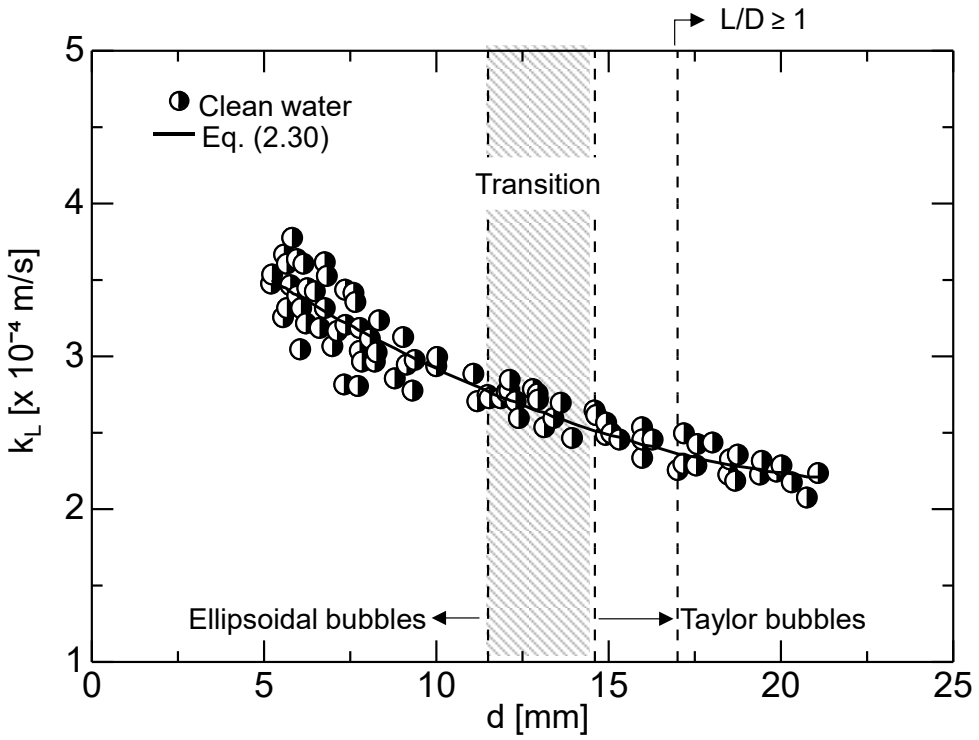

Fig. 2.18 Fitting equations of k_L^0 (D = 18.2 mm)

The fact that the measured E for D = 18.2 mm shown in Fig. 2.19 are almost the same as those for D = 18.2 mm suggests that the dependence of E on d is not affected by the pipe diameter. Due to the high Pe (3.6 x 10^5–1.4 x 10^6), the concentration boundary layer formed at the bubble interface is extremely thin. As a result, a change in D does not influence the mass transfer in the boundary layer, and the pH effect in Eq. (2.20) is valid for both D. Although the shape and motion of a bubble are both influenced by D, the dimensionless diameter d^* may be used to define both. Because of this, the term d^* in Eq. (2.20), which is supposed to represent the bubble size effect, works quite well. As can be seen in Fig. 2.20, the enhancement factor correlation yields a good agreement and 91% of the data for D = 18.2 mm are contained within an error range of ± 10%.

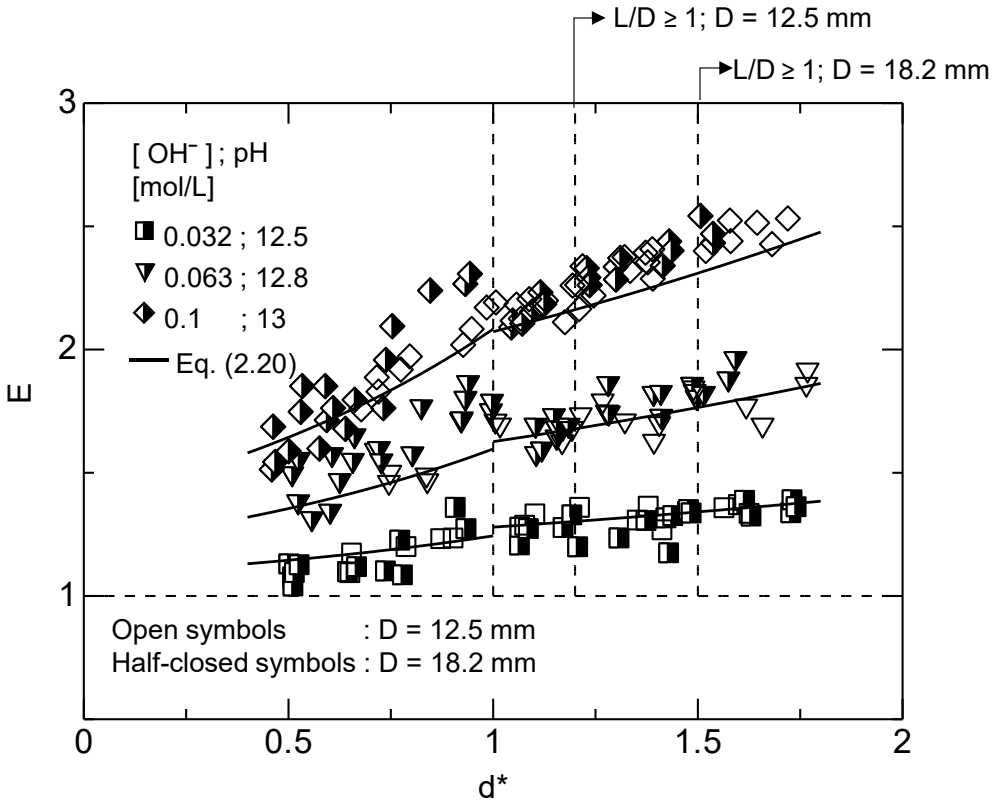

Fig. 2.19 Enhancement factor for each d^*

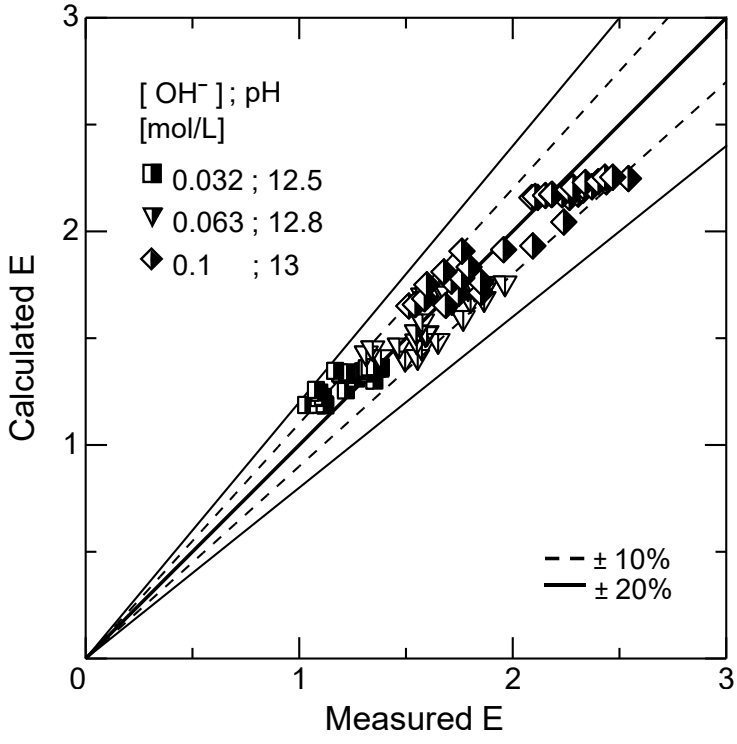

Fig. 2.20 Measured and calculated E in D = 12.5 and 18.2 mm

Comparison between the *Sh* correlation Eqs. (2.1), (2.20) and (2.23) and the data of *D* = 18.2 mm is shown in Fig. 2.21. The dependence of $Sh/Pe^{1/2}$ on *d** is well reproduced by the correlation. As shown in Fig. 2.22, the *Sh* correlation can evaluate 88% of the data with errors less than ±10%.

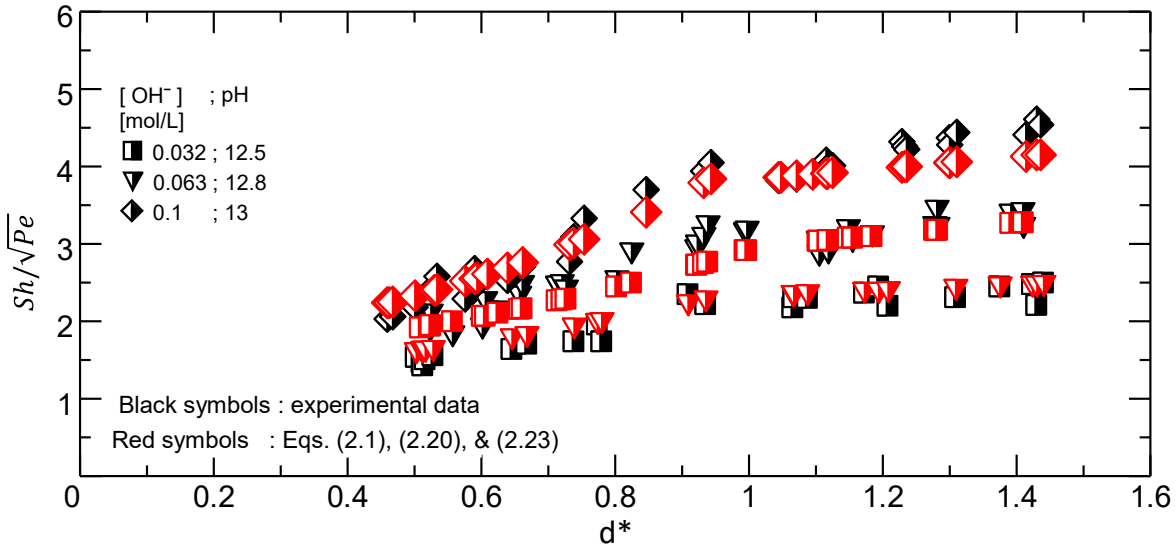

Fig. 2.21 $Sh/Pe^{1/2}$ vs. *d** (*D* = 18.2 mm)

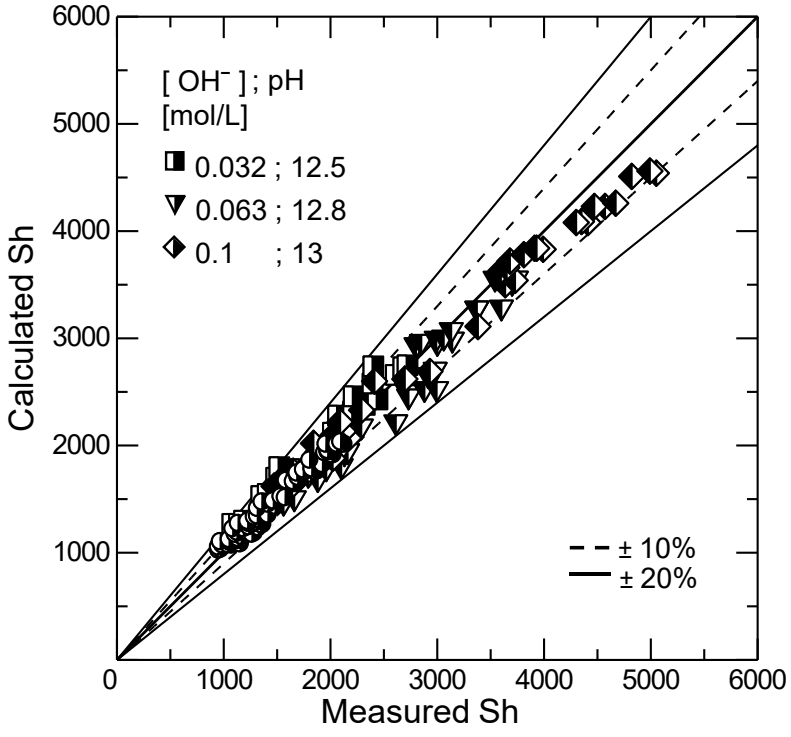

Fig. 2.22 Measured and calculated *Sh* in *D* = 18.2 mm

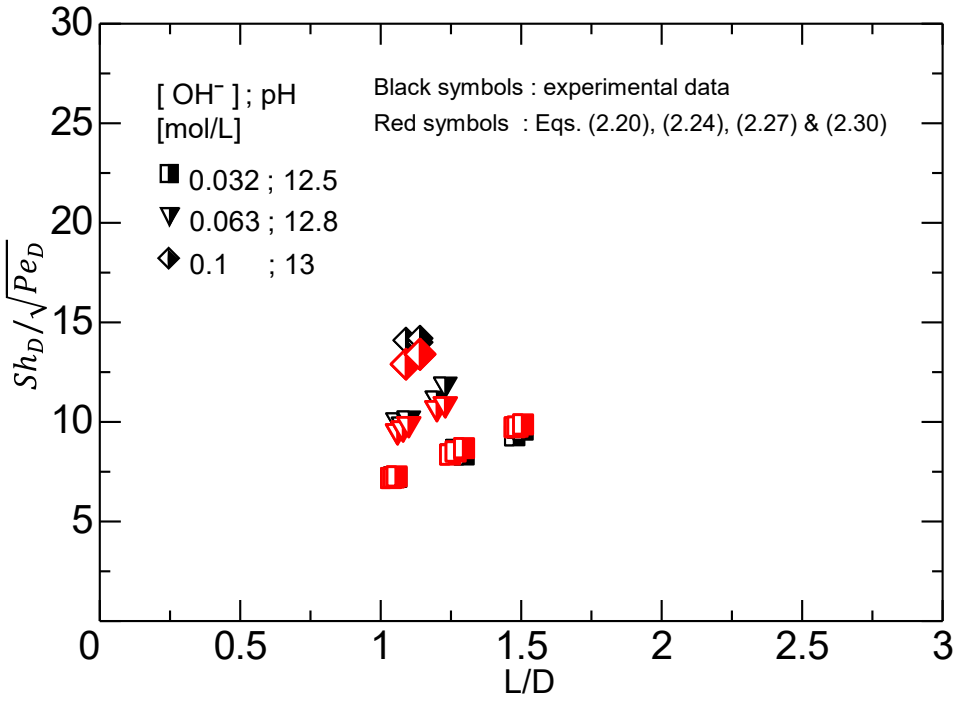

Fig. 2.23 $Sh_D/Pe_D^{1/2}$ vs. L/D in D = 18.2 mm

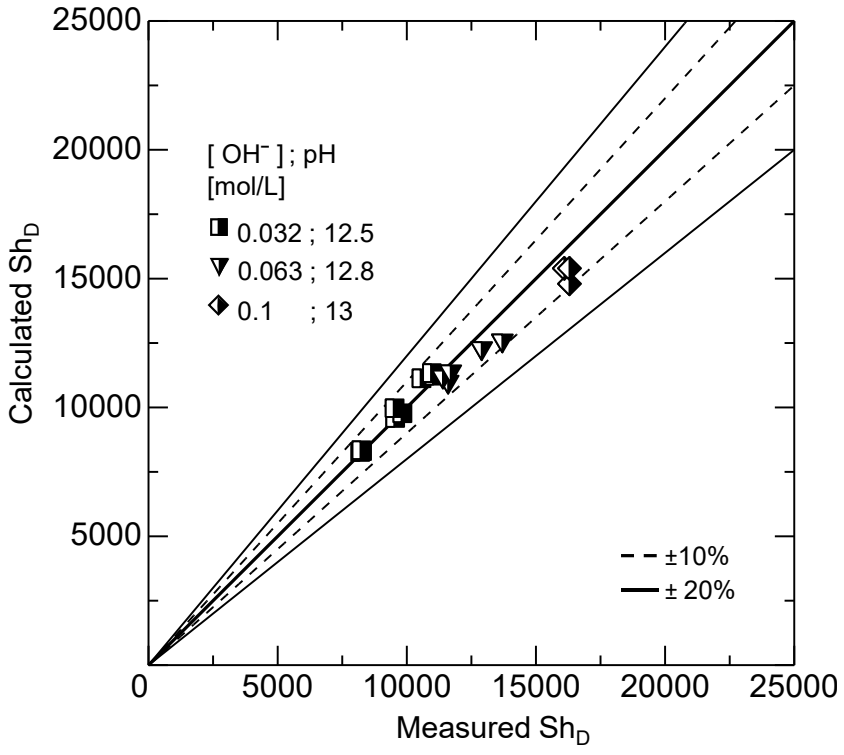

Fig. 2.24 Comparison between measured and calculated Sh_D in D = 18.2 mm

Although the data for $L/D \geq 1$ are limited, Fig. 2.23 shows $Sh_D/Pe_D^{1/2}$ versus L/D for D = 18.2 mm. For pH = 12.5 and 12.8, $Sh_D/Pe_D^{1/2}$ values increase with increasing pH and L/D. The combination of Eqs. (2.20), (2.24), (2.27), and (2.30) gives good evaluation as shown in Fig. 2.24, i.e., where 95% of the data are within 10% error margins.

2.4 Conclusion

Single CO_2 bubbles rising through a vertical pipe filled with a NaOH solution were measured to understand the effects of pH and the bubble diameter d on the enhancement factor E. The experiments were carried out for a wide range of the dimensionless bubble diameter λ which is the ratio of the bubble diameter to the pipe diameter, $0.4 < \lambda < 1.4$, and for the sodium hydroxide concentration, $12 \leq pH \leq 13.15$. Appendix B tabulates all the data, which would be of use for validation of numerical methods. The conclusions obtained are as follows:

1. E for $7 \leq pH \leq 12$ is almost unity, i.e. the presence of NaOH does not affect the mass transfer due to low concentration, while the measured E increases with increasing both pH and d for $pH \geq 12.25$.
2. The enhancement factor model based on the two-film theory and a flat interface (Fleischer et al., 1996) is not applicable to ellipsoidal and Taylor bubbles.
3. The proposed empirical correlation of E for single bubble of $0.4 \leq \lambda \leq 1.4$ and $7 \leq pH \leq 13.15$ gave good agreement with 93% of the data to within ±10% errors. The correlation was also applicable to D = 18.2 mm.
4. The measured Sherwood numbers can be evaluated by combining the proposed E correlation and available correlations of the Sherwood number without chemical reaction.

References

[1] R. Pan, J. Green, and C. Maldarelli, "Theory and experiment on the measurement of kinetic rate constants for surfactant exchange at an air/water interface," *J Colloid Interface Sci*, vol. 205, no. 2, pp. 213–230, 1998, doi: 10.1006/jcis.1998.5559.

[2] D. M. Himmelblau, "Diffusion of dissolved gases in liquids," *Chem Rev*, vol. 64, no. 5, pp. 527–550, 1964, doi: 10.1021/cr60231a002.

[3] D. W. van Krevelen and P. J. Hoftijzer, "Sur la solubilite des gaz dans les solutions aqueouses," *Ind. 21st Congr. Int. Chim. Ind.*, p. 168, 1948.

[4] J. G. Ratcliff, G.A, Holdcroft, "Diffusivities of gases in aqueous electrolyte solutions," *Transactions of the Institution of Chemical Engineers*, vol. 41, pp. 315–319, 1963.

[5] G. F. Versteeg and W. P. M. van Swaal, "Solubility and diffusivity of acid gases (CO_2, N_2O) in aqueous alkanolamine solutions," *J Chem Eng Data*, vol. 33, no. 1, pp. 29–34, 1988, doi: 10.1021/je00051a011.

[6] S. Weisenberger and A. Schumpe, "Estimation of gas solubilities in salt solutions at temperatures from 273 K to 363 K," *AIChE Journal*, vol. 42, no. 1, pp. 298–300, 1996, doi: 10.1002/aic.690420130.

[7] S. Hosoda, S. Abe, S. Hosokawa, and A. Tomiyama, "Mass transfer from a bubble in a vertical pipe," *Int J Heat Mass Transf*, vol. 69, pp. 215–222, 2014, doi: 10.1016/j.ijheatmasstransfer.2013.10.031.

[8] S. Hosokawa and A. Tomiyama, "Image Processing of Bubble Shape and Motion Based on Curvature Evaluation from Bubble Image," in *Proceedings of 6th World Conference on Experimental Heat Transfer, Fluid Mechanics and Thermodynamics*, p. 6–a–10, 2005.

[9] J. Aoki, K. Hayashi, S. Hosokawa, and A. Tomiyama, "Effects of surfactants on mass transfer from single carbon dioxide bubbles in vertical pipes," *Chem Eng Technol*, vol. 38, no. 11, pp. 1955–1964, 2015, doi: 10.1002/ceat.201500063.

[10] C. Fleischer, S. Becker, and G. Eigenberger, "Detailed modeling of the chemisorption of CO_2 into NaOH in a bubble column," *Chem Eng Sci*, vol. 51, no. 10, pp. 1715–1724, 1996, doi: 10.1016/0009-2509(96)00030-9.

[11] K. Hayashi, S. Hosoda, G. Tryggvason, and A. Tomiyama, "Effects of shape oscillation on mass transfer from a Taylor bubble," *International Journal of Multiphase Flow*, vol. 58, pp. 236–245, 2014, doi: 10.1016/j.ijmultiphaseflow.2013.09.009.

[12] S. Hosoda, G. Tryggvason, S. Hosokawa, and A. Tomiyama, "Dissolution of single carbon dioxide bubbles in a vertical pipe," *Journal of Chemical Engineering of Japan*, vol. 48, no. 6, pp. 418–426, 2015, doi: 10.1252/jcej.14we241.

[13] H. W. Jia and P. Zhang, "Mass transfer of a rising spherical bubble in the contaminated solution with chemical reaction and volume change," *Int J Heat Mass Transf*, vol. 110, pp. 43–57, 2017, doi: 10.1016/j.ijheatmasstransfer.2017.02.095.

[14] J. Boussinesq, “Calcul du pouvoir refroidissant des fluides,” *J. Math.*, vol. 1, pp. 285–332, 1905.

[15] Y. Hori, K. Hayashi, S. Hosokawa, and A. Tomiyama, “Mass transfer from single carbon-dioxide bubbles in electrolyte aqueous solutions in vertical pipes,” *Int J Heat Mass Transf*, vol. 115, pp. 663–671, 2017, doi: 10.1016/j.ijheatmasstransfer.2017.07.087.

[16] M. Filla, “Gas absorption from a slug held stationary in downflowing liquid,” *The Chemical Engineering Journal*, vol. 22, no. 3, pp. 213–220, 1981, doi: 10.1016/0300-9467(81)80016-0.

[17] Y. Nakahara and A. Tomiyama, “Shapes and Rising Velocities of Single Bubbles in Vertical Pipes,” *Trans. Jpn. Soc. Mech. Eng. B*, vol. 69, no. 685, pp. 2001–2009, 2003, doi: 10.1299/kikaib.69.2002.

Chapter 3
Application of Physical Absorption Mass Transfer Correlation for Single Bubble to Bubble-Slug Flow in Vertical Pipe

3.1 Introduction

In Chapter 2, the effects of chemical absorption on the mass transfer of a single carbon dioxide (CO_2) bubble in a vertical pipe was investigated, and a correlation equation for predicting mass transfer was developed. In a previous study, Abe [1] extended the mass transfer correlation for a single CO_2 bubble to a system with multiple bubbles and obtained a good prediction. Therefore, the single-bubble correlation may be used to estimate mass transfer in multi-bubble systems containing liquid phases other than water. Before applying the enhancement factor proposed in the previous chapter to multiple bubble systems, it would be necessary to examine whether we can obtain good prediction for mass transfer in multiple bubble systems with various kinds of physical absorption.

Hence, in this chapter, physical absorption in bubble-slug flows in a vertical pipe was numerically simulated under three different conditions: pure water system (Case 1), a system with electrolyte, NaCl (Case 2), and a system including surfactant and electrolyte, NaCl-1-octanol mixture (Case 3). Mass transfer correlations proposed in previous studies for each scenario [2,3] were implemented into a three-dimensional one-way bubble tracking method [4,5]. In addition, experiments on bubbly-slug flows in a vertical pipe were carried out, and the collected data were used to validate the extended numerical method.

3.2 Experiment and measurement method

3.2.1 Experimental condition

The experiments were performed using pure water (Case 1), an aqueous sodium chloride solution (NaCl) with concentration of C_N = 14 wt.% (Case 2), and an aqueous NaCl-

1-Octanol mixture with a surfactant concentration of C_{sol} = 0.17 mol/m^3 and C_N = 14 wt.% (Case 3). Fig. 3.1 shows the measured σ at the interface between an air bubble and NaCl-1-octanol mixed aqueous solution by using a pendant bubble method [6] for several concentration conditions (C_{sol} [mol/m^3], C_N [wt.%]). Due to the surface inactive effect of NaCl, the surface tension in Case 2 is slightly higher than in Case 1. In Case 3, the value of σ is almost the same as the 1-Octanol aqueous solution of C_{sol} = 0.77 mol/m^3 where the bubbles are sufficiently contaminated (dashed line in Fig. 3.1: σ = 0.051 N/m). Therefore, Case 3 can be used as the case contaminated by NaCl and 1-Octanol.

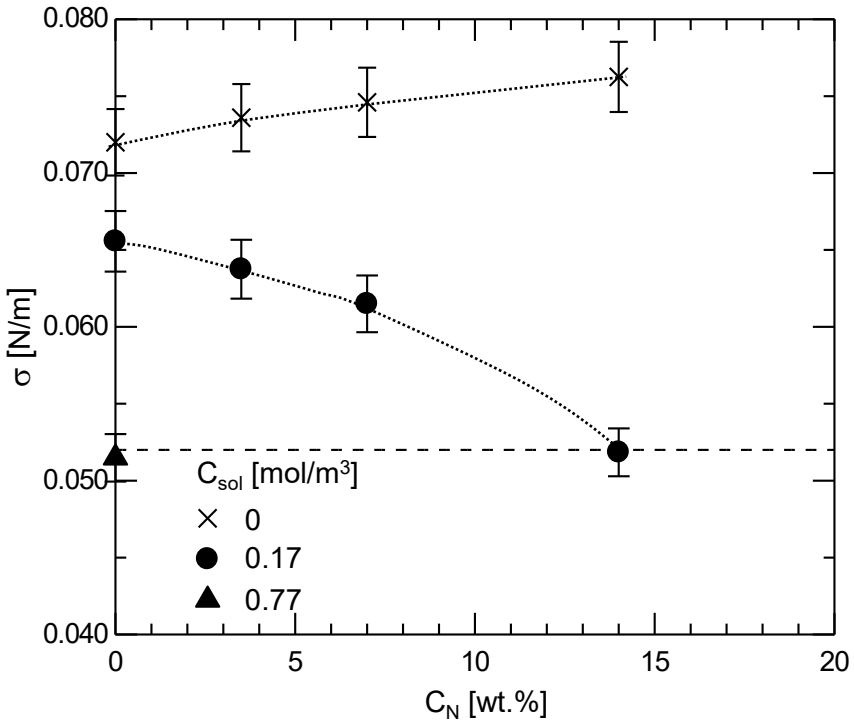

Fig. 3.1 Interfacial tension between NaCl-1-octanol mixed aqueous solution and air

Table 3.1 Experimental conditions

Case	C_{sol} [mol/m^3]	C_N [wt.%]	Re_L	J_L [m/s]	J_G [m/s]	σ [N/m]	ρ_L [kg/m^3]	μ_L x10^{-3} [Pa·s]	Sc
Case 1：Pure water	0	0	7000	0.250	0.120	0.072	997	0.89	420
Case 2：aqueous NaCl solution	0	14	7000	0.299	0.120	0.076	1095	1.17	712
Case 3：aqueous NaCl-1-octanol mixed solution	0.17	14	7000	0.299	0.120	0.052	1095	1.17	712

Table 3.1 shows the experimental conditions. J_L [m/s] is the volume flux of the liquid phase, J_G [m/s] is the volume flux of the gas phase, and Re_L is the Reynolds number of the liquid phase defined by

$$Re_L = \frac{\rho_L J_L D}{\mu_L} \quad (3.1)$$

Here, ρ_L [kg/m^3] is the liquid phase density, μ_L [Pa.s] is the liquid viscosity, C_{sat} [mol/m^3] is the solubility of CO_2 in the liquid phase, and D_L [m^2/s] is the diffusion coefficient. The experiment was performed at the same Re_L = 7000 and J_G = 0.12 m/s as Tamai's experiment using air and water [5]. Sc is the Schmidt number, which is a dimensionless number representing the ratio of viscosity to diffusion.

$$Sc = \frac{\mu_L}{\rho_L D_L} \quad (3.2)$$

Since the amount of 1-octanol added was very small (O (10^{-2}) wt.%), The physical properties of NaCl solution were used in case 3. ρ_L was measured using a standard hydrometer (JISB-1525), and μ_L was measured using a tuning fork vibrating viscometer (A & D Corporation, SV-A10).

Tables 3.2 show the liquid phase properties and transport coefficients [7,8] of CO_2, nitrogen (N_2), and oxygen (O_2) under each condition, where C_{Sat} [mol/m^3] is the gas concentration at the bubble interface, C_L [mol/m^3] is the gas concentration in the liquid phase and D_L [m^2/s] is the diffusion coefficient.

Table 3.2 Gas phase transport coefficients (298 K) [7,8]

	C_{Sat} [mol/m^3]			C_L [mol/m^3]			$D_L \times 10^{-9}$ [m^2/s]		
	CO_2	N_2	O_2	CO_2	N_2	O_2	CO_2	N_2	O_2
Case 1	34.0	0.66	1.3	0.011	0.51	0.27	1.90	2.00	2.30
Case 2	19.4	0.29	0.7	0.006	0.22	0.15	1.50	1.58	1.82
Case 3	19.4	0.29	0.7	0.006	0.22	0.15	1.50	1.58	1.82

3.2.2 Experimental setup

Fig. 3.2 shows an outline of the experimental setup. For the test part, an acrylic resin vertical circular pipe of inner diameter D = 25.0 mm and a length of 5000 mm was used. The external shape of the imaging unit was made rectangular to reduce optical distortion generated on the wall of the pipe.

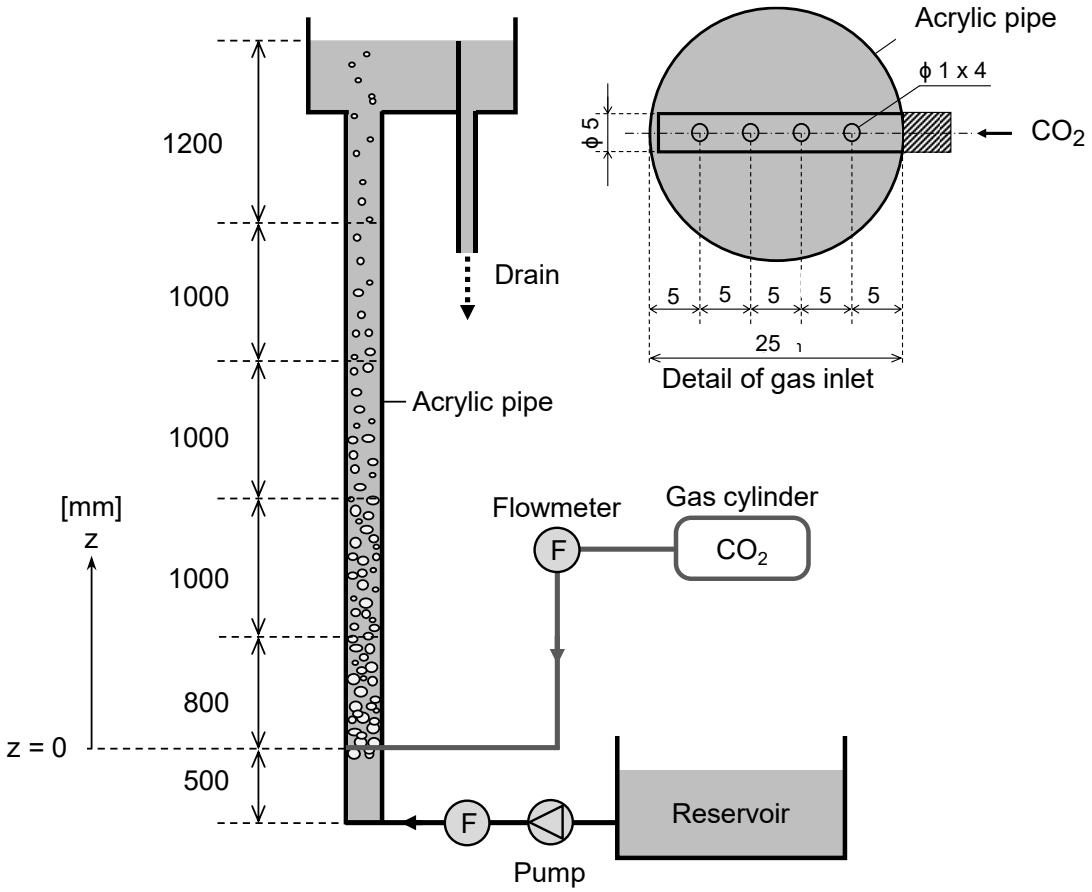

Fig. 3.2 Experimental setup

The liquid phase was supplied by the pump (Iwaki, MD-30FX-N) and flowed from the lower part of the test section through the flow meter (Nippon Flowcell, NSP-5). The liquid temperature T was kept at 25±1.0 ºC. Carbon dioxide (CO_2: Sumitomo Seika Co., Ltd., purity 99.9 vol.%) was used for the gas phase. CO_2 was supplied from the gas cylinder, depressurized to 0.2 MPa by the regulator (CKD, R600-20), and then flowed from the bottom of the test section through the flow meter (KOFLOC, 8500MC) and the bubble inlet. The bubble inlet was a gas sparger consisting of a circular pipe with four orifices on the underside to distribute the flow rate uniformly [9]. The diameter of the sparger was 5 mm. The diameter of each orifice was 1 mm, and the spacing between consecutive orifices was 5 mm. The level of liquid surface was kept constant by overflowing and draining the liquid phase to assure a constant static

pressure in the test section. The channel was opened to the atmosphere to keep the CO_2 concentration in the liquid phase flowing into the test section constant. Hereafter, z [m] and r [m] will be referred to as the vertical coordinate measured from the sparger position and the radial position from the pipe axis, respectively.

3.2.3 Measurement method of bubble diameter and time average local void fraction

Flow observation was performed using a high-speed video camera (Integrated Design Tool, Motion Pro X-3) to observe the flow state and measure the bubble diameter distribution. The recording conditions were the frame rate of 500 frame/s and the resolution of 0.10 mm/pixel. A fluorescent light source was used as the light source, and it was placed directly opposite to the camera with the test section and diffuser for light diffusion interposed. 500 bubbles passing through each section were extracted from the flow image, and image processing was performed to calculate the bubble diameter d [m]. The method described in Section 2.2.3 was used to calculate d. Since the image was taken from one direction, the bubble section was assumed to be circular in this measurement. The measurement error of d was ±5.0%.

The radial distribution of the time-averaged local void fraction α_G was measured using the point electrode probe method [10–12]. The point-electrode probe method is a method of detecting phases based on the difference in electrical conductivity between the gas phase and the liquid phase, and can measure local quantities [12] This method determines the phase based on the difference in electrical conductivity between the gas and liquid phases; however, pure water has a very low electrical conductivity, making phase identification difficult. Therefore, in Case 1, 1.0 wt.% tap water was added to the water purified by Millipore (Elix 3.0). Preliminary experiments have confirmed that the addition of a small amount of tap water does not affect mass transfer.

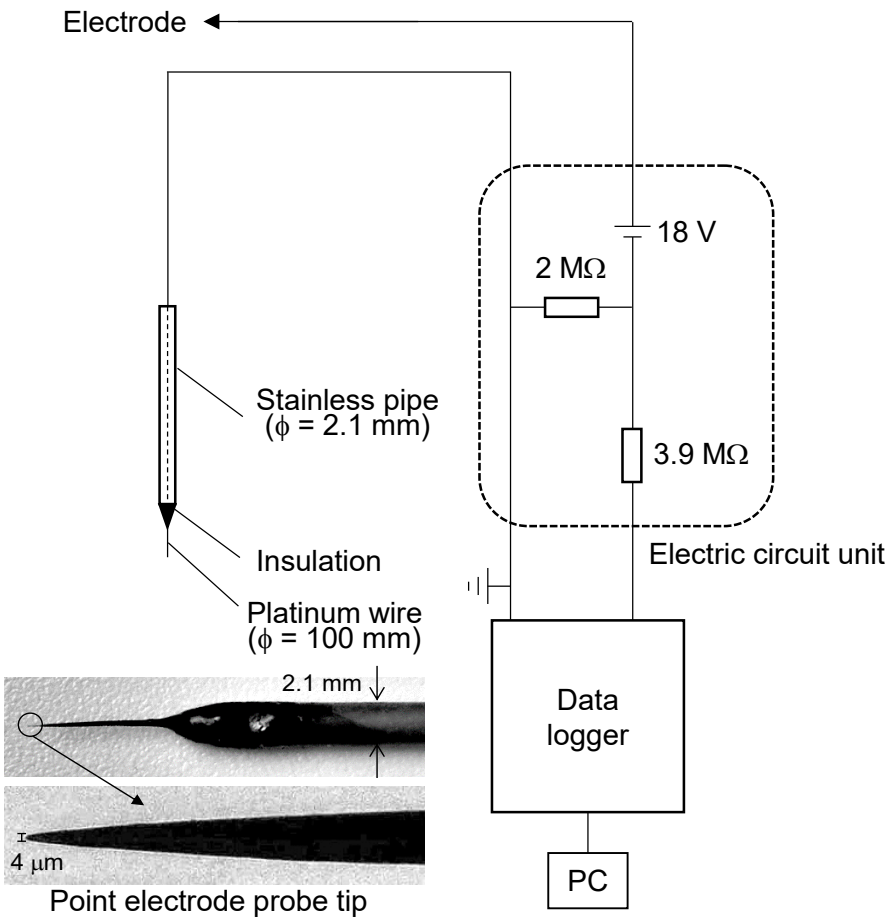

Fig. 3.3 Point electrode probe measurement system

Fig. 3.3 shows the point electrode probe measurement system. The measurement system consists of the point electrode probe, the electric circuit, the data logger (Yokogawa Electric Corporation, WE7000), and the computer. The platinum wire 100 μm in diameter connected to a conductor was passed through the stainless-steel tube of 2.1 mm outer diameter, and all parts except the tip of the platinum wire were insulated with enamel paint. The tip of the platinum wire and the conductor placed below the gas phase inlet acted as electrodes, and the voltage across the resistor (2 MΩ) in the figure was captured by the computer through the data logger. The sampling rate was 20 kHz. For accurate local void fraction measurement by the point electrode probe method, the tip of the probe must be sharp enough so as not to interfere with bubble motion. To obtain a signal with a high signal-to-noise ratio (SNR), a resistor was attached between the data logger and the probe and its resistance value was adjusted. In this experiment, the resistance was set at 3.9 MΩ to obtain a voltage signal with a high SNR.

The voltage signal was binarized to 1 for the gas phase and 0 for the liquid phase using two-point multiple threshold discrimination [13]. α_G was calculated from the binarized signal $B(t)$ using the following equation

$$\alpha_G = \frac{1}{t_M}\int_{t_1}^{t_1+t_M} B(t)dt \qquad (3.3)$$

where t [s] is the time, t_M is the measurement time, and t_1 is the measurement start time. In this experiment, t_M was set at 300 s, which is the time at which α_G converges sufficiently.

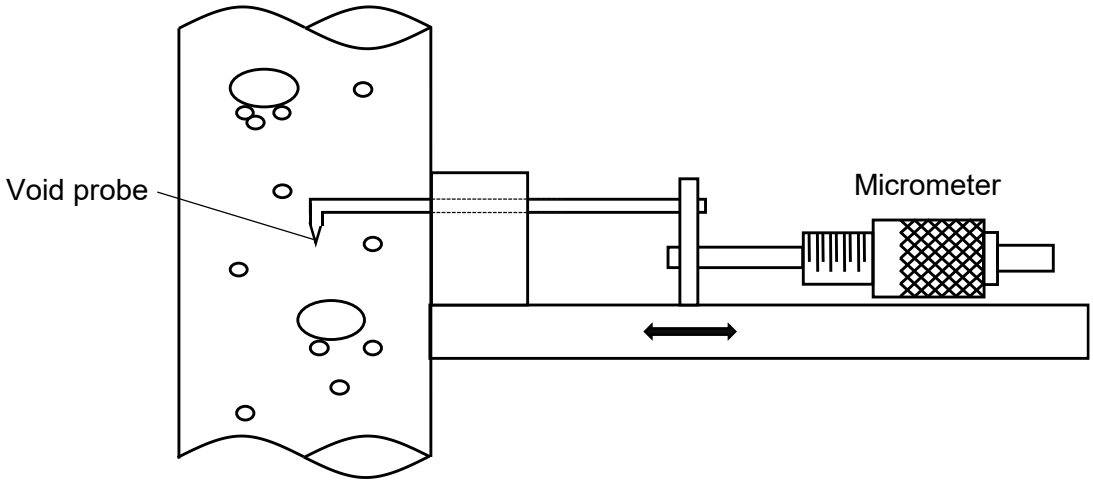

Fig. 3.4 Void fraction measurement

Fig. 3.4 shows a schematic of the measurement section. The measurement section consists of the transparent acrylic resin tube for measurement, the void probe, and the micrometer. The inaccuracy in the *r*-coordinates of the measurement spots was reduced by using the void probe bent at a straight angle. The micrometer was used to move the void probe to the measurement point in the *r*-direction. Measurements were taken at four cross sections (dashed lines in Fig.3.2) in the vertical position z = 0.8-3.8 m, at intervals of 1.0 mm in the r direction, for a total of 13 points. Preliminary experiments confirmed the axisymmetricity of the radial α_G distribution at each measurement section and the measurement error by this method was to within ±2.1 %.

3.3 Bubble dissolution data of gas-liquid two-phase bubble flow in a vertical pipe

3.3.1 Bubble diameter distribution at inlet and flow pattern

Bubble diameter distributions at the bubble inlet are required as the inlet boundary condition for bubble tracking simulation. Therefore, the bubble diameter distribution was measured immediately after the bubble inlet (z <50 mm). Fig. 3.5 shows the measurement results. The horizontal axis in the figure represents the bubble diameter d classified by a width of 0.5 mm. The probability density function (pdf) of d for $3 < d < 4$ mm in Case 1 and 2 are larger than in Case 3. The measured bubble size was used as the inlet condition for bubble tracking simulation.

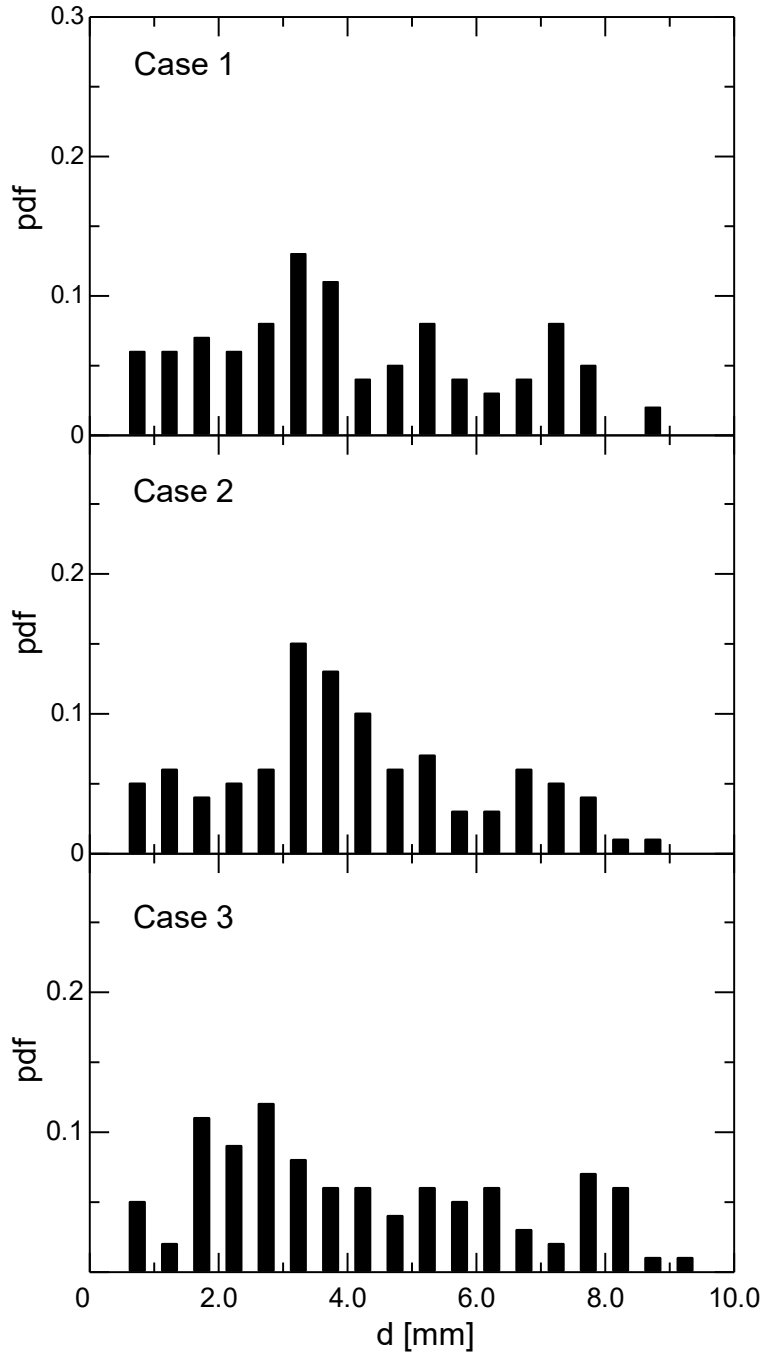

Fig. 3.5 Inlet bubble diameter distribution

Fig. 3.6 shows bubbly flow images. For comparison, a bubble image of a pure water-air system is also shown in the same figure. The flow state of bubbles in a vertical pipe differs greatly depending on the presence or absence of mass transfer. In the clean water-air bubble flow without mass transfer, bubble clusters are formed, and bubbles that have grown to large bubbles by coalescence of bubble clusters repeatedly merge with other large bubbles and small bubbles entrained in the wake, and grow to larger bubbles. Cases 1-3, which involve mass

transfer, show flow fields with a sparse bubble distributions along the pipe axis. Because bubbles dissolve before reaching $d > d_T$, the diameter at which they turn into Taylor bubbles. The bubble diameter downstream is the smallest in Case 1 and the largest in Case 3. Since the k_L of bubbles in the contaminated system is significantly lower than that in the clean system, Taylor bubbles are generated by bubble coalescence at z = 4.0 m in Case 3.

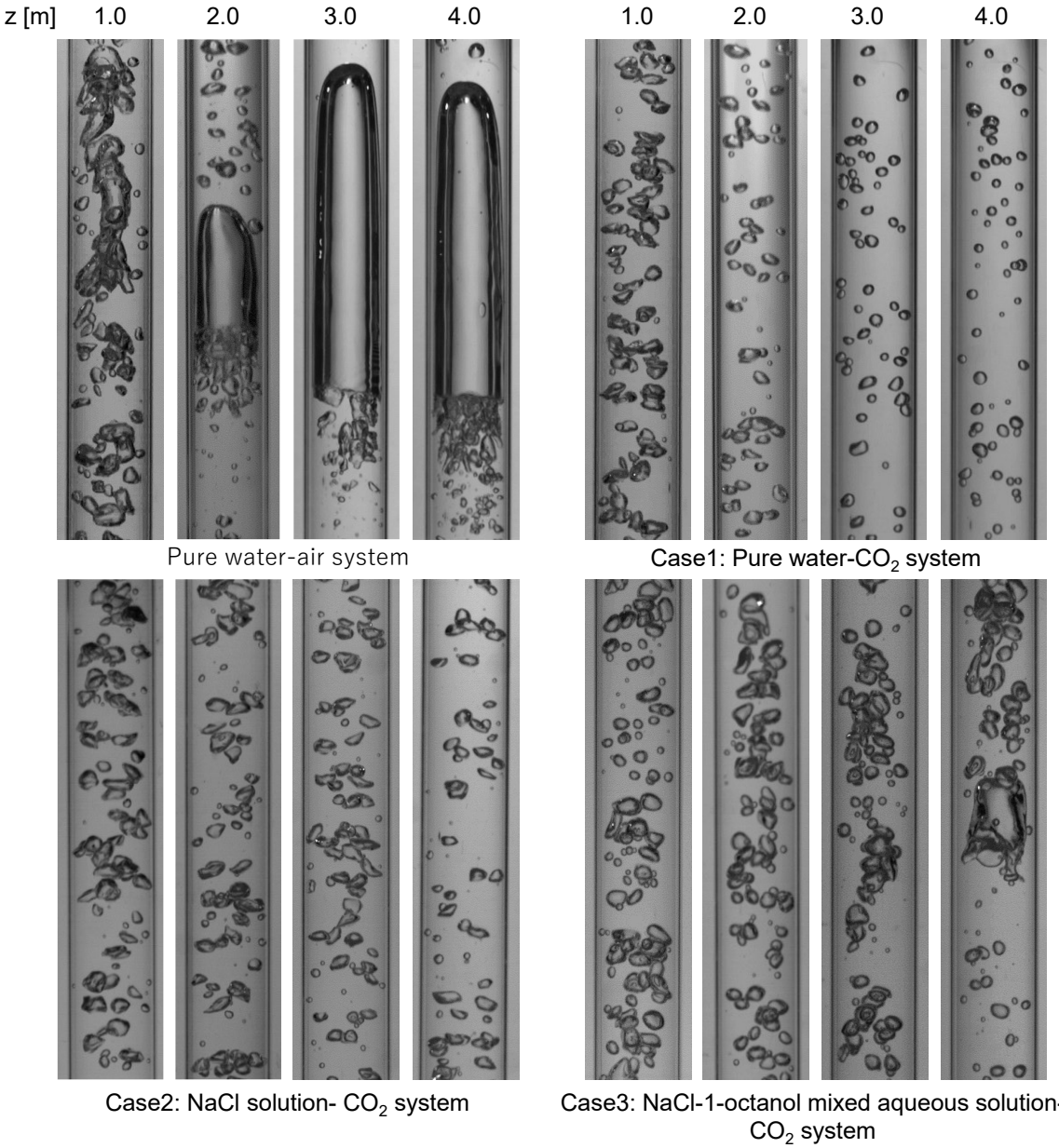

Fig. 3.6 Flow pattern for each cases

3.3.2 Radial void fraction distribution and bubble diameter distribution

The measurement results of α_G and bubble diameter distributions at each measurement position in the vertical direction are shown in Figs. 3.7 and 3.8. The left figure is the results of α_G distributions with the horizontal axis representing the r coordinate normalized by the pipe radius R_P [m]. Meanwhile, the right figure is bubble diameter distributions with the horizontal axis representing d classified by a width of 0.5 mm, and the vertical axis represents the total bubble volume Θ_{Bn} [m^3] to the total gas volume of each bubble class.

In Case 1 (Fig. 3.7), the α_G distribution, which is a core peaking distribution with the peak in the center of the pipe in the upstream part, transited to a wall peaking distribution with the peak near the wall as going downstream. It is known that in a clean water-air bubble flow in a vertical pipe, the direction of lift acting on the bubbles is directed toward the pipe wall when d <5 mm, and toward the pipe center when d > 5 mm [14]. According to the measured bubble diameter distribution, there are many bubbles of d > 5 mm immediately after the inlet, but the number of bubbles with d < 5 mm increases toward the downstream. In other words, the reversal of the direction of lift due to the decrease in d is the cause of the transition of the α_G distribution. On the other hand, in Case 2 (blank square symbol in Fig. 3.8) the core peak is maintained down to the downstream. This is because the bubbles in the NaCl aqueous solution have a lower k_L than the bubbles in pure water, so that the bubbles expand and coalesce due to the decrease in hydrostatic pressure faster than the d decrease due to dissolution. A similar tendency was observed in Case 3 (blank triangle symbol in Fig. 3.8). In addition, as shown in the flow state observation results in the previous section (Fig. 3.6), Taylor bubbles of $d > d_T$ that are not generated in Case 1 and Case 2 (d_T = 15.2 mm) are generated by bubble coalescence in Case 3 (d_T = 13.8 mm) because of much lower k_L than other cases.

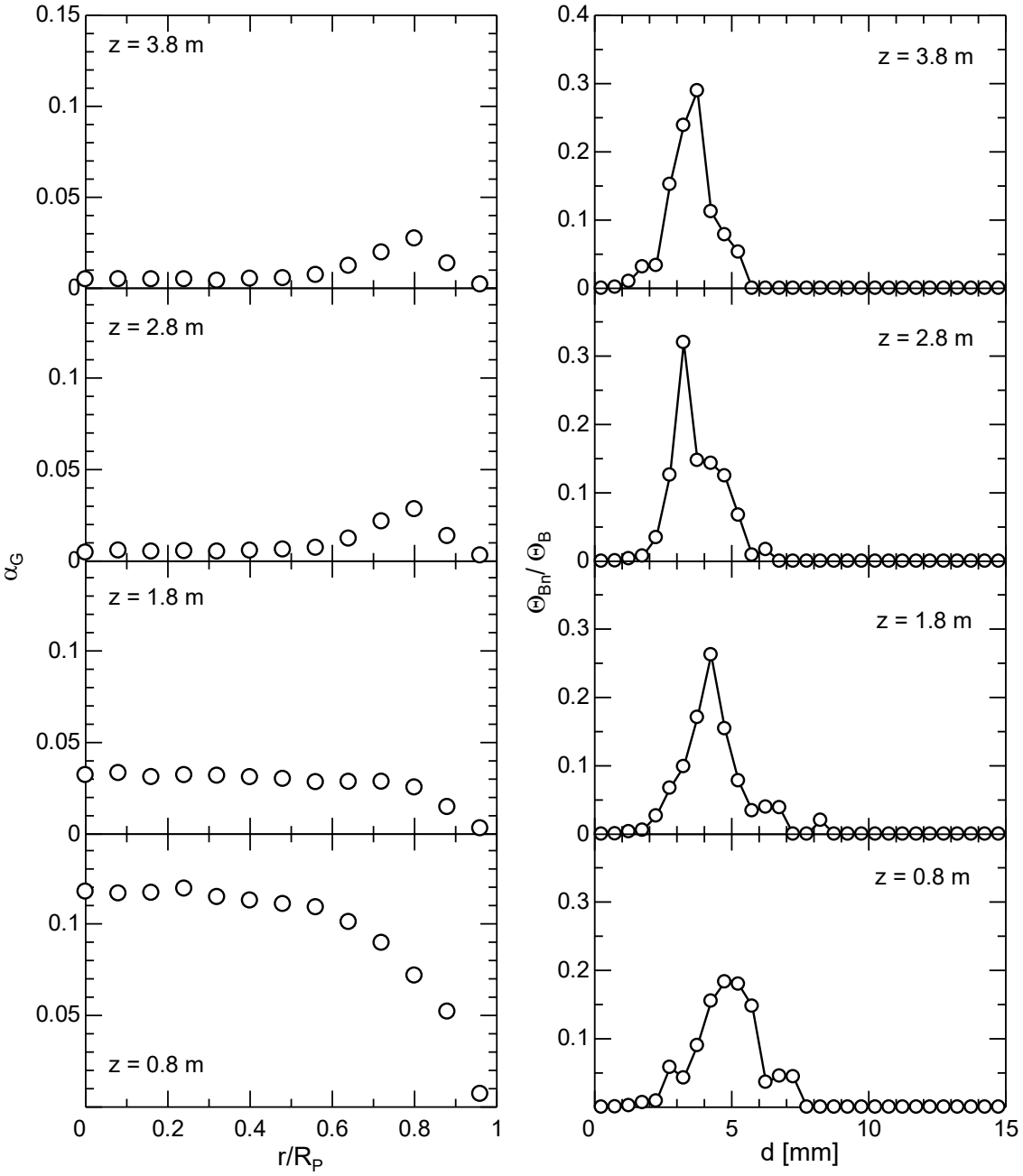

Fig. 3.7 Distribution of void fraction and bubble diameter in radial direction (Case 1)

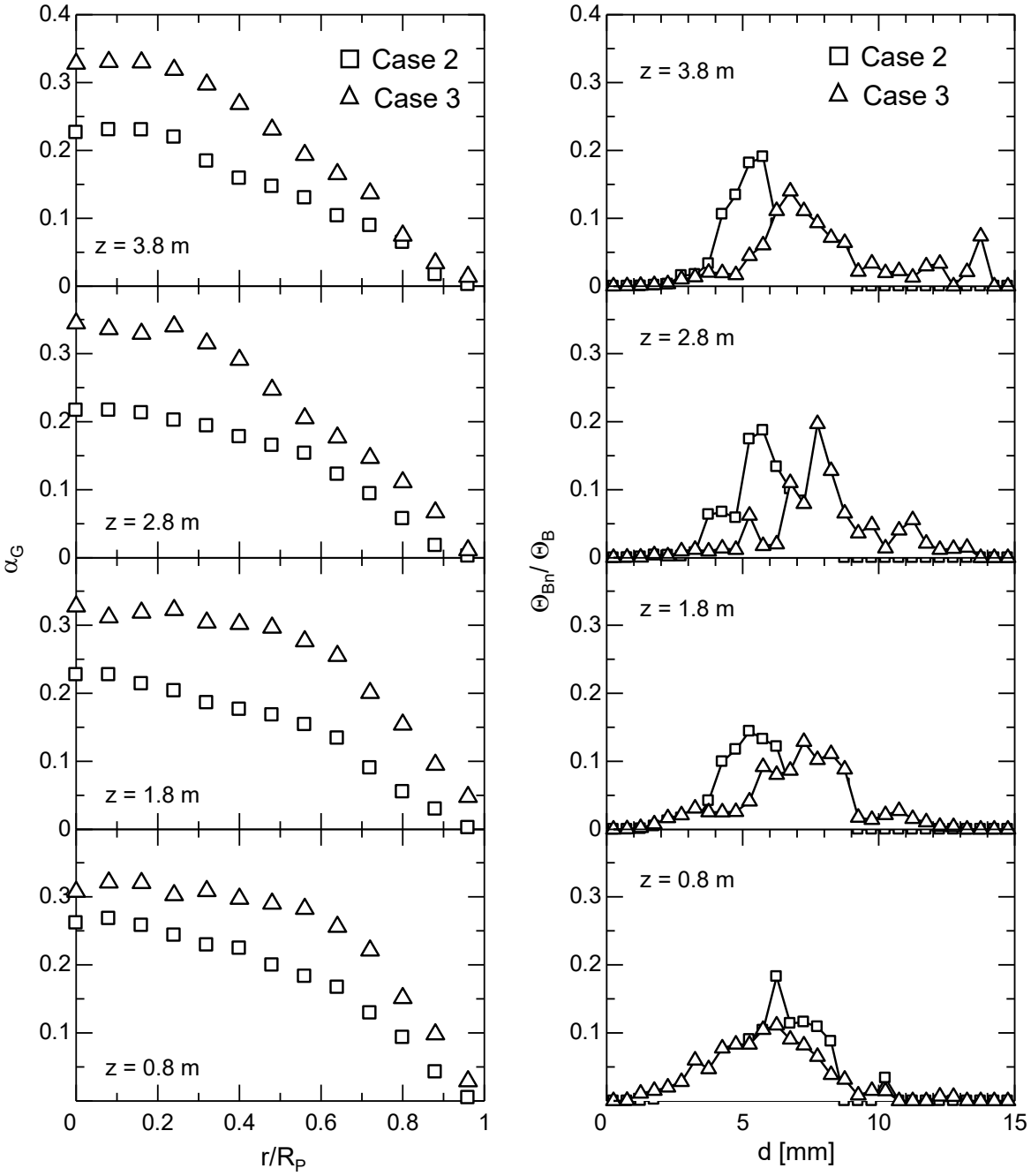

Fig. 3.8 Distribution of void fraction and bubble diameter in radial direction of Case 2 (□) and Case 3 (Δ)

3.4 Three-dimensional one-way bubble tracking method

The bubble tracking method predicts bubble flows in a Lagrangian manner. Since the local variables such as the bubble diameter, velocity, and position of each bubble in the flow field are directly obtained as dependent variables, the volume fraction of each phase and the gas-liquid boundary area are calculated without numerical diffusion. Therefore, it is an effective method for predicting bubble-liquid mass transfer [1]. A model or solution of the equation of liquid motion is used for the liquid flow field around the bubble. The method of using a model of the liquid flow field is called one-way bubble tracking method [15,16]. In this section, we incorporate the mass transfer correlation into the three-dimensional one-way bubble tracing method proposed by Tamai et al [5].

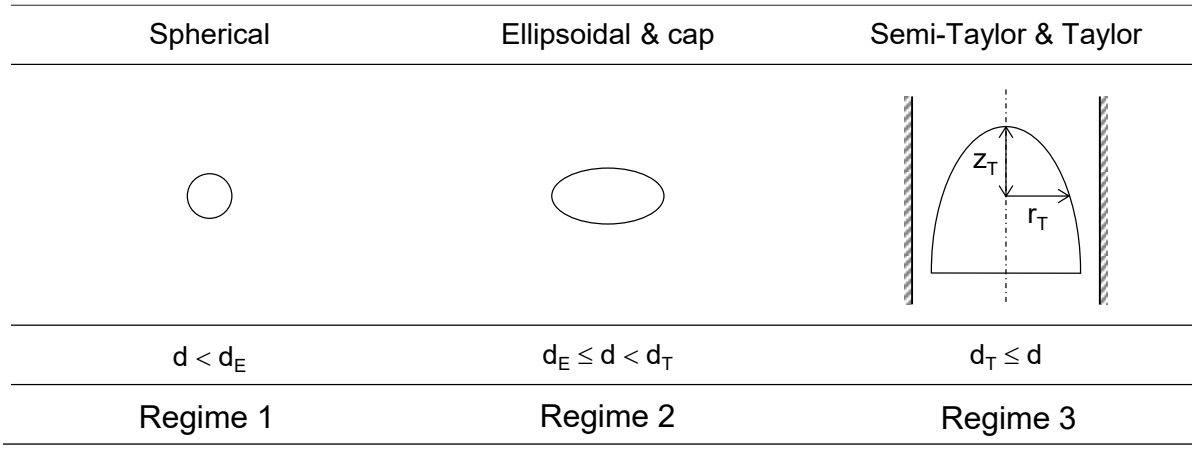

Fig. 3.9 Bubble shape considered in bubble tracking method [2,3]

As shown in Fig. 3.9, bubbles are classified into three shapes, i.e., spherical (Regime 1), ellipsoidal and cap (Regime 2), and semi-Taylor and Taylor bubbles (Regime 3) according to the bubble diameter d [4,5]. Bubbles are spherical when $d < d_E$ [m], where d_E is obtained from the following equation [14].

$$\frac{32}{81\mathrm{A}^2}\sqrt{\frac{Eo^3}{M}} = \frac{4}{Eo} + 1 \qquad (3.4)$$

where A is a constant with the value 16 for a clean system, and 24 for a contaminated system.

The Eötvös number *Eo* and the Morton number *M* are defined by.

$$Eo = \frac{\Delta\rho g d^2}{\sigma} \quad (3.5)$$

$$M = \frac{\Delta\rho g \mu^4}{\rho_L^2 \sigma^3} \quad (3.6)$$

Here, $\Delta\rho$ [kg/m^3], g [m/s^2], and σ [N/m] are the gas-liquid density difference, the gravitational acceleration, and the interfacial tension, respectively. The aspect ratio E of an elliptical bubble ($d_E \leq d < d_T$) gives a random value between the lower limit E_{min} and the upper limit E_{max} [17] given by.

$$E_{min} = \max\left(1 + 0.016 Eo^{1.12} Re_L^{-0.388}, 0.45\right) \quad (3.7)$$

$$E_{max} = \frac{1}{1 + 0.16 Eo^{0.76}} \quad (3.8)$$

The bubble changes to a Taylor bubble when $d = d_T$. The d_T of the clean system and the contaminated system are 15.2 mm and 13.8 mm [18] at D = 25.0 mm, respectively. The form of a large bubble is represented using the shape function [19] given by

$$r_T{}^* = 0.9 - \left(z_T{}^{*0.7} + 0.9^{1/a}\right)^a \quad (3.9)$$

$$r_T{}^* = \frac{r_T}{R_P},\ z_T{}^* = \frac{z_T}{R_P} \quad (3.10)$$

$$a = \min\left(3.26 \times 10^{-4}\, Re_L - 2.83,\ 2.29 \times 10^{-5}\, Re_L - 2.36\right) \quad (3.11)$$

Here, r_T [m] is the radial position of the bubble interface, and z_T [m] is the vertical downward distance from the bubble tip (Fig. 3.9).

3.4.1 Regime 1 and 2 (Spherical, ellipsoidal and cap bubbles)

The motion of spherical, ellipsoidal and cap bubbles (regime 1 and 2) are predicted using

$$(\rho_G + C_{VM}\rho_L)\frac{\mathrm{d}\boldsymbol{V}_B}{\mathrm{d}t} = C_{VM}\rho_L\frac{\mathrm{d}\boldsymbol{V}_L}{\mathrm{d}t} + \boldsymbol{F}_D + \boldsymbol{F}_L + \boldsymbol{F}_F + \boldsymbol{F}_W + \boldsymbol{F}_B \quad (3.12)$$

where ρ_G [kg/m^3] is the gas phase density, C_{VM} is the virtual mass coefficient, $\boldsymbol{V}_B$ is the bubble velocity, $\boldsymbol{V}_L$ is the liquid phase velocity, $\boldsymbol{F}_D$ [N] is the drag force, $\boldsymbol{F}_L$ [N] is the lift force, $\boldsymbol{F}_F$ [N] is the force causing non-rectilinear motion, $\boldsymbol{F}_W$ [N] is the wall force, and $\boldsymbol{F}_B$ [N] is the buoyancy force.

In the evaluation of the drag $\boldsymbol{F}_D$, the following equation [19] taking into account the effect of the pipe wall is used.

$$\boldsymbol{F}_D = -\frac{3}{4d}C_D\Phi(\lambda)\rho_L|\boldsymbol{V}_B - \boldsymbol{V}_L|(\boldsymbol{V}_B - \boldsymbol{V}_L) \quad (3.13)$$

where C_D is the drag coefficient for a single bubble in an infinite stagnant liquid and $\Phi(\lambda)$ is the wall effect multiplier given by

$$\Phi(\lambda) = \max\{\ 1,\ 4[1.13\exp(-\lambda) + (1-\lambda^2)^{1.5}]^{-2}\} \quad (3.14)$$

where λ (= d/D) is the diameter ratio. The V_T of a clean single bubble can take various values depending on the instantaneous bubble shape as well as the physical properties and bubble diameter [20]. Therefore, C_D is given as a uniform random value between lower limit value C_{Dmin} and the upper limit value C_{Dmax} for Cases 1 and 2 with a bubble diameter range $1 < d <$ 5 mm:

$$C_{Dmin} = \max\left(\frac{48}{Re}, \frac{8Eo}{3(Eo+4)}\right) \quad (3.15)$$

$$C_{Dmax} = \frac{7(Eo+1.5)}{3(Eo+4)} \quad (3.16)$$

where *Re* is the bubble Reynolds number defined by

$$Re = \frac{\rho_L |\boldsymbol{V}_B - \boldsymbol{V}_L| d}{\mu_L} \quad (3.17)$$

Bubbles are fully contaminated in Case 3, and therefore, $C_D = C_{Dmax.}$ For all the cases, C_D for $d > 5$ mm is given by

$$C_D = \frac{8Eo}{3(Eo + 4)} \quad (3.18)$$

The following equation [21] is used for $\boldsymbol{F}_L$.

$$\boldsymbol{F}_L = -C_{Li}\rho_L(\boldsymbol{V}_B - \boldsymbol{V}_L) \times \mathrm{rot}\boldsymbol{V}_L \quad (3.19)$$

where C_{Li} is the lift coefficient given by

$$C_{Li} = \begin{cases} \min[0.288\tanh(0.121\,Re),\ f(Eo_H)] & \text{for } Eo_H < 4 \\ f(Eo_H) & \text{for } otherwise \end{cases} \quad (3.20)$$

$$f(Eo_H) = 0.0011Eo_H^3 - 0.016Eo_H^2 - 0.020Eo_H + 0.47 \quad (3.21)$$

$$Eo_H = \frac{\Delta\rho g d_H^2}{\sigma} \quad (3.22)$$

Eo_H is the Eötvös number whose representative length is the major diameter d_H of the bubble.

The C_L correlations proposed for clean bubbles are applicable to Cases 1 and 2. Hayashi and Tomiyama [22] pointed out that C_L correlations for clean bubbles are also applicable to contaminated bubbles, provided that Eo_H is evaluated for the adsorption-desorption equilibrium and the Hatta number is large. Therefore, the correlation Eq. (3.20) would also be applicable to bubbles in Case 3.

The following centrifugal force is used for $\boldsymbol{F}_F$ to take into account spiral and zigzagging motions of bubbles [23, 24].

$$\boldsymbol{F}_F = (\rho_G + C_{VM}\rho_L)\, s\, \omega^2\, (\sin\omega t\mathbf{e}_1 + \cos\omega t\mathbf{e}_2) \quad (3.23)$$

where $\boldsymbol{e}_1$ and $\boldsymbol{e}_2$ are unit vectors orthogonal to each other in the horizontal plane, and $\boldsymbol{e}_2 = 0$ in the zigzagging motion

$$s = (-21St + 2.7)d \quad (3.24)$$

$$\omega = \frac{2\pi|(\boldsymbol{V}_B - \boldsymbol{V}_L) \cdot \mathbf{n}_z|}{d}\mathrm{St} \quad (3.25)$$

Here s is the amplitude [m] and ω is the angular velocity [rad/s] of the bubble oscillating motion. $\boldsymbol{n}_z$ is the unit vector pointing vertically upward. The Strouhal number *St* is given by

$$St = \begin{cases} \min(0.09,\ 0.057\,Eo^{0.67}) & \text{for spiral motion} \\ 0.09 & \text{for zigzagging motion} \end{cases} \quad (3.26)$$

It is assumed that 90% of the bubbles at the inlet are helical and 10% are zigzagging. Furthermore, a zigzagging bubble changes its morphology to a spiral motion with a 90% probability when it collides with another bubble or the pipe wall.

The following correlation is used for the wall force $\boldsymbol{F}_W$ [25]

$$\boldsymbol{F}_W = C_W \frac{\rho_L}{2}|(\boldsymbol{V}_B - \boldsymbol{V}_L) \cdot \mathbf{n}_z|^2 \mathbf{n}_r \quad (3.27)$$

$$C_W = -0.05d\left(\frac{1}{r_T^2} + \frac{1}{(D - r_T)^2}\right. \quad (3.28)$$

where C_W is the wall force coefficient and $\boldsymbol{n}_r$ is the unit vector in the radial direction of the pipe.

The buoyancy $\boldsymbol{F}_B$ is evaluated by

$$\boldsymbol{F}_B = (\xi\rho_L - \rho_G)\mathrm{g} \quad (3.29)$$

where ξ is a parameter to account for the fact that there is no pressure gradient in the axial direction in the descending free-falling liquid film around Taylor bubbles, ξ = 0 for small bubbles in the descending film, and ξ = 1 for other bubbles.

In order to consider the effect of the liquid phase fluctuation velocity due to shear-induced turbulence and bubble-induced turbulence on the movement of small bubbles, the following

equation that considers velocity fluctuations is used when computing the bubble position at a new time:

$$x(t+\Delta t) = x(t) + (\boldsymbol{V}_B + \boldsymbol{V}')\Delta \boldsymbol{t} \quad (3.30)$$

where, $\boldsymbol{x}$ [m] is the bubble position and $\boldsymbol{V}'$ [m/s] is the velocity fluctuation due to turbulence. $\boldsymbol{V}'$ is evaluated by the following formula considering the liquid phase turbulence scale.

$$\boldsymbol{V}' = \beta_{SI}\boldsymbol{V}'_{SI} + \beta_{BI}\boldsymbol{V}'_{BI} \quad (3.31)$$

$$\beta_{SI} = \min(1, l_{mSI}/d), \beta_{SI} = l_{mBI}/d \quad (3.32)$$

The subscripts *SI* and *BI* mean the shear-induced turbulence and the bubble-induced turbulence, respectively, β is a coefficient indicating the degree of turbulence vorticity influence on bubble motion, and l_m [m] is the mixture length representing the turbulence length scale. Since no shear-induced turbulence occurs under laminar flow conditions, only the bubble-induced turbulence is considered. The following models are used for l_{mSI} and l_{mBI} respectively [26,27]

$$\frac{l_{mSI}}{R_P} = 0.06\left(\frac{r}{R_P}\right)^4 - 0.08\left(\frac{r}{R_P}\right) + 0.14 \quad (3.33)$$

$$l_{mBI} = 0.6d \quad (3.34)$$

$\boldsymbol{V}_{SI}$' and $\boldsymbol{V}_{BI}$' are random variables following the normal distribution:

$$f(|\boldsymbol{V}'|) = (2\pi\zeta^2)^{-1/2}\exp\left(-(|\boldsymbol{V}'| - \overline{\boldsymbol{V}}')^2/2\zeta^2\right) \quad (3.35)$$

$\overline{\boldsymbol{V}}'$ is the mean value and ζ is the standard deviation. The standard deviation ζ_{SI} of $\boldsymbol{V}_{SI}$' is evaluated by the following formula by Laufer [28].

$$\zeta_{SI,r} = V_{B0}\left\{-0.35\left(1 - \frac{r}{R}\right) + 1.06\right\} \quad (3.36)$$

$$\zeta_{SI,\theta} = V_{B0}\left\{-0.97\left(1 - \frac{r}{R}\right) + 1.58\right\} \quad (3.37)$$

$$\zeta_{SI,z} = V_{B0}\left\{-1.48(1-\frac{r}{R})+2.12\right\} \quad (3.38)$$

where, the subscripts r, θ, and z denote the radial direction, circumferential direction, and vertical direction, respectively. The typical terminal velocity V_{B0} of a bubble is evaluated by the following equation.

$$V_{B0} = \sqrt{2}[g\sigma(\rho_L-\rho_G)/{\rho_L}^2]^{0.25} \quad (3.39)$$

On the other hand, regarding the standard deviation ζ_{BI} of V'_{BI}, it is considered that the bubble-induced fluctuation velocity is smaller than V_{B0}, so that $\zeta_{BI} = 0.3V_{B0}$ [1]

3.4.2 Regime 3 (Taylor bubbles)

The large bubbles are assumed to rise in the center of the pipe, the vertical velocity V_B is evaluated by the sum of the liquid phase velocity CV_L at the pipe center, the bubble terminal velocity V_T, and the wake velocity of a preceding large bubble V_W.

$$V_B = CV_L + V_T + V_W \quad (3.40)$$

$$C = 1.18 + 0.32exp\,[0.0017(2300-Re_L) \text{ for } Re_L > 2300 \quad (3.41)$$

The terminal velocity V_T of semi-Taylor and Taylor bubbles are evaluated by using the following correlation

$$Fr_D = \sqrt{\frac{\gamma\cdot\varepsilon}{\frac{\varepsilon}{0.35^2}+\eta}} \quad (3.42)$$

where γ, η, ε are defined as

$$\gamma = \left(1+\frac{3.87}{Eo_D^{1.68}}\right)^{-18.4} \quad (3.43)$$

$$\eta = \frac{1}{Re_D}(1-0.05\sqrt{Re_D}) \quad (3.44)$$

$$\varepsilon = 0.0025[3 + \gamma] \quad (3.45)$$

Here Re_D and Eo_D are the the Reynolds number and the Eötvös number, respectively, defined by

$$Re_D = \frac{\rho_L V_B D}{\mu_L} \quad (3.46)$$

$$Eo_D = \frac{(\rho_L - \rho_G) g D^2}{\sigma} \quad (3.47)$$

Then V_T is calculated as:

$$V_T = Fr_D \sqrt{\frac{(\rho_L - \rho_G) g D}{\rho_L}} \quad (3.48)$$

The wake velocity V_W is calculated by using

$$\mathbf{V}_W(r, Z) = \begin{cases} V_T \left[V^* - (V^* - 1) \left(1 - \frac{z}{L_m} \right)^2 \right] f(r) \mathbf{n}_z & \text{for } 0 \le Z \le L_m \\ \dfrac{V_T}{\chi \left(\frac{z - L_m}{D} \right)^2 + \frac{1}{V^*}} f(r) \mathbf{n}_z & \text{for } L_m < Z \end{cases} \quad (3.49)$$

$$V^* = \frac{V_{max}}{V_T} = 3.5 - 2.6 \exp(-2.3\lambda^3) \quad (3.50)$$

where Z is the distance from the tail of the bubble heading downward, V^* is the dimensionless value of the maximum rise velocity V_{max} in the wake region of the large bubble with V_T. The distance of L_m from the bubble trailing edge to the position where V_{max} is evaluated by

$$\frac{L_m}{D} = \begin{cases} \lambda - 0.4 & \text{for } 0 \le \lambda \le 1.35 \\ 590 \exp(-5.5\lambda) + 0.6 & \text{for } 1.35 < \lambda \end{cases} \quad (3.51)$$

The coefficient χ is given by

$$\chi = \begin{cases} 0.81\lambda^2 + 0.2\lambda & \text{for } 0 \le \lambda \le 1.4 \\ 58\exp(-3\lambda) + 1 & \text{for } 1.4 < \lambda \end{cases} \quad (3.52)$$

and *f(r)* the radial factor is given by

$$f(r) = \begin{cases} \cos\dfrac{\pi r}{2R_W} & \text{for } 0 < r < R_W \\ -\dfrac{(2-4/\pi){R_W}^2}{R_P^2 - {R_W}^2}\sin\dfrac{r - R_W}{R_P - R_W}\pi & \text{for } R_W < r < R_P \end{cases} \quad (3.53)$$

where R_W is the radius of the updraft region in the wake:

$$R_W = (-0.025z/D + 0.67)R_P \quad (3.54)$$

3.4.3 Liquid Velocity

The momentum equation of the liquid phase is not solved, while the liquid velocity is given by a model, in which the presence of large bubbles affects the liquid velocity distribution. The velocity field is divided into the following four regions: 1) undisturbed region, 2) large bubble tip area, 3) liquid film region, and 4) large bubble wake region shown in Fig. 3.10. The liquid velocity in region 1 is given by the 1/7th power law for single-phase flows.

$$\boldsymbol{V}_L(r) = 1.2V_L(1 - r/R_P)^{1/7}\boldsymbol{n}_z \quad (3.55)$$

Region II is the tip region of large bubbles ranging from z_T = 0.5D to –0.2D, and the small bubbles existing in this region are pushed forward by the flow of the liquid phase induced by the large cell motion or are caught in the liquid film flow around the large bubbles. In order to take this into consideration, the liquid phase velocity distribution in Eq. (3.55) is superimposed with the solution of the potential flow calculated by the boundary-fitted grid method [4]. The liquid film region 3 is from z_T = –0.2D to the bottom edge of the bubble. The film velocity in this region is assumed to be uniform and the velocity magnitude is determined by the continuity equation.

$$\boldsymbol{V}_L(z) = \frac{(J_G + J_L)R_P^2 - \boldsymbol{V}_B \cdot \boldsymbol{n}_z {r_T}^2}{R_P^2 - {r_T}^2}\boldsymbol{n}_z \qquad (3.56)$$

r_T in Eq. (3.56) is obtained using the large bubble shape function of Eqs (3.9) and (3.10). The wake region 4 starts from $Z = 0$ and ends at $Z = 16D$. The liquid velocity in this region is given by the linear sum of the liquid phase velocity distribution of Eq. (3.55) and the wake velocity distribution of Eq. (3.49) in section 3.4.2.

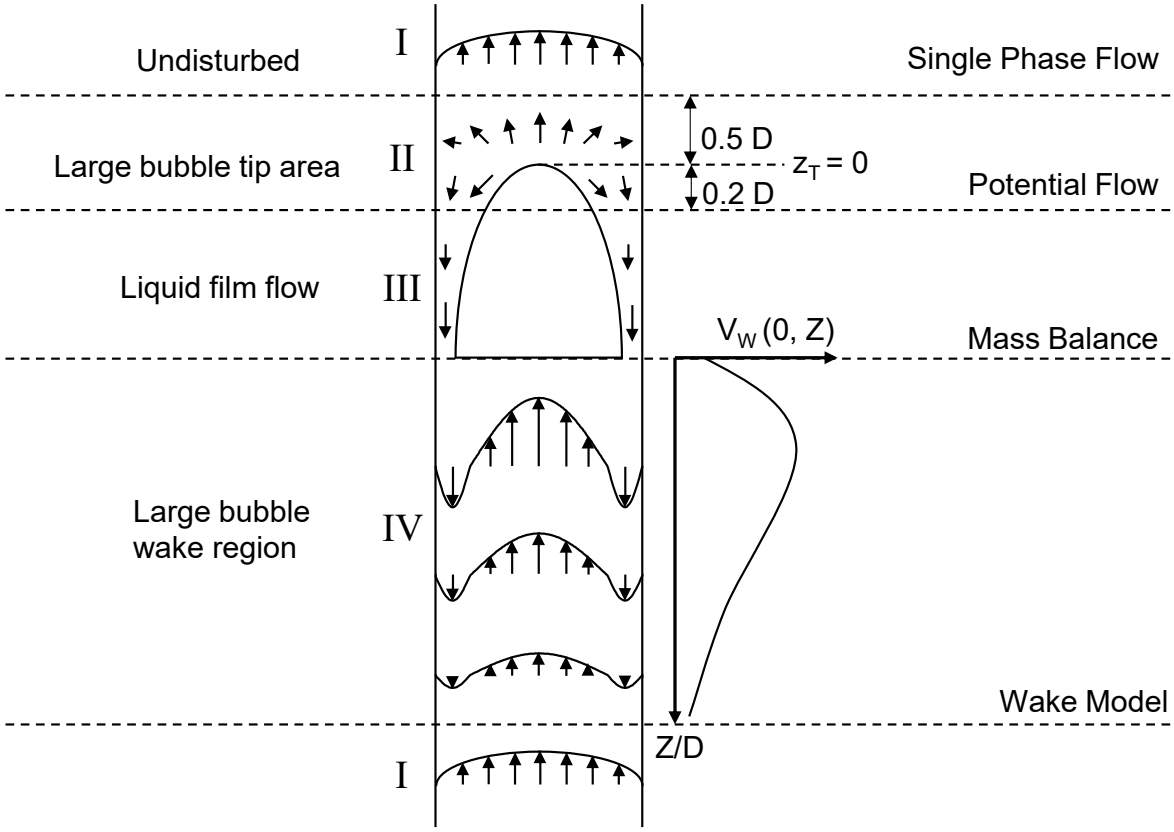

Fig. 3.10 Liquid phase velocity

3.4.4 Bubble coalescence and clustering

Small bubbles in a certain area ($\Delta z/D \leq 0.2$) below the rear end of the large bubble are regarded as clustered bubbles and rise at the same speed as the large bubble. Since clustered bubbles may be detached from the wake due to factors such as vortex shedding and turbulence [29], clustered small bubbles are also moved to the downflow region of the large bubble wake with probability P_{E1}. P_{E1} is given by.

$$P_{E1} = 10\left\{1 - 0.9\exp\left[-0.1\left(\frac{d_L}{D}\right)^6\right]\right\}\Delta t \qquad (3.57)$$

On the other hand, some of small bubbles flowing in the downflow region near the wall of the pipe are entrained in the vortex behind the large bubble. Therefore, small bubbles existing in the downflow area near the pipe wall are moved to the upflow area in the center of the pipe with a probability P_{E2}:

$$P_{E2} = 2\left\{1 - 0.9\exp\left[-0.1\left(\frac{d_L}{D}\right)^6\right]\right\}\Delta t \qquad (3.58)$$

Bubble coalescence processes are classified into three elementary processes: bubble approach, liquid film thinning, and bubble coalescence, and it is reported that each elementary process depends on factors such as bubble size, relative velocity, and interface contamination [30,31]. However, it is difficult to consider these various factors in a real flow field where many bubbles interfere. Therefore, it is determined whether or not bubbles are coalesced by the coalescence probability P_C.

The coalescence probability P_C should be modeled as a function of bubble diameter, relative velocity between bubbles, turbulent velocity, contact time, contact area, etc. However, at present, there is a lack of knowledge on the effects of these factors on bubble coalescence. Therefore, in this calculation, P_C of small bubbles is evaluated as a function of Δt ($P_C = C_P\Delta t$). Here C_P is an experimental coefficient, and a recommended value is given for a clean system, i.e., $C_P = 0.05$ under this condition. C_P of the contaminated system cannot be evaluated with the same value as that of the clean system due to the effect of the surfactant to suppress the coalescence of bubbles [31]. In this calculation, $C_P = 0.038$ is set from a comparison of photographed images of the flow state of the aqueous NaCl-1-octanol mixed aqueous solution-air system and calculation results. Although the actual bubble coalescence process has some time duration from the contact of bubbles to coalescence [32], this method assumes that the bubbles coalesce and deform instantaneously. The volume-weighted average of both bubbles is used for the position and velocity of the bubbles after merging. $P_C = 1$ is for large bubbles. The bubble position after merging is calculated by fixing the tip coordinates of the preceding large bubble. It is assumed that coalescence between small bubbles and large bubbles does not occur at the tip and body of the large bubbles, so it occurs only in the bubble cluster at the rear end of the large bubbles. That is, when the total volume of clustered small bubbles exceeds the maximum packing (74.1%), all clustered small bubbles are merged with the large bubbles.

3.4.5 Bubble dissolution and mass transfer

The rate of change in CO_2 moles inside a bubble is calculated as

$$\frac{\mathrm{d}n}{\mathrm{d}t} = -k_L A_B (C_{int} - C_0) \quad (3.59)$$

where A_B is the bubble surface area, C_0 is the CO_2 concentration in the liquid phase, and C_{int} is the concentration of CO_2 at the bubble interface mass transfer coefficient. The mass transfer k_L is evaluated using correlations for single bubbles proposed by Hori et al.[2]. The Sherwood numbers of spheroidal and semi-Taylor bubbles in clean water (Case 1) and NaCl solution (Case 2) are given by

$$Sh = f(d^*)Pe^{1/2} \quad (3.60)$$

$$f(d^*) = \begin{cases} \frac{2}{\sqrt{\pi}}(0.33d^{*2} + 0.28d^* + 1.0) & \text{for } d^* \leq 1 \\ 0.18d^* + 1.6 & \text{for } d^* > 1 \end{cases} \quad (3.61)$$

where *Sh*, *d** and *Pe* are the Sherwood number, the dimensionless bubble diameter, and the Peclet number, respectively, and they are defined by

$$Sh = \frac{k_L d}{D_{CO_2}} \quad (3.62)$$

$$d^* = d/d_T \quad (3.63)$$

$$Pe = \frac{|V_B - V_L| d}{D_L} \quad (3.64)$$

The following Sherwood number correlation by Filla [33] is used for Taylor bubbles

$$Sh_D = 5.1(L/D)^{0.8}\sqrt{Pe_D} \quad (3.65)$$

where Sh_D and Pe_D are the modified Sherwood and Peclet numbers defined as:

$$Sh_D = \frac{k_L A_B}{D_{CO_2} D} \quad (3.66)$$

$$Pe_D = \frac{|V_B - V_L|D}{D_L} \quad (3.67)$$

L/D is evaluated using the following empirical correlation proposed by Nakahara and Tomiyama[19]:

$$L/D = (0.586 - 0.216\lambda + 0.844\lambda^2)\lambda \quad (3.68)$$

In case 3, mass transfer coefficients of spheroidal and semi-Taylor bubbles in the contaminated system under the combined NaCl-1-octanol can be evaluated by using the following correlation [3]:

$$Sh = F(d^*)Re^{1/2}Sc^{1/3} \quad (3.69)$$

$$F(d^*) = -0.10d^{*2} + 0.88d^* + 0.6 \quad (3.70)$$

$$Sh_D = [A(\theta)\left(\frac{L}{d_T}\right)^2 + B(\theta)\left(\frac{L}{d_T}\right) - 7]Re_D^{1/2}Sc^{1/3} \quad (3.71)$$

where

$$\theta = \frac{k_a\Gamma_m}{k_d d_T} \quad (3.72)$$

$$A(\theta) = -5.6\ x\ 10^{-5}\theta^{-1.2} \quad (3.73)$$

$$B(\theta) = 2.8\ \theta^{-0.19} \quad (3.74)$$

For 1-octanol, the adsorption rate constant k_a = 170 m^3/ms, the desorption rate constant k_d = 68/s, and the saturation concentration Γ_m= 7.5 x 10^{-6} mol/m^2

The amount of material m_p [mol] of the gas *p* (= CO_2, N_2, O_2) in the bubble and the time change of the bubble diameter due to dissolution are calculated using the mass transfer correlation equation of a single bubble. However, since this system is a multi-bubble system, the change in the CO_2 concentration C_{LCO2} [mol/m^3] in the liquid phase accompanying the dissolution of CO_2 cannot be ignored. Assuming that the effect of diffusion is negligible compared to advection in the vertical transport of dissolved CO_2, the following one-dimensional mass conservation equation taking into account the CO_2 transfer rate *Q* [mol/m^3·s] from bubbles is used to calculate the change in C_{LCO2} [10]:

$$\frac{\partial C_{LCO2}}{\partial t} + J_L \frac{\partial C_{LCO2}}{\partial z} = Q \qquad (3.75)$$

The changes in the concentrations of N_2 and O_2 in the liquid phase are so small that they are ignored.

3.4.6 Simulation condition

The calculation was performed under the conditions of D = 25.0 mm, a pipe length of 5 m, and a time interval of 0.005 s, up to 500 s, which was sufficient for evaluating the time average value. The measured values shown in Fig. 3.5 were used for the inlet boundary conditions. Considering three types of gas components, CO_2, N_2 and O_2, the initial CO_2 mole fraction was set at 0.999. The remaining components were N_2 and O_2, and the mole fraction was determined from the air component ratio (79:21). Calculation time was about 5 hours using a personal computer (CPU: Core i7, Memory: 4 GHz).

3.5 Comparison of measured and predicted flows

3.5.1 Comparison of flow patterns

Fig.3.11 shows comparisons between measured and predicted flow patterns of the pure water-air system and the flow pattern of Case 1-3. The center of each image is the z-coordinate position shown at the top of the figure. The predicted results show the flow fields at the same time arranged side by side in each section. The experiment using an air-water system was first carried out to obtain a reference case without mass transfer. The left-side figure of Fig. 3.11a shows high-speed video images. Bubbles are dispersed at z = 1.0 m, but bubble clustering can be seen in the pipe center region. Bubble coalescence events increase the mean bubble size and the formation of a Taylor bubble is seen at z = 2.0 m. Small bubbles are entrained in the near wake of the Taylor bubble. The flow is still developing between z = 2 and 3 m, i.e., Taylor bubbles still grow and become longer. The right-side figure shows predicted bubble distributions at each elevation. Being similar to the experiment, the flow structure at z = 1.0m is bubbly and the increase in z enhances the formation and growth of Taylor bubbles. Although the number of small bubbles behind Taylor bubbles in the prediction is much less than that in the experiment, the structure and development of the flow are predicted well with the present numerical model.

Fig. 3.11b (left figure) shows a flow in Case 1. Bubbles are well dispersed at z = 1.0 m. The bubble sizes are smaller than the air-water case. The bubble size decreases as z increases up to 2m and no Taylor bubbles are formed at that elevation, meaning that the reduction of the bubble size due to dissolution is faster than the bubble growth rate by coalescence. The bubble sizes at z = 3.0m are smaller than those at z = 2.0 m, whereas the bubble sizes at z = 3.0 and 4.0m are not so much different. The spatial evolution of the flow structure with mass transfer in the experiment is well reproduced in the numerical prediction as shown in the right figure of Fig. 3.11b.

Fig. 3.11c shows Case 2. The flow structure and its evolution along z are similar to those in Case 1. However, the bubble sizes are slightly larger than in Case 1, which can be attributed to the reduction of k_L due to the presence of NaCl [2]. The numerical prediction reproduces well not only the flow structure but also the slight difference in the bubble size from Case 1.

The presence of 1-octanol in the NaCl solution (Case 3) causes a drastic change in the evolution of the flow compared with Case 2, i.e., the bubble sizes do not reduce for z = 2.0–3.0 m and bubble clustering are observed at z = 3.0 m. The formation of bubble clusters induces frequent bubble coalescence events, resulting in the formation of Taylor bubbles at z = 4.0 m. The large difference in the flow structure from Case 2 is due to the combined effect of NaCl and 1-octanol, which largely decreases k_L.

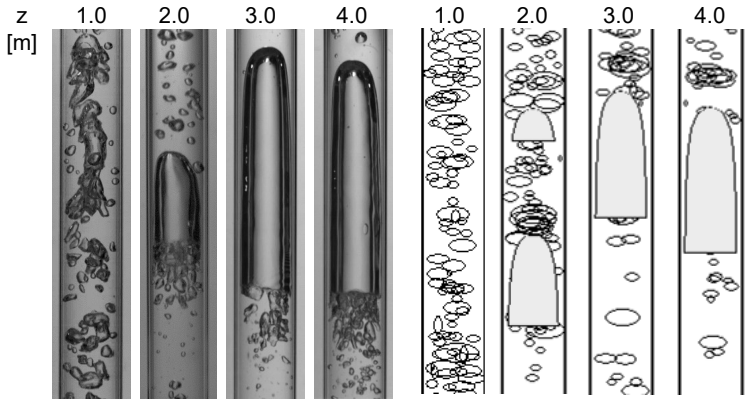

(a) Pure water-air system

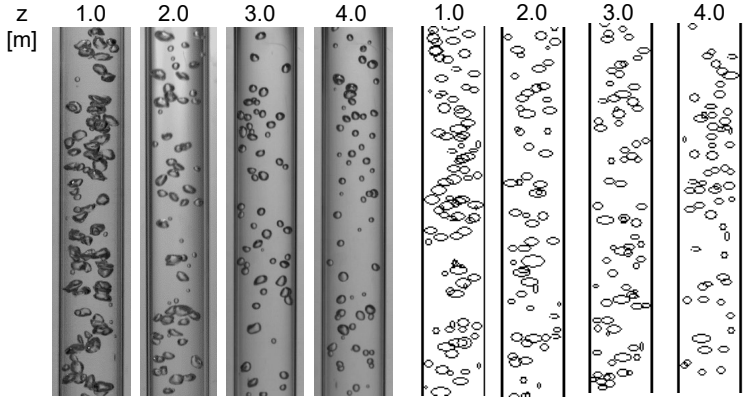

(b) Case1: Pure water-CO_2 system

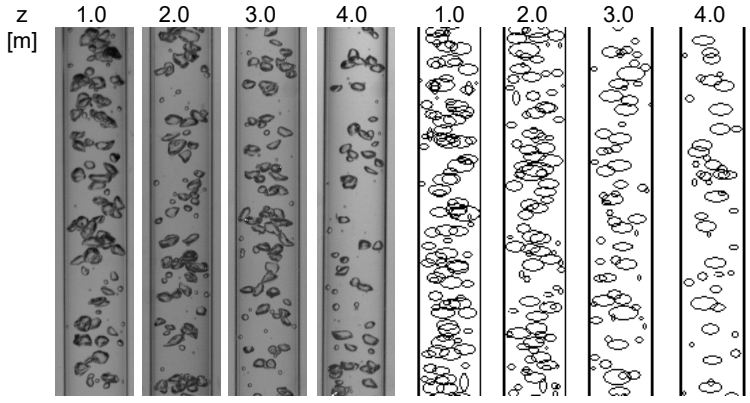

(c) Case2: NaCl solution- CO_2 system

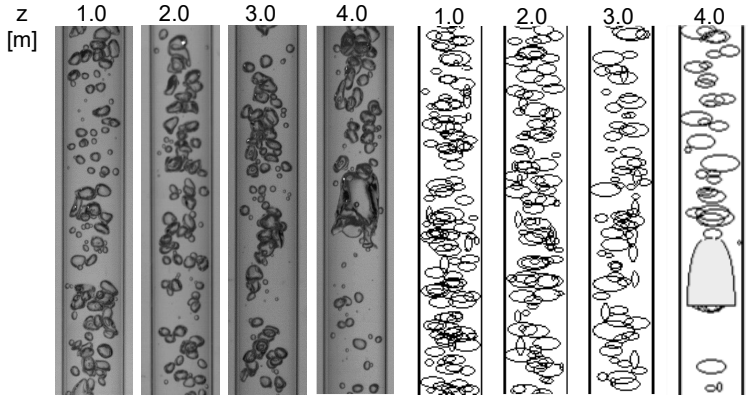

(d) Case3: NaCl-1-octanol mixed aqueous solution- CO_2 system

Fig. 3.11 Comparison of experiment and simulation flow structure for each cases

3.5.2 Comparison of radial void fraction distribution and bubble diameter distribution

Fig. 3.12-3.15 shows a comparison of measured and predicted α_G distribution and bubble diameter distribution at each measurement position in the vertical direction. The vertical axis in the left figure is the time-averaged local void fraction α_G normalized by the area-average void fraction $<\alpha_G>$. The α_G distribution and bubble size distribution were well predicted in the simulation. In Case 1, similarly to the experimental results, the number of bubbles with $d < 5$ mm increased downstream, and the tendency of the α_G distribution to transition to the wall peaking was predicted. Even in Case 3, the transition to the slug flow downstream due to the coalescence of bubbles was successfully calculated.

From the figures, it was found that the bubble dissolution process of bubble flow and slug flow in a vertical pipe can be well predicted by the mass transfer correlation of a single bubble in NaCl aqueous solution and NaCl-1-octanol mixed aqueous solution. Therefore, this correlation constructed based on the mass transfer data of a single bubble rising in a stagnant liquid can also predict the mass transfer of a multi-bubble flow system well. In this experiment, *Sc* was much larger than 1, and the concentration boundary layer was much thinner than the velocity boundary layer. Therefore, the velocity change around the bubble due to other bubbles or liquid flow has little effect on mass transfer. This is the reason why mass transfer was well evaluated by the single-bubble correlation even in a multi-bubble system. However, this calculation does not take into account the effect of interference between bubbles on gas-liquid mass transfer, for example, the effects of collision, coalescence, or breakup between bubbles on mass transfer. By constructing models for these phenomena, further improvement would be required.

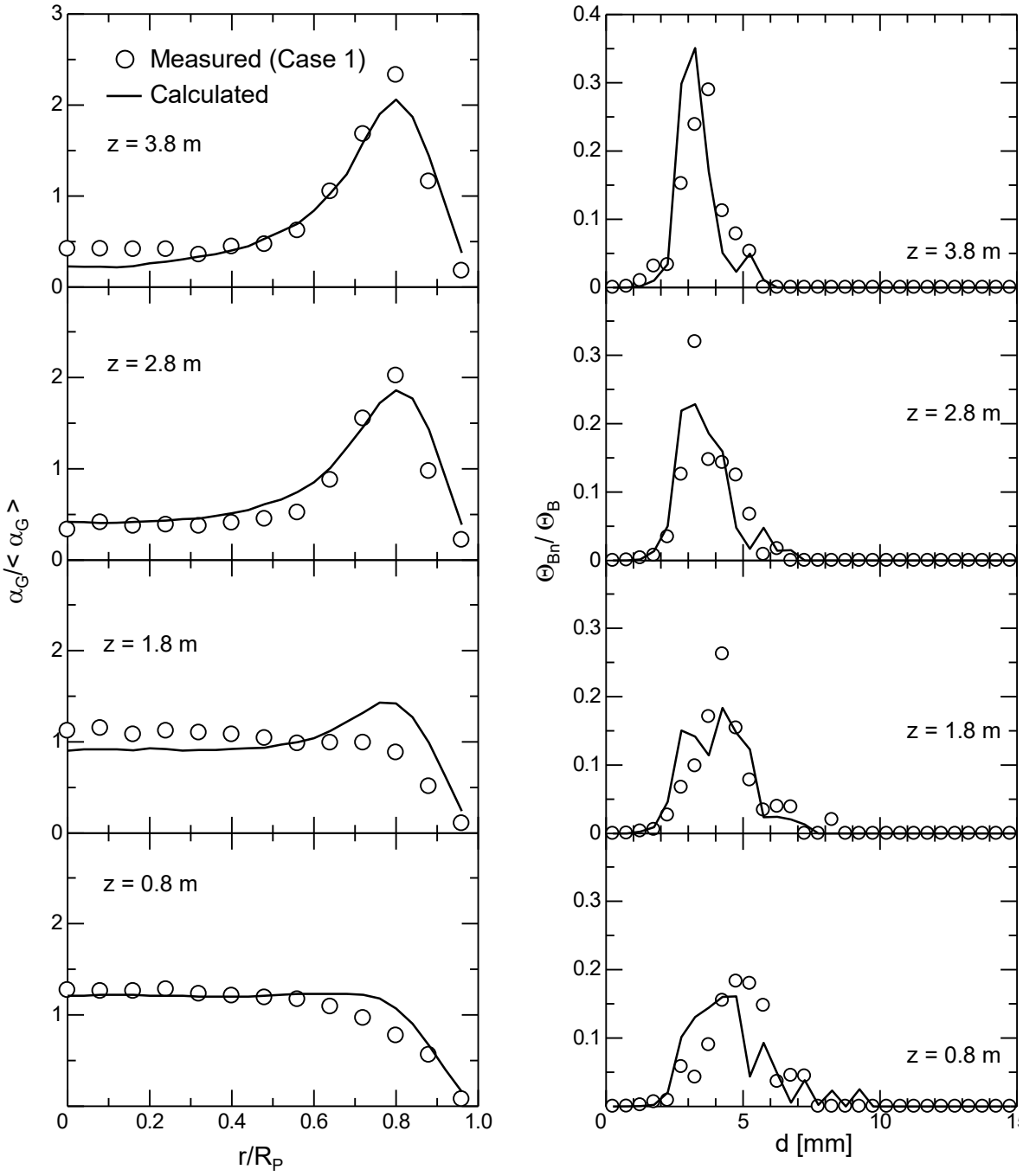

Fig. 3.12 Comparison of experiment and simulation results Case 1

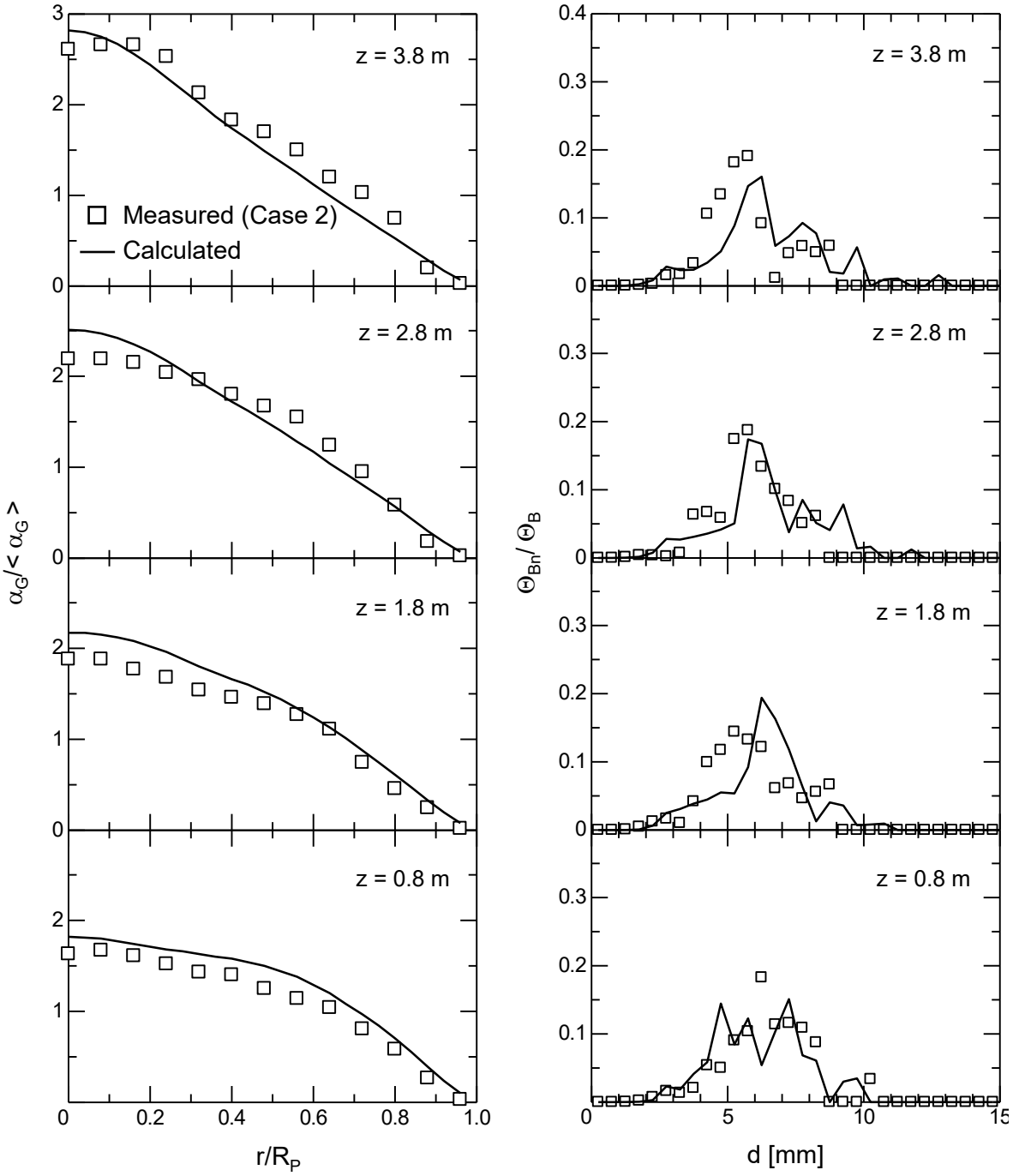

Fig. 3.13 Comparison of experiment and simulation results Case 2

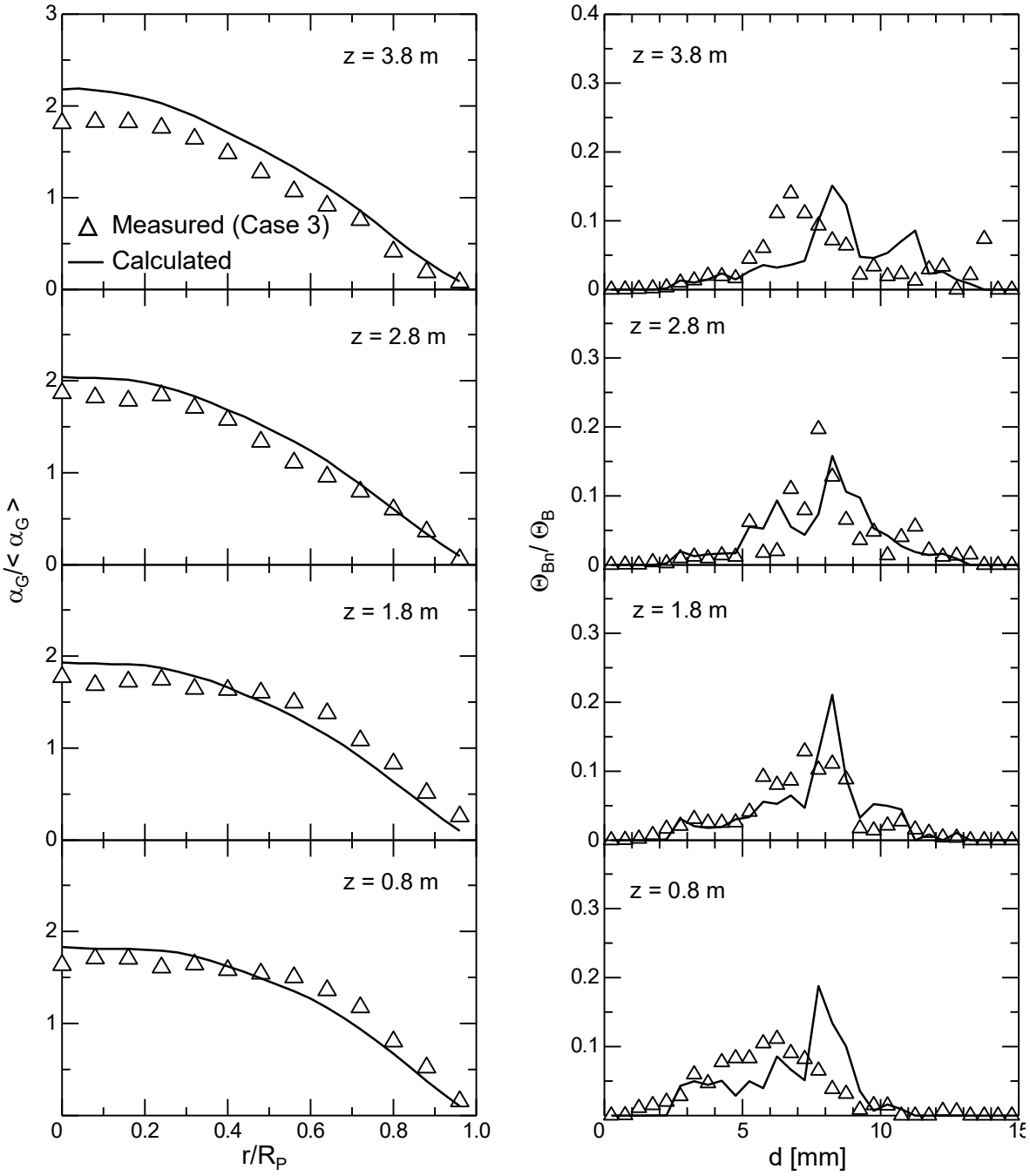

Fig. 3.14 Comparison of experiment and simulation results Case 3

3.6 Conclusion

As a first step to validate the implementation of the mass transfer models into the three-dimensional one-way bubble tracking method, mass transfer correlations of single bubble constructed by previous study [2,3] with different kinds of liquid phases other than pure water were used in numerical simulation. The predicted results of bubble-slug flows were compared with experimental results. The validity of the mass transfer calculation in the multi-bubble flow

system using the correlations was verified. As a result, the following conclusions were obtained.

1. The effects of electrolyte and the combined effects of electrolyte and surfactant on the flow pattern, radial void fraction distribution, and radial bubble diameter distribution of bubbles were measured for a pipe of 25.0 mm in diameter, the liquid phase Reynolds number of 7000, and the gas phase volume flux of 0.120 m/s.
2. The numerical simulations well reproduced the characteristics of the flows observed in the experiments and the predicted void and bubble size distributions agreed well with the data, implying that the mass transfer correlations developed for single bubbles are applicable to bubbly flows of high Schmidt number systems.

References

[1] S. Abe, “Study on gas-liquid mass transfer in carbon dioxide-water bubble flow in vertical pipe (in Japanese),” Doctoral dissertation, Kobe University, 2009.

[2] Y. Hori, K. Hayashi, S. Hosokawa, and A. Tomiyama, “Mass transfer from single carbon-dioxide bubbles in electrolyte aqueous solutions in vertical pipes,” *Int J Heat Mass Transf*, vol. 115, pp. 663–671, 2017, doi: 10.1016/j.ijheatmasstransfer.2017.07.087.

[3] Y. Hori, D. Bothe, K. Hayashi, S. Hosokawa, and A. Tomiyama, “Mass transfer from single carbon-dioxide bubbles in surfactant-electrolyte mixed aqueous solutions in vertical pipes,” *International Journal of Multiphase Flow*, vol. 124, Mar. 2020, doi: 10.1016/j.ijmultiphaseflow.2020.103207.

[4] H. Tamai, “Prediction of gas-liquid two-phase bubble and slag flow in a vertical pipe based on three-dimensional one-way bubble tracking method (in Japanese),” Doctoral dissertation, Kobe University, 2002.

[5] H. Tamai and A. Tomiyama, “Prediction of Undeveloped Bubbles and Slag Flows Based on Three-Dimensional One-Way Bubble Tracking Method (1st Report, Model and Calculation Example, in Japanese),” *Transactions of the Japan Society of Mechanical Engineers (Part B)*, vol. 70, pp. 880–887, 2004.

[6] R. Pan, J. Green, and C. Maldarelli, “Theory and experiment on the measurement of kinetic rate constants for surfactant exchange at an air/water interface,” *J Colloid Interface Sci*, vol. 205, no. 2, pp. 213–230, 1998, doi: 10.1006/jcis.1998.5559.

[7] D. M. Himmelblau, “Diffusion of dissolved gases in liquids,” *Chem Rev*, vol. 64, no. 5, pp. 527–550, 1964, doi: 10.1021/cr60231a002.

[8] *The Chemical Engineering Association, 4th edition, Chemical Engineering Fact Sheet (in Japanese)*. Maruyama Corporation, 1978.

[9] R. Sato, “Study on the flow inside and outside a diffuser pipe (in Japanese),” Doctoral dissertation, Kobe University, 2018.

[10] S. Abe, H. Okawa, S. Hosokawa, and A. Tomiyama, “Dissolution of a Carbon Dioxide Bubble in a Vertical Pipe,” *Journal of Fluid Science and Technology*, vol. 3, no. 5, pp. 667–677, 2008, doi: 10.1299/jfst.3.667.

[11] S. Kojima, “Study on the flow in a slurry bubble tower (in Japanese),” Doctoral dissertation, Kobe University, 2015.

[12] *Atomic Energy Society of Japan (ed.), Multiphase Flow Measurement Methods (in Japanese)*. Morikita Publishing, 2002.

[13] T. Hibiki and M. Ishii, “Two-group interfacial area transport equations at bubbly-to-slug flow transition,” *Nuclear Engineering and Design*, vol. 202, no. 1, pp. 39-76, 2000, doi: 10.1016/S0029-5493(00)00286-7.

- [14] A. Tomiyama, H. Tamai, I. Zun, and S. Hosokawa, “Transverse migration of

single bubbles in simple shear rows," *Chemical Engineering Science*, vol. 57, pp. 1849–1858, 2002, doi: 10.1016/S0009-2509(02)00085-4.

[15] A. Tomiyama, "Numerical prediction of flow containing bubbles (in Japanese)," *JSME (B)*, vol. 66, pp. 1618–1626, 2000.

[16] K. Hayashi, "Study on numerical prediction method for two-phase flow based on interface tracking method," Doctoral Dissertation, Kobe University, 2007.

[17] R. M. Wellek, A. K. Agrawal, and A. H. P. Skelland, "Shapes of liquid drops moving in liquid media," *American Institute of Chemical Engineers Journal*, vol. 12, pp. 854–862, 1966, doi: 10.1002/aic.690120506.

[18] J. Aoki, "A Study on Dissolution Process of Carbon Dioxide Bubbles in Polluted Systems in Vertical Tubes (in Japanese)," Doctoral Thesis, Kobe University, 2017.

[19] A. Tomiyama and Y. Nakahara, "Shapes and rising velocities of single bubbles in vertical pipe (in Japanese)," *Transactions of the Japan Society of Mechanical Engineers (Part B)*, vol. 69, 2003, doi: 10.1299/kikaib.69.2002.

[20] A. Tomiyama, G. P. Celata, S. Hosokawa, and S. Yoshida, "Terminal velocity of single bubbles in surface tension force dominant regime." *International Journal of Multiphase Flow* , vol. 28, pp. 1497–1519, 2002, doi: 10.1016/S0301-9322(02)00032-0.

[21] A. Tomiyama, "Drag, lift and virtual mass forces acting on a single bubble," in *Proceedings of 3rd International Symposium on Two-Phase Flow Modeling and Experimentation*, 2004, pp. 22–24.

[22] K. Hayashi and A. Tomiyama, "Effects of surfactant on lift coefficients of bubbles in linear shear flows," *International Journal of Multiphase Flow* , vol. 99, pp. 86–93, 2018, doi: 10.1016/j.ijmultiphaseflow.2017.10.003 .

[23] D. S. Sa'adiyah, K. Hayashi, R. Kurimoto, and A. Tomiyama, "Spatial Evolution of CO2-Contaminated Water Bubble Flows in a Vertical Pipe," *Chem Ing Tech*, vol. 93, no. 1–2, pp. 247–259, Jan. 2021, doi: 10.1002/cite.202000138.

[24] R. Kurimoto, K. Hayashi, and A. Tomiyama, "Bubble tracking simulations using simple models for fluctuating bubble motion," 2020. *Multiphase Science and Technology* , vol. 32, pp. 221–236, 2020, doi: 10.1615/MultScienTechn.2020034484.

[25] A. Tomiyama, A. Sou, I. Zun, N. Kanami, and T. Sakaguchi, "Effects of Eötvös Number and Dimensionless Liquid Volumetric Flux on Lateral Motion of a Bubble in a Laminar Duct Flow," in *Multiphase Flow 1995*, Elsevier, 1995, pp. 3–15. doi: 10.1016/b978-0-444-81811-9.50005-6.

[26] J. Nikuradse, "Gesetzmässigkeit der Turbulenten Strömung in Glatten Rohren," *Forsh. Arb. Ing. Wes.*, vol. 356, 1932.

[27] Y. Sato and K. Sekoguchi, "Liquid velocity distribution in two-phase bubble flow," *International Journal of Multiphase Flow* , vol. 2, pp. 79–95, 1975, doi: 10.1016/0301-9322(75)90030-0.

[28] J. Laufer, “The structure of turbulence in fully developed pipe flow,” *NASA Technical Reports Server* , 1954.

[29] A. Tomiyama, Y. Makino, I. Zun, and T. Sakaguchi, “Bubble shape modelling for a 3D two-way bubble tracking method,” in *Proceedings of 3rd International Conference on Multiphase Flow, CD-ROM*, 1998.

[30] M. J. Prince and H. W. Blanch, “Bubble Coalescence and Break-Up in Air-Sparged Bubble Columns,” *AIChE Journal*, vol. 36, no. 10, pp. 1485–1499, 1990, doi: 10.1002/aic.690361004.

[31] S. Takagi, T. Ogasawara, M. Fukuta, and Y. Matsumoto, “Surfactant effect on the bubble motions and bubbly flow structures in a vertical channel,” *Fluid Dyn Res*, vol. 41, no. 065003, 2009, doi: 10.1088/0169-5983/41/6/065003.

[32] S. Ojima, S. Sasaki, K. Hayashi, and A. Tomiyama, “Effects of particle diameter on bubble coalescence in a slurry bubble column,” *Journal of Chemical Engineering of Japan*, vol. 48, no. 3, pp. 181–189, Mar. 2015, doi: 10.1252/jcej.14we248.

[33] M. Filla, “Gas absorption from a slug held stationary in downflowing liquid,” *The Chemical Engineering Journal*, vol. 22, no. 3, pp. 213–220, 1981, doi: 10.1016/0300-9467(81)80016-0.

Chapter 4
Application of Chemical Absorption Enhancement Factor to Bubbly-Flow in Vertical Pipe

4.1 Introduction

Based on chapter 3, investigated were the experiments and predicted simulations of CO_2 in multiple bubble system with various kind of physical absorption, including surfactant and electrolyte. Even though the mass transfer correlations used were created for single bubbles, they gave accurate predictions of the spatial evolution of flow structure in the multi-bubble system. This is because the concentration boundary layer at the surface of a bubble with a high Schmidt number is extremely thin and the mass transfer rate is not as significantly influenced by the motion of adjacent bubbles. In this chapter, the enhancement factor for chemical absorption is implemented into the bubble tracking method to examine its applicability to bubbly flow with chemical absorption.

Chemical absorption is investigated for two volume fluxes of the gas phase J_G with NaOH aqueous solution of pH = 13. The results were then compared with a clean system case. The measurement method of the experiment results in this chapter is different from the previous chapter. Since the dissolution of bubbles in chemical absorption is very fast and the accuracy is very important, a 3D image processing method is used to calculate both time-averaged void fraction and bubble diameter distribution at several axial locations in a vertical pipe. The experimental results are compared with one-way bubble tracking prediction.

4.2 Experiment and measurement method

4.2.1 Experimental condition

The experiments for CO_2 bubbly flows were carried out for two different J_G. For each J_G two cases were investigated, i.e., pure water (pH ≈ 7) and NaOH aqueous solution (pH = 13) cases. The experimental conditions were summarized in Table 4.1. Re_L, J_L [m/s], and J_G [m/s]

are the liquid Reynolds number, the liquid volume flux, and the gas volume flux, respectively. It should be noted that J_G listed in the table is based on mass flow rates measured at the gas inlet and will not be used as the inlet condition in the simulation. The details on this will be explained in the next section.

σ [N/m], ρ_L [kg/m^3], μ_L [Pa.s] are the surface tension, the liquid density and the liquid viscosity, which were measured by a pendant bubble method, a standard hydrometer (JISB-1525), and a tuning fork vibrating viscometer (A & D Corporation, SV-A10), respectively.

Table 4.1 Experimental conditions

Case	pH	Re_L	J_L [m/s]	J_G^* [m/s]	σ [N/m]	ρ_L [kg/m^3]	μ_L x10^{-3} [Pa·s]	Sc
Case 1 A : Pure water	7	7000	0.250	0.01	0.072	997	0.89	420
Case 1 B : aqueous NaOH solution	13	7000	0.250	0.01	0.069	1001	0.91	478
Case 2 A : Pure water	7	7000	0.250	0.02	0.072	997	0.89	420
Case 2 B : aqueous NaOH solution	13	7000	0.250	0.02	0.069	1001	0.91	478

*J_G were measured by a mass flow controller and was not be used as inlet conditions in simulation

Tables 4.2 show the phyisical properties [1,2] of CO_2, under each condition, where C_{Sat} [mol/m^3] is the gas concentration at the bubble interface, C_L [mol/m^3] is the gas concentration in the liquid phase and D_L [m^2/s] is the diffusion coefficient. The details on the calculation of C_{Sat} and D_L can be seen in section 2.2.1. Since the experiments were carried out in the degassed system, the presence of N_2 and O_2 were neglected.

Table 4.2 CO_2 gas phase transport coefficient under each condition (298 K) [1,2]

	C_{Sat} [mol/m^3]	C_L [mol/m^3]	$D_L \times 10^{-9}$ [m^2/s]
Case 1A & 2A	34.0	0.0110	1.92
Case 2A & 2B	32.7	0.0112	1.90

4.2.2 Experimental setup

A schematic of the experimental apparatus is shown in Fig. 4.1. The apparatus consists of the test section, the upper tank, the gas phase inlet, the pump (Iwaki, MD-30FX-EN), the mixer (NITTO METAL INDUSTRY), the glove box (Azwan), the tank, the agitator (Azwan, SMT-101), the pH meter (TOA DKK, HDM-136A, measurement accuracy ±0.03), the vacuum pump (ULVAC, GLD-137-CC), the pH meter (TOA DKK, HDM-136A, measurement accuracy ±0.03), the flowmeter (Nippon Flow Cell, NSP-5), and the mass flow controller (KOFLOC, 8500MC). The liquid phase in the test section was water purified by using Millipore, Elix5UV. Sodium hydroxide (NaOH) (Fujifilm Wako Pure Chemicals, 1310-73-2) was used as the solute. NaOH was added to the purified water and was thoroughly stirred in an argon-purged mixer. In order to prevent NaOH from reacting with carbon dioxide in the air, granular NaOH was weighed and fed into the mixer in an argon-purged glove box. The pH of NaOH was set at 13.0, with a tolerance of ±0.03.

The liquid phase was supplied by the pump and flowed in from the bottom of the test section via the flow meter. The temperature of the liquid phase was set at 25±1.0°C. The gas phase was carbon dioxide (CO_2: Sumitomo Seika Co., Ltd., purity 99.9 vol.%), which was supplied from the gas cylinder, depressurized to 0.2 MPa by the regulator, and supplied from the bottom of the test section via the mass flow controller and a bubble inflow section. The diffuser tube of the bubble inflow section had diffuser holes facing vertically downward to ensure uniform diffusion of air from each hole. The flow channel was purged by argon and closed to the atmosphere to avoid the intrusion of other chemical elements from the air. Hereafter, z [m] is the vertical coordinates of the test section.

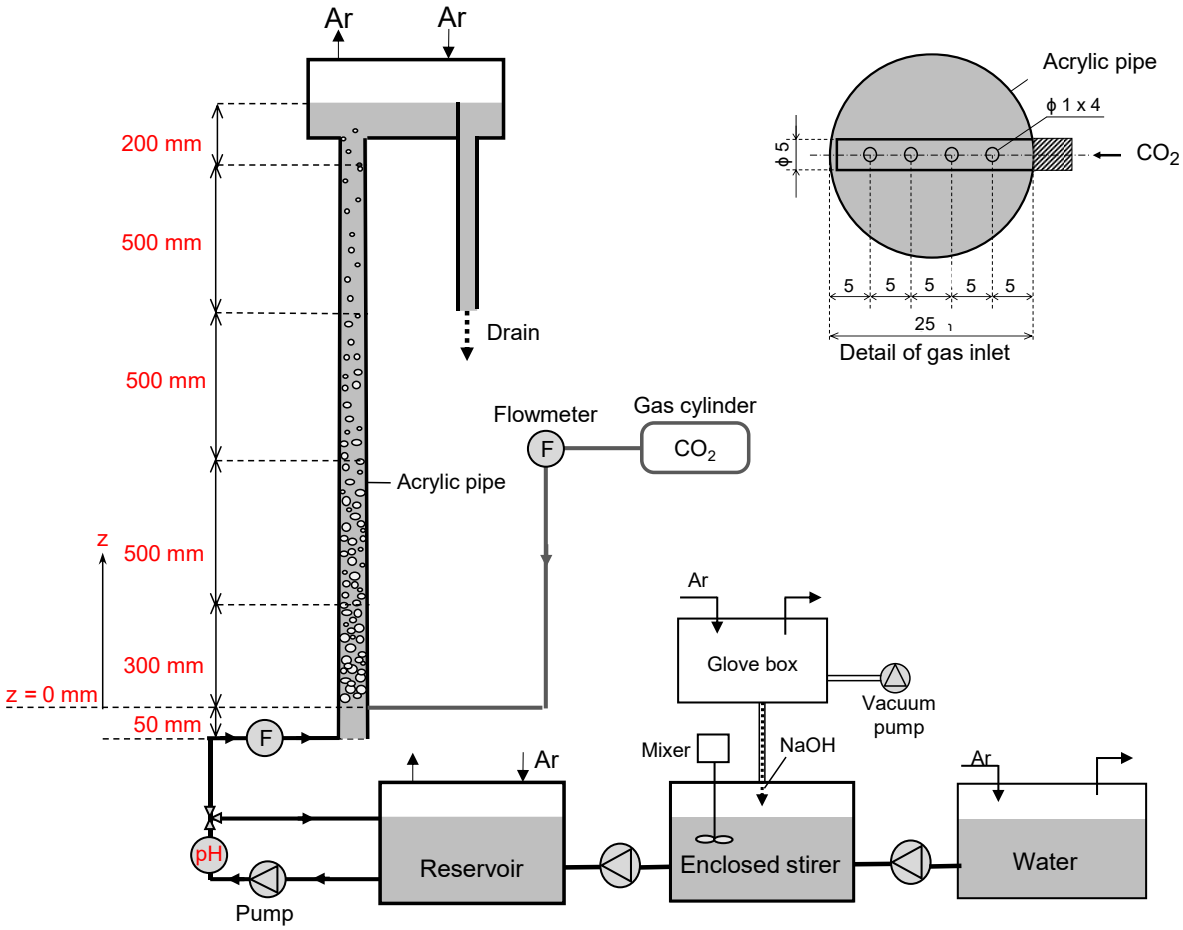

Fig. 4.1 Experimental setup

4.2.3 Measurement method of bubble diameter and time average void fraction

The flow observations were carried out at z = 0.3, 0.8, 1.3 and 1.8 m, where the elevations represent the center position of flow images. The length of flow observation area were 100 mm and the images were captured by high-speed cameras (Integrated Design Tool, M3) from two orthogonal directions. The position of the high-speed camera and the test section are shown in Fig. 4.2. Red and green LEDs were used as light sources to suppress reflected and scattered light generated at the bubble interface by the lateral light source. The frame rate was 400 frame/s and the resolution was 0.08 mm/pixel. The test section consisted of a circular tube made of fluorinated ethylene propylene (FEP) resin. The inner diameter of the pipe was D = 25.0 mm. The pipe was inserted into an acrylic duct and filled with water. The refractive indices of water (1.333) and FEP (1.338) are almost equal, so that bubble images with reduced distortion due to light refraction were obtained.

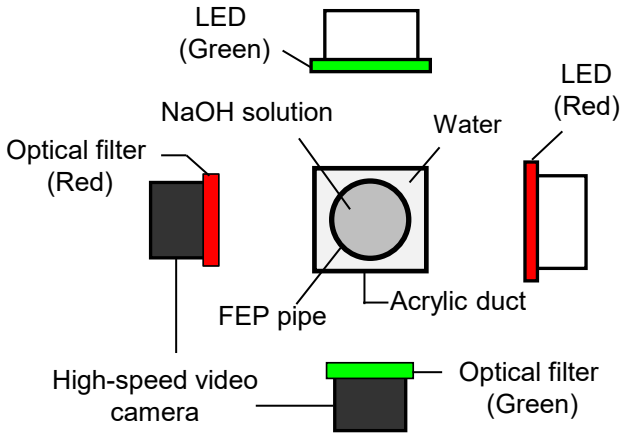

Fig. 4.2 Flow observation setup

Bubble size distributions were obtained from 800 bubbles passing through the center of each elevation. Image processing in section 2.2.3 was performed to calculate the sphere-volume equivalent bubble diameters d [m]. Because the image was taken from two directions, the measurement error of d was lowered to ±2.0%. Since the dissolution of CO_2 in a NaOH system is very fast due to chemical absorption, the measurement of d cannot be performed immediately after the gas inlet, therefore in this study, the bubble diameter at z = 0.3 m will be used as the inlet condition in simulations while J_G at z = 0.3 m estimated in simulation so as to obtain the same void fraction in the simulation and experiment.

Being different from the previous chapter in which the radial distribution of the time-averaged local void fraction α_G were measured using the point electrode probe method[3]–[5], only volume averaged void fraction $< \alpha_G >$ at each elevation was measured from the bubble size distributions. The total number of frames used for obtaining $< \alpha_G >$ was 4800.

4.3 Bubble dissolution data of gas-liquid two-phase bubble flow in a vertical pipe

4.3.1 Bubble diameter distribution at inlet and flow pattern

As mentioned in section 4.2.3, for the inlet boundary condition for bubble tracking simulation, the bubble diameter distribution at z = 0.3 m was used. Figs. 4.3 and 4.4 show the measurement results for each J_G. Bubble diameters were classified with bins of 0.5. For all cases, bubble diameter were less than 8 mm, with the NaOH cases much less than the pure water case. Cases with larger J_G have larger bubble sizes. In case 1A, the highest probability

density function (pdf) is in $4 < d < 5$ mm while in Case 1B there are two peaks in $3 < d < 4$ mm and $d < 1$ mm. Since the measurement of pdf was done for $z = 0.3$ m, it is possible to have many tiny bubbles ($d < 1$ mm) even at $z = 0.3$ m in Case 1 B because the bubbles were mostly going through fast dissolution due to chemical absorption.

In Fig. 4.4 different peaks can be seen between the pure water system (Case 2 A) and the NaOH system (Case 2 B) for $J_G = 0.02$ m/s. The pdf peak is at $d = 5$ mm in Case 2 A, while the peaks in Case 2 B are at $d = 1.5$ mm and $d = 4$ mm.

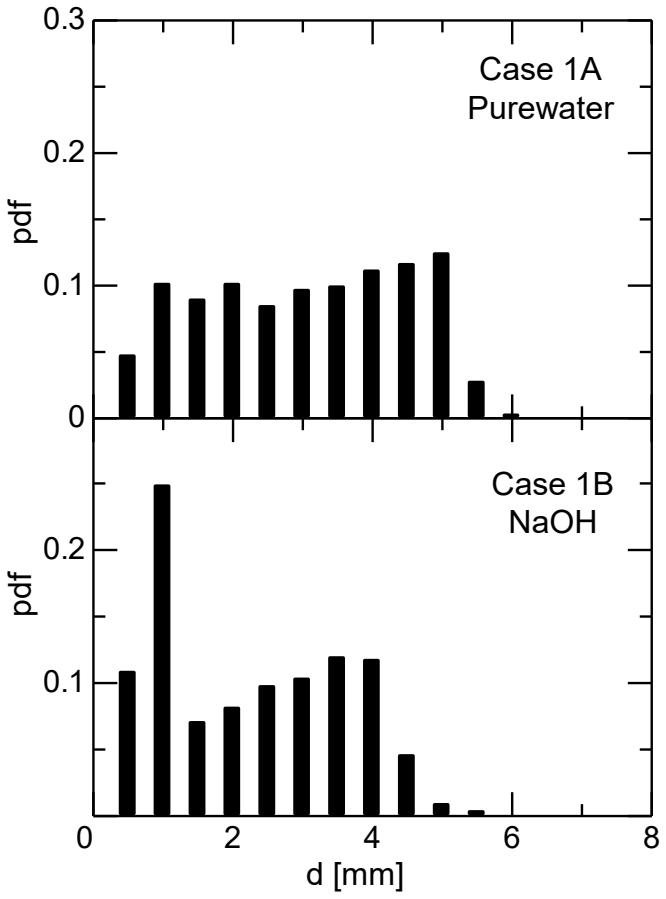

Fig. 4.3 Inlet bubble diameter distribution for $J_G = 0.01$ m/s

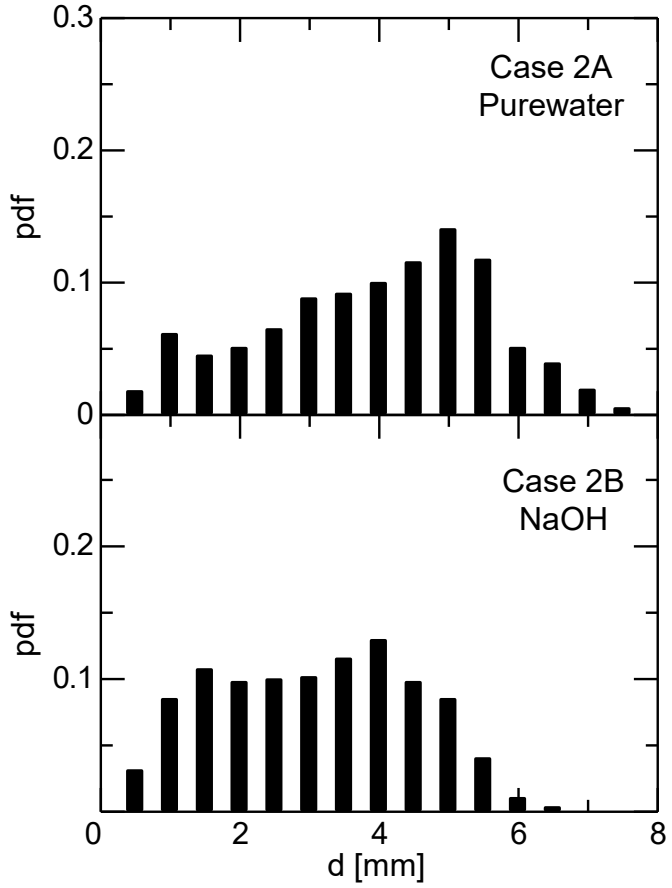

Fig. 4.4 Inlet bubble diameter distribution for J_G = 0.02 m/s

The flow patterns are shown in Fig. 4.5. In the CO_2-pure water system, the bubble diameter decreases as increasing the elevation. This is of course due to the physical dissolution of bubbles. With the presence of chemical absorption in the system, the bubble diameter downstream become much smaller due to the enhancement of the dissolution rate. In case 1B (J_G = 0.01 m/s), the bubble diameters at z = 1.8 m were very small, i.e., d < 1 mm.

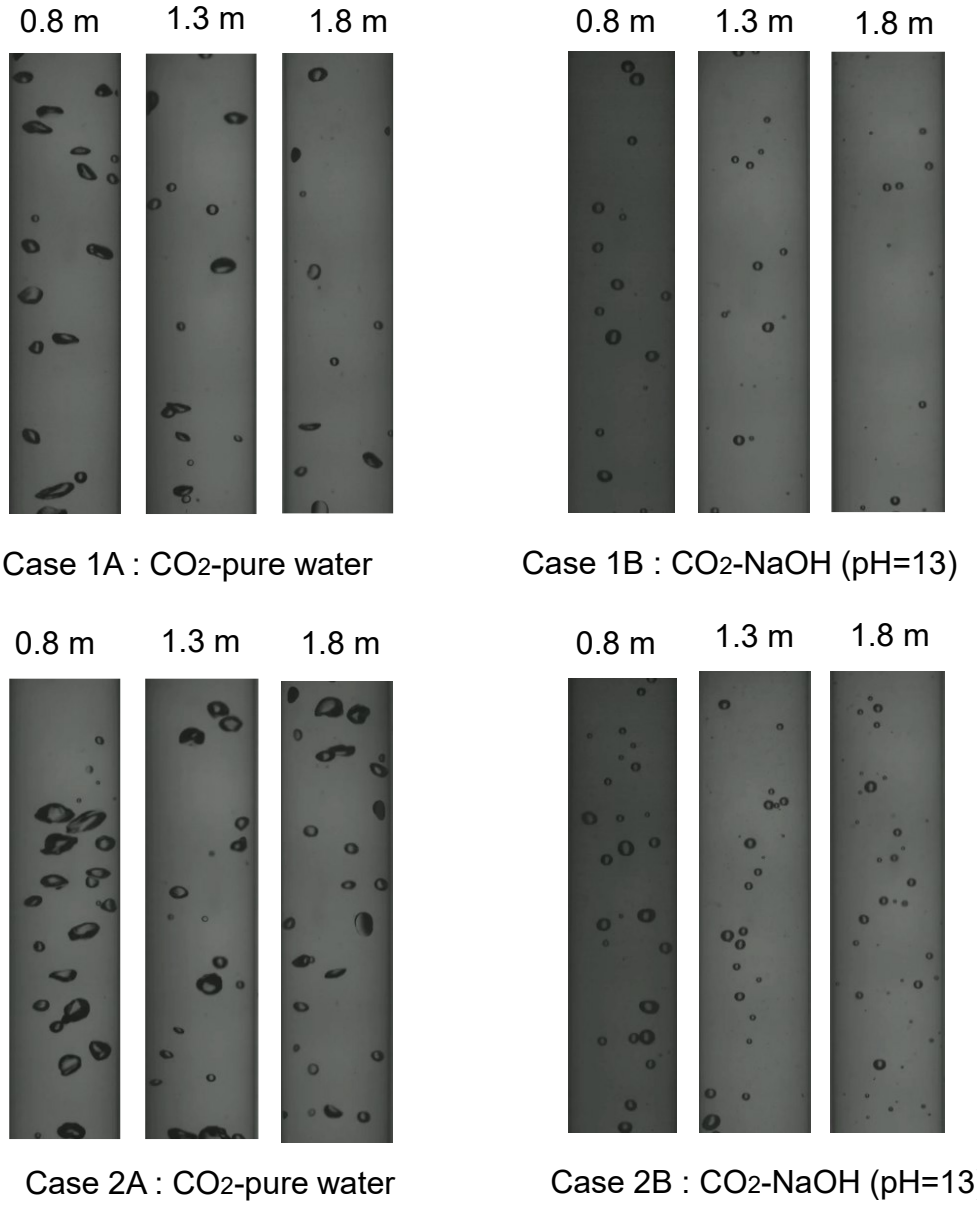

Fig. 4.5 Flow pattern for J_G = 0.01 m/s (Case 1 A and B) and J_G = 0.02 m/s (Case 2 A and B)

4.3.2 Mean void fraction and bubble diameter distribution

The measured $< \alpha_G >$ and bubble size distribution at each elevation are shown in Figs. 4.6 and 4.7. In Case 1 A and B, $< \alpha_G >$ start from different values. This is because at z = 0.3 m CO_2 bubbles have already dissolved a lot in the NaOH system. This also applies to Case 2 A and B. In downstream of the NaOH system, almost all CO_2 bubbles were dissolved and $< \alpha_G >$ is only 6.7 x 10^{-4} in Case 1 B, and 1.75 x 10^{-3} in Case 2 B.

The vertical axis of the bubble size distribution is the ratio of the total bubble volume Θ_{Bn} [m^3] of each bubble class to the total gas volume Θ_B. Different peaks can be seen between

the pure water and the NaOH systems, where from upstream to downstream the peaks in the NaOH cases moves to smaller bubble diameters faster than the pure water cases.

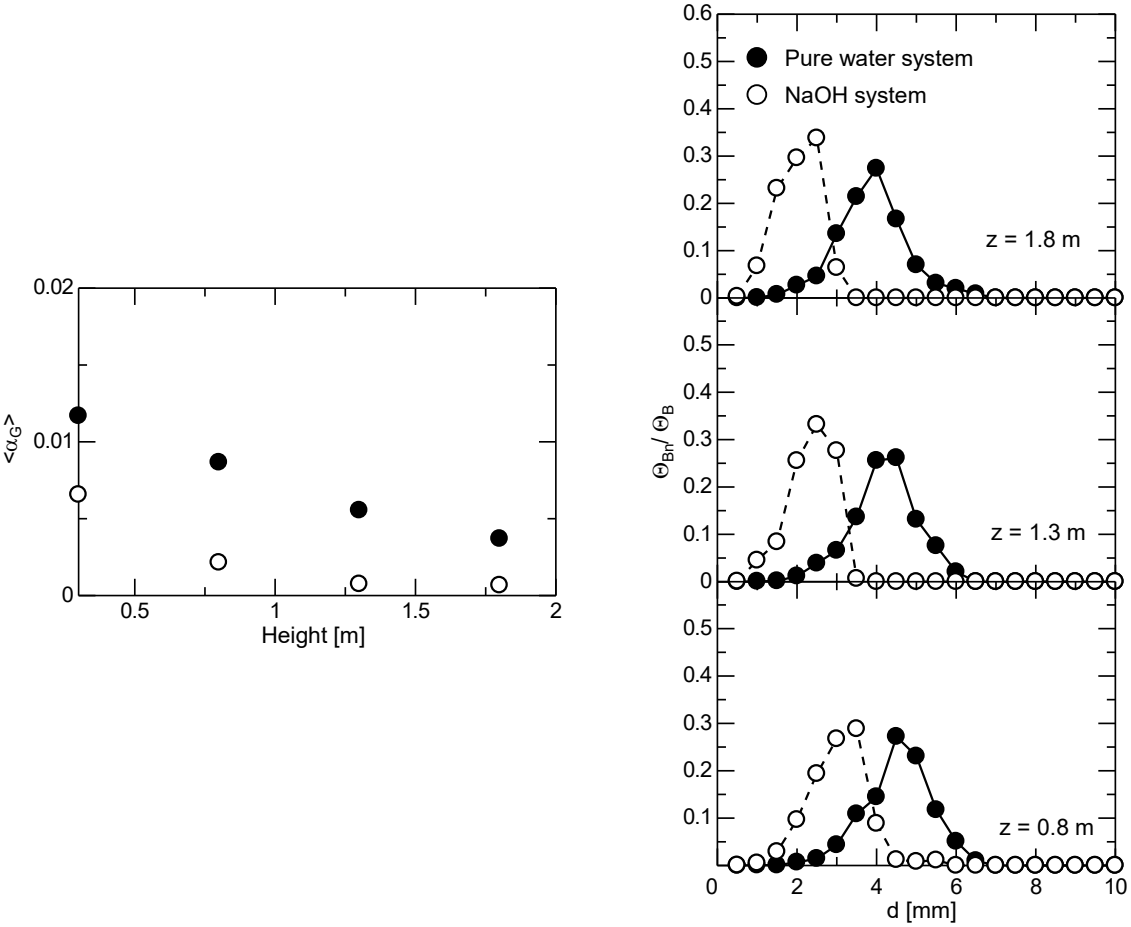

Fig. 4.6 Mean void fraction and bubble diameter at each elevation of Case 1 A and B

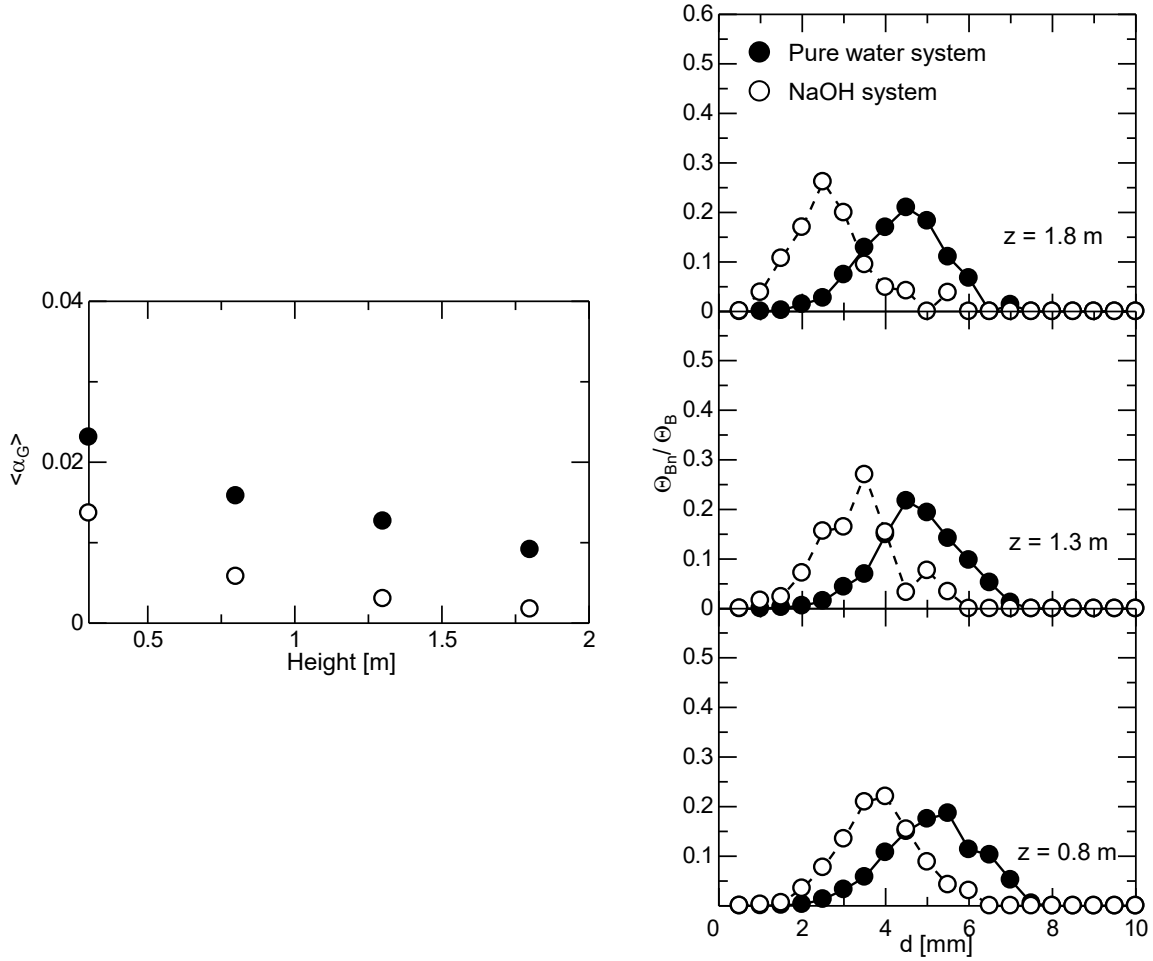

Fig. 4.7 Mean void fraction and bubble diameter at each elevation of Case 2 A and B

4.4 Numerical simulation

The three-dimensional one-way bubble tracking method given in chapter 3 [6] was used. Basically, the mass transfer correlation used in all the cases in this section was the same, except for the enhancement factor correlation proposed in Chapter 2. The mass transfer correlation for clean system proposed by Hosoda [7] and corrected by Hori [8] was:

$$Sh^0 = \begin{cases} \frac{2}{\sqrt{\pi}}\left(0.34\, d^{*2} + 0.28 d^* + 1\right)\sqrt{Pe} & \text{for } d^* < 1 \\ (0.18\, d^* + 1.6)\ \sqrt{Pe} & \text{for } d^* \geq 1 \end{cases} \qquad (4.1)$$

where Sh^0 is the Sherwood number for the clean system, $d^* = d/d_T$, and Pe is the Peclet number defined by

$$Pe = \frac{V_B d}{D_L} \quad (4.2)$$

For the NaOH system, the enhancement factor correlation proposed in Chapter 2 was implemented to account for chemical absorption:

$$Sh = E\, Sh^0 \quad (4.3)$$

where

$$E = \begin{cases} 1 + \exp(2.98\,\mathrm{pH} + 1.04d^* - 39.7) & \text{for } d^* < 1 \\ 1 + \exp(2.69\,\mathrm{pH} + 0.40d^* - 35.3) & \text{for } 1 \le d^* < 1.8 \end{cases} \quad (4.4)$$

Since both cases were free from other chemical substances such as N_2 and O_2, only the change in the CO_2 concentration C_{LCO2} [mol/m^3] in the liquid phase due to the dissolution of CO_2 was taken into account. The change in C_{LCO2} was simulated using the following one-dimensional mass conservation equation which takes into account the CO_2 transfer rate Q [mol/m^3·s] from bubbles [3].

$$\frac{\partial C_{LCO2}}{\partial t} + J_L \frac{\partial C_{LCO2}}{\partial z} = Q \quad (4.5)$$

Since the chemical reaction occurs in the system after the dissolution of CO_2, the change of the hydroxide ion in NaOH and other chemical products needs to be considered. Table 4.3 is the parameter values for chemical reaction between NaOH and CO_2 [9]. The parameter values listed in Table 4.3 were used in the calculation of chemical reaction of each ion in the liquid.

Table 4.3 Parameter values for chemical reaction

Reaction	Kinetic constant [m^3/(mol.s)]	Equilibrium constant [m^3/mol]
$CO_2 + OH^- \leftrightarrow HCO_3^-$	5.0	6.1 x 10^4
$HCO_3^- + OH^- \leftrightarrow CO_3^{2-} + H_2O$	1 x 10^4	5.88

4.5 Comparison of measured and predicted flows

4.5.1 Comparison of flow patterns

Fig. 4.8 shows a comparison of measured and predicted flow patterns. The axial elevation of the center of each image is shown at the top of each image. The predicted images show similar pattern with the measured images, where at the downstream bubble diameters become smaller in the pure water system, and much smaller in the NaOH system. The comparison indicate that the bubble dissolution processes with/without chemical absorption is predicted well.

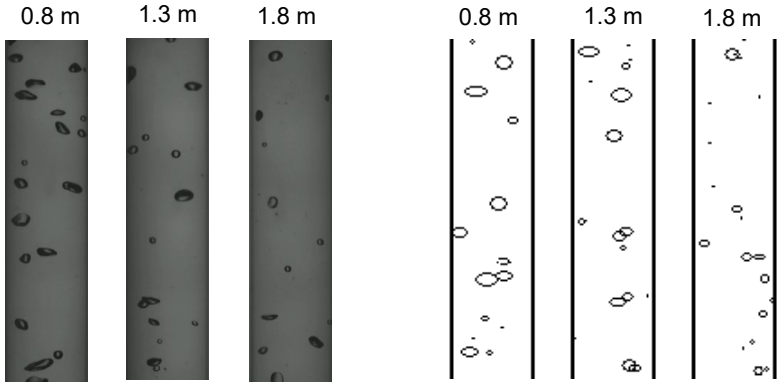

Case 1A : CO_2-pure water

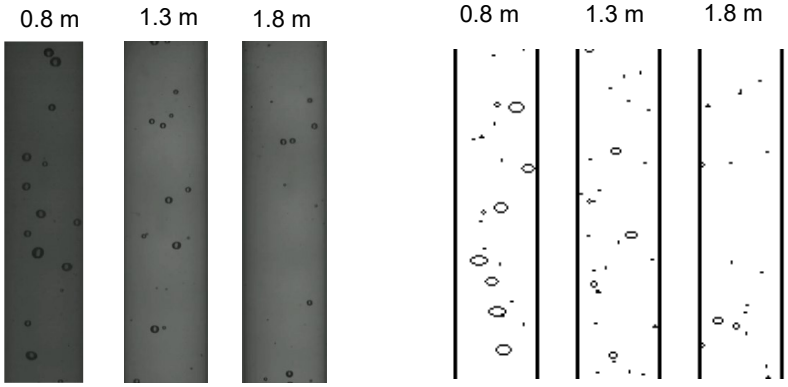

Case 1B : CO_2-NaOH (pH=13)

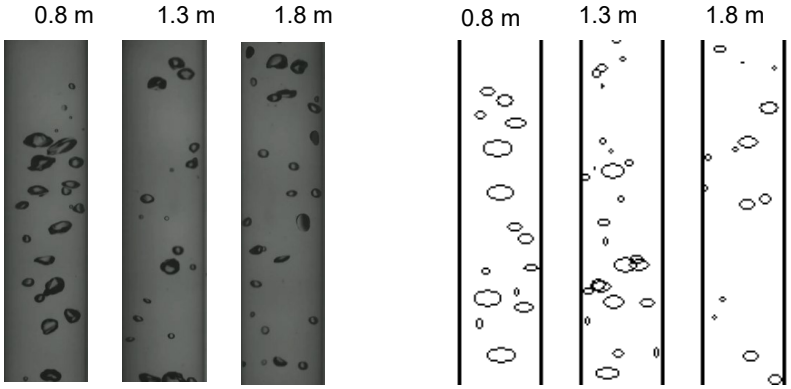

Case 2A : CO_2-pure water

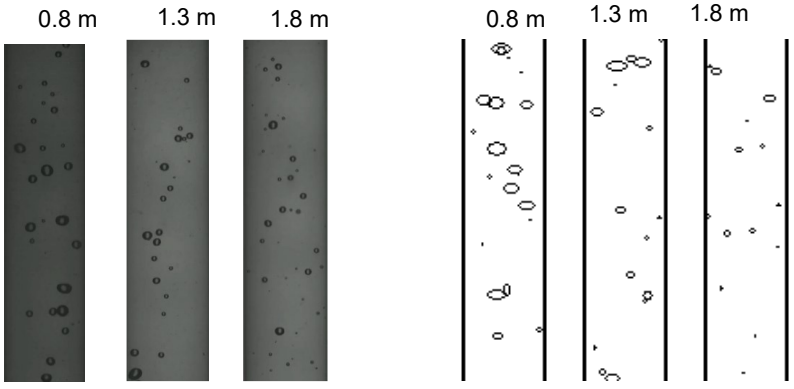

Case 2B : CO_2-NaOH (pH=13)

Fig. 4.8 Comparison of experiment and simulation flow structure for each cases

4.5.2 Comparison of mean void fraction and bubble diameter distribution

The spatial evolution of measured and predicted mean void fractions $<\alpha_G>$ are shown in Fig. 4.9. For both J_G, the measured $<\alpha_G>$ for aqueous NaOH solution at z = 0.3 m are lower than those of the pure water system because CO_2 bubbles in the former dissolved a lot in $0 \leq z \leq 0.3$ m due to chemical absorption, $<\alpha_G>$ for Case 1 A and 1 B start from 0.012 and 0.007, while for Case 2 A and 2 B start from 0.023 and 0.013. In the numerical calculation, the measured $<\alpha_G>$ at z = 0.3 m is the inlet condition together with the pdfs of bubble size distributions shown in Figs. 4.3 and 4.4. Since it was difficult to measure J_G at z = 0.3 m, the value of J_G then was tuned via trial and error in the calculation to obtain the same $<\alpha_G>$ at z = 0.3 m as those in the experiments. J_G = 0.0045 m/s was used in Case 1 A, while J_G = 0.005 m/s was used in Case 1 B. For Case 2 A and 2 B, J_G = 0.01 m/s gave good agreement between measured and predicted $< \alpha_G >$ at z = 0.3 m. In the pure water systems, $<\alpha_G>$ is well predicted by using the available mass transfer correlation of single bubbles for the clean system [8]. The aqueous NaOH solution systems are also well predicted by using the enhancement factor correlation Eq. (4.4), whereas we cannot obtain good predictions of $<\alpha_G>$ without the E correlation as expected. This confirms that the enhancement factor correlation, Eq. (4.4), should be taken into account for obtaining good predictions for bubbly flows with chemical absorption.

Fig. 4.10 shows comparisons of measured and predicted bubble size distributions at three axial elevations. Its vertical axis is the ratio of the total bubble volume Θ_{Bn} [m^3] of each bubble class to the total gas volume Θ_B. The values of d were classified with bins of 0.5 mm width. The cases with chemical absorption, Case 1 B and 2 B, have smaller bubble sizes at each axial position than the cases without chemical absorption, Case 1 A and 2 A. The chemical absorption in the systems significantly increases the dissolution of CO_2 bubbles. The one-way bubble tracking method gives reasonable predictions for spatial evolution of bubble size distributions for all the cases.

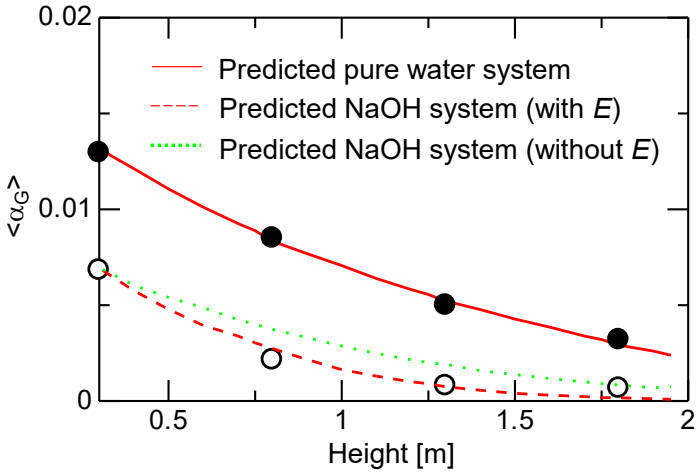

(a) Case 1: $J_G = 0.01$ m/s

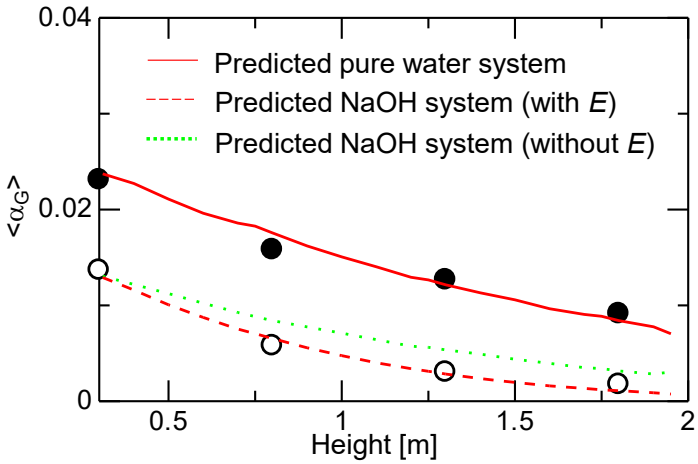

(a) Case 2: $J_G = 0.02$ m/s

Fig. 4.9 Comparison of mean void fractions

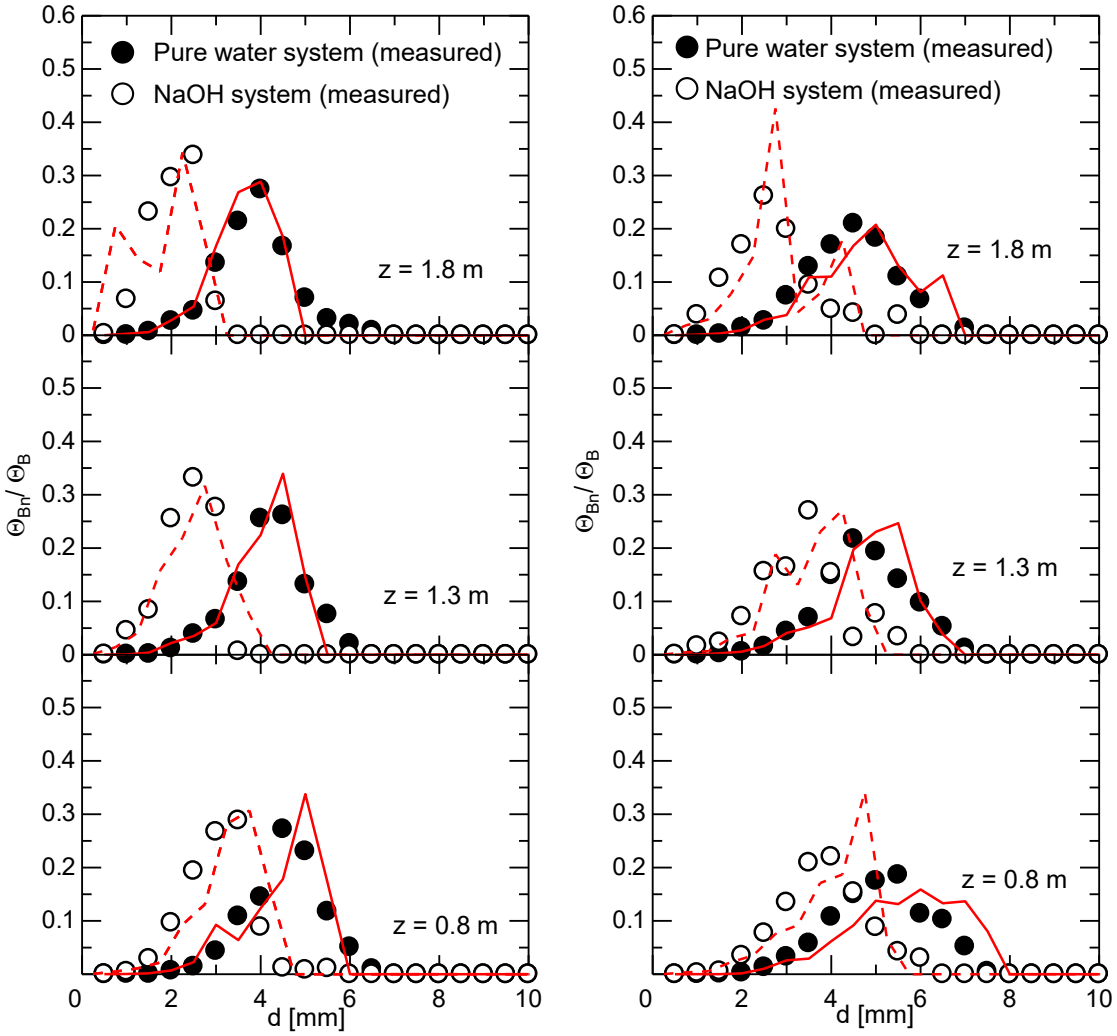

(a) Case 1: J_G = 0.01 m/s (a) Case 2: J_G = 0.02 m/s

Fig. 4.10 Comparison of bubble diameter distributions

4.6 Conclusion

The combination of the enhancement factor of chemical absorption proposed in Chapter 2 and the available mass transfer correlation of a clean system from the previous study [8] was implemented into the three-dimensional one-way bubble tracking method to examine its applicability to bubbly flow with chemical absorption. Experiments were also carried out to obtain the data for validation. Here is the conclusion of this section:

1. The spatial evolutions of flow patterns, mean void fractions, and bubble diameter distributions of CO_2 bubbly flows with or without chemical absorption were measured

for a pipe diameter of 25.0 mm, a liquid phase Reynolds number of 7000, and two gas phase volume fluxes, i.e., 0.01 and 0.02 m/s.

2. Implementation of the enhancement factor correlation together with the available mass transfer correlation for single bubbles in a clean system into the one-way bubble tracking method can produce good results of the characteristics of the flow patterns, mean void fraction, and bubble size distributions.

References

[1] D. M. Himmelblau, “Diffusion of dissolved gases in liquids,” *Chem Rev*, vol. 64, no. 5, pp. 527–550, 1964, doi: 10.1021/cr60231a002.

[2] *The Chemical Engineering Association, 4th edition, Chemical Engineering Fact Sheet (in Japanese)*. Maruyama Corporation, 1978.

[3] S. Abe, H. Okawa, S. Hosokawa, and A. Tomiyama, “Dissolution of a Carbon Dioxide Bubble in a Vertical Pipe,” *Journal of Fluid Science and Technology*, vol. 3, no. 5, pp. 667–677, 2008, doi: 10.1299/jfst.3.667.

[4] S. Kojima, “Study on the flow in a slurry bubble tower (in Japanese),” Doctoral dissertation, Kobe University, 2015.

[5] *Atomic Energy Society of Japan (ed.), Multiphase Flow Measurement Methods (in Japanese)*. Morikita Publishing, 2002.

[6] H. Tamai and A. Tomiyama, “Prediction of Undeveloped Bubbles and Slag Flows Based on Three-Dimensional One-Way Bubble Tracking Method (1st Report, Model and Calculation Example, in Japanese),” *Transactions of the Japan Society of Mechanical Engineers (Part B)*, vol. 70, pp. 880–887, 2004.

[7] S. Hosoda, S. Abe, S. Hosokawa, and A. Tomiyama, “Mass transfer from a bubble in a vertical pipe,” *Int J Heat Mass Transf*, vol. 69, pp. 215–222, 2014, doi: 10.1016/j.ijheatmasstransfer.2013.10.031.

[8] Y. Hori, K. Hayashi, S. Hosokawa, and A. Tomiyama, “Mass transfer from single carbon-dioxide bubbles in electrolyte aqueous solutions in vertical pipes,” *Int J Heat Mass Transf*, vol. 115, pp. 663–671, 2017, doi: 10.1016/j.ijheatmasstransfer.2017.07.087.

[9] N. Shimada, A. Tomiyama, M. Maekawa, T. Suzuta, and T. Ozaki, “A Numerical Method for Solving Bubbly Flow with Chemisorption in a Bubble Column (In Japanese),” *KAGAKU KOGAKU RONBUNSHU*, vol. 31, no. 6, pp. 377–387, 2005, doi: 10.1252/kakoronbunshu.31.377.

Chapter 5
Conclusion

Mass transfer phenomena, in which gas in bubbles is dissolved in the surrounding liquid phase, are used in various post-combustion CO_2 captures such as Gas-Lift Advanced Dissolution (GLAD) systems, bubble column reactors and gas absorbers. In designing the bubble column reactor with chemical absorption, it is necessary to understand the flow characteristics in the system. The flow characteristics change significantly due to changes in the bubble diameter, shape, and rising speed of the bubbles due to mass transfer. Specifically for chemical absorption, the enhancement factor E needs to be considered to define how fast the absorption rate is in the system. However, E correlations obtained so far have been based on an analytical theory which has not been validated against experimental data for multi-bubble systems. Hence in this study, experiments of single CO_2 bubbles with various shapes were carried out with several NaOH concentrations and its applicability to bubbly flow was examined.

In Chapter 2, the mass transfer from a single CO_2 bubbles in a stagnant liquid in a vertical pipe of diameter D = 12.5mm was investigated using the aqueous NaOH solution. The experiments were carried out for a wide range of the dimensionless bubble diameter λ, which is the ratio of the bubble diameter to the pipe diameter, $0.4 \leq \lambda \leq 1.4$, and for the sodium hydroxide concentration, $12 \leq \mathrm{pH} \leq 13.15$. The image processing was performed for the bubble images, and the mass transfer coefficient k_L was measured from the time change of the bubble diameter. The value of E for each bubble is obtained by comparing k_L of the chemical absorption with those of the physical absorption k_L^0. The experimental results confirmed that E for $7 < \mathrm{pH} < 12$ is almost unity, i.e., the presence of NaOH does not affect the mass transfer due to low concentration, while E increases with increasing both pH and d for pH > 12.25. The enhancement factor model based on the two-film theory and a flat interface by Fleischer et al. is not applicable to single bubbles because E changes not only because of pH but also by the shapes of bubble d^*, where d^* ($= d/d_T$) is the ratio of the bubble diameter to the bubble diameter at the transition from ellipsoidal to semi-Taylor bubbles. The proposed empirical correlation of E for single bubbles of $0.4 \leq \lambda \leq 1.4$ and $7 \leq \mathrm{pH} \leq 13.15$ gave good agreement with 93% of

the data to within ±10% errors. The correlation was also applicable to bubbles in the pipe diameter D = 18.2 mm.

In Chapter 3, examined was whether it is possible to obtain good predictions for mass transfer in multi-bubble systems with various kinds of physical absorption before applying the enhancement factor proposed in Chapter 2 to multi-bubble systems. Physical absorption in bubbly-slug flow in a vertical pipe was numerically simulated for three conditions: a pure water system, a system with electrolyte, NaCl, and a system including surfactant and electrolyte, NaCl-1-octanol mixture. The available mass transfer correlations are implemented into the bubble tracking method. In addition, experiments on bubbly-slug flows in a vertical pipe were carried out, and the obtained data were used to validate the extended numerical method. The spatial evolution of the flow patterns, radial void fraction distributions, and radial bubble diameter distributions of bubbles, were measured for a pipe of 25.0 mm in diameter, the liquid phase Reynolds number of 7000, and the gas volume flux of 0.120 m/s. The predicted and measured spatial evolution give good agreement, implying that the available mass transfer correlations developed for single bubbles are applicable to bubbly flows of high Schmidt number systems. In a system with a high Schmidt number, the thickness of concentration boundary layer is very small so that the effect of other bubbles or velocity changes around the bubbles due to the liquid flow on the mass transfer is negligible. Therefore, the spatial evolutions were well predicted.

In Chapter 4, the E correlation of chemical absorption proposed in Chapter 2 was implemented into the bubble tracking method to examine its applicability to bubbly flows with chemical absorption. The experiments were carried out for two gas volume flux conditions to validate the predicted results with or without chemical absorption. Since the dissolution of bubbles in chemical absorption is very fast, the image processing method is used to calculate both mean void fractions and bubble diameter distributions at several axial locations in a vertical pipe. The proposed E correlations implemented into a three-dimensional one-way bubble tracking method together with available mass transfer correlations for a clean system gave good predictions of the flow patterns, mean void fractions, and bubble diameter distributions.

In summary, the mass transfer with chemical absorption from single bubbles of various shapes and NaOH concentrations flowing in a vertical pipe were investigated this study. In addition, an enhancement factor correlation was proposed to predict bubble dissolution in aqueous NaOH solution. Before applying the proposed E correlation to the multi-bubble

system, the validity of the available mass transfer correlations with various kinds of physical absorption was examined using the bubble tracking method. Furthermore, it was clarified that the proposed *E* correlation can predict dissolving bubbly flows in a vertical pipe with or without chemical absorption.

List of publications

1. D. S. Sa'adiyah, Y. Matsuo, M. Schlüter, R. Kurimoto, K. Hayashi, and A. Tomiyama, "Effects of chemical absorption on mass transfer from single carbon dioxide bubbles in aqueous sodium hydroxide solution in a vertical pipe," *Chem Eng Sci*, 245, 1-11, 2021
2. D. S. Sa'adiyah, K. Hayashi, R. Kurimoto, and A. Tomiyama, "Spatial Evolution of CO_2-Contaminated Water Bubble Flows in a Vertical Pipe," *Chem Ing Tech*, 93, no.1–2, 247–259, 2021

Acknowledgement

All praises belong to Allah Subhanahu Wata'ala, the Most Gracious and the Most Merciful, and prayers and peace be upon Muhammad, His servant and messenger. Alhamdulillah, because of Allah blessing, I can finish my doctoral journey and write the dissertation entitled, "Mass transfer in bubbly flows with or without chemical absorption".

I want to express my gratitude to everyone who assisted me in completing my dissertation. Special appreciation to Prof. Akio Tomiyama, my doctoral supervisor, for his insightful remarks, inspiration, and invaluable advice. In addition, I would like to express my gratitude to Prof. Kosuke Hayashi and Prof. Ryo Kurimoto for their insightful input during my study. I would also like to thank my CO_2 research team, Mr. Yohei Hori, Mr. Yuki Matsuo, and Mr. Kanto Sato, for their assistance during the experiments. I want to thank the Ministry of Education, Culture, Sports, Science, and Technology for the scholarship. I would also like to thank my colleagues at the Institut Teknologi Kalimantan for the joy, help, discussion, and support they provided. Thank you to all the Multiphase Fluid Dynamics Laboratory student members who are always willing to assist me with experiments and contribute their research time.

Finally, I would like to thank my husband, Samsu Dlukha Nurcholik, and my beloved son, Hezarfen Ihsan Nurcholik, for all their patience and love. I also like to express my admiration to my father, Suroto, my mother, Ety Hartati, and my sister, Rizky Dwi Meilan Sari. Their encouragement and support have helped me through tough times and elevated my spirits anytime I felt unmotivated.

Doctoral Dissertation, Kobe University
“Mass transfer in bubbly flows with or without chemical absorption”, 102 pages

Submitted on January, 20, 2023

The date of publication is printed in cover of repository version published in Kobe University Repository Kernel